



DEVELOPMENT OF A DIMENSIONAL MEASUREMENT SYSTEM FOR HOT FORGED PARTS AT ELEVATED TEMPERATURE

A thesis submitted in fulfilment of the requirements for the degree of Doctor of Philosophy (PhD)

PhD candidate: Muthair Hafeez
Supervisors: Prof. David Butler & and Dr. Remi C Zante

DEPARTMENT OF DESIGN, MANUFACTURING AND ENGINEERING
MANAGEMENT

Dedication
To my parents

Acknowledgements

This thesis is the outcome of research conducted between 2017 and 2023 in the United Kingdom at the University of Strathclyde and the AFRC Strathclyde.

I am really grateful to my Supervisor, Dr David Butler, for facilitating this thesis, for engaging talks, for encouraging and for his irreplaceable years of support. Dr David Butler deserves special recognition for motivating me to pursue a Ph.D. and for reviewing various preliminary concepts. Furthermore, I would like to thank Alaster McDonach for supportive talks and Dr Remi C Zante for co-supervising my work. I would also like to acknowledge the support and guidance provided by Professor Jorn Mehnen during the final stages of this thesis.

I would like to thank Liza Hall from the AFRC Metrology lab for their amazing conversations and help in conducting lab-based experiments. I would like to thank Dr Muftooh Ur Rehman Siddiqi for providing an enjoyable working environment and for his informal knowledge transfer.

In private, I want to thank my wife Laraib Atique for her inspiration and endurance throughout the years. Finally, I'd like to thank my parents and siblings. I want to express my gratitude for their assistance, patience, trust, and support during my Ph.D. studies.

Abstract

Precision in-process dimensional measurement during high-temperature metal forming operations, such as hot forging, is key to guaranteeing product quality, enhancing material utilization, and ensuring process consistency. Conventional post-process measurement methods, including coordinate measuring machines (CMMs) and callipers, involve cooling prior to inspection, which causes delays, raises scrap rates, and reduces efficiency in flaw detection. Although next-generation optical systems such as GOM ATOS can achieve high-accuracy 3D scanning, they cannot be used for real-time in-process measurement in the harsh forging environment because of thermal expansion issues, glare, and material reflectivity. This warrants the development of a non-contact measuring system capable of providing accurate and reliable real-time dimensional measurement.

This work reports the development and validation of a real-time non-contact dimension measurement system tailored to hot forging applications. It is based on optical metrology techniques and advanced image processing algorithms exploiting photogrammetry for the provision of high-precision measurements under high temperature conditions. The system was developed to work effectively within the temperature range of 900°C to 1200°C, with the desired measurement accuracy of ± 1 mm at both the pixel and sub-pixel levels, thereby ensuring adherence to industrial tolerances for forged components.

Experimental validation was carried out both in laboratory and hot forging environments to confirm the accuracy and reliability of the proposed system. The system's performance was also benchmarked against the commercial GOM ATOS optical scan system through the assessment of the key parameters of measurement error, repeatability, and robustness in mild steel workpiece length and diameter measurement. Statistical analysis, such as confidence interval analysis, error quantification, and comparative analysis, also guaranteed that the measurement errors were within ± 1 mm for the majority of the length and diameter measurements of workpieces, with reproducible and consistent measurements.

The results of this research have provided a worthy contribution through a low-cost and scalable solution for real-time dimensional measurement for high-temperature forgings.

Mitigating Circumstances

The thesis was undertaken during a period which included the COVID lockdown and thus conducting experiments within the laboratories of the AFRC proved to be a challenge. A mitigation strategy was developed by the author which involved undertaking a series of limited experiments in industry in Pakistan.

Table of Contents

Dedication	1
Acknowledgements.....	2
Abstract.....	3
Discrimination.....	5
1 Introduction	12
1.0 Background	12
1.1 Problem statement	13
1.1.1 Key challenges.....	14
1.2 Research aim and objectives	15
1.3 Thesis organization	16
2 Literature review.....	18
2.0 Introduction	18
2.1 Quality control in the forging process	18
2.2 Forging temperature range.....	29
2.3 Advancements and challenges in vision-based hot forging measurement	31
2.4 Current dimensional methods for measurement of hot forging.....	36
2.4.1 Quality control at elevated temperature.....	36
2.4.2 Parts measurement at elevated temperature.....	37
2.4.3 Forging process optimization.....	51
2.5 Summary of review	53
2.6 Research gap and Justification of the research project.....	56
2.7 Objective metrics	57
3 Proposed methodology and preliminary studies.....	59
3.0 Introduction	59
3.1 Preliminary experiments.....	60
3.1.1 Fringe projection system.....	60
3.1.2 Specification of the GOM ATOS system.....	61
3.1.3 Justification for selecting the GOM ATOS system.....	62
3.2 Preliminary investigation to compare non-contact with contact-based measurement system at room temperature.....	64
3.3 Evaluation of the GOM ATOS performance at elevated temperature	68
3.3.1 Dimensional measurement results of heated samples	69

3.3.2	Comparison of GOM ATOS and CMM at elevated temperature	73
3.4	Proposed dimensional measurement system at elevated temperature	74
3.4.1	Experimental setup	77
3.4.2	Material and part geometry.....	78
3.4.3	Furnace and Camera Specifications	79
3.4.4	The dimensional measurement processes	81
3.4.5	Camera calibration	83
3.4.6	Image acquisition of hot part.....	87
3.4.7	Image processing of monochrome image.....	87
3.4.8	Image processing of I-R image	89
3.4.9	Physical filtering	92
3.4.10	Image de-noising.....	94
3.4.11	Blob analysis.....	96
3.5	Validation of proposed system	98
3.5.1	Part measurement at room temperature using a CMM.....	98
3.5.2	Elevated temperature measurements using proposed system.....	99
3.5.3	Justification of proposed system in current research.....	101
3.6	Conclusion.....	101
4	Photogrammetry system evaluation.....	104
4.0	Introduction	104
4.1	Part specifications, scanning methodology, and calibration process.....	106
4.1.1	Overview of experimental samples and preparation	106
4.1.2	Scanning methodology using the GOM ATOS system	108
4.1.3	Calibration of the GOM ATOS scanner.....	108
4.1.4	Justification for using a non-telecentric lens system.....	108
4.1.5	Analysis of distance-related magnification error and mitigation techniques.....	109
4.2	Measurement approach and system setup	110
4.2.1	Camera calibration of proposed system	111
4.2.2	Image scale calculation	111
4.2.3	Image segmentation approach	112
4.3	Interface for dimensional measurements of parts	117
4.4	Experiment and analysis at pixel level	120
4.4.1	Results of diameter and length measurements of heated samples before forging ...	121
4.4.2	Results of diameter and length measurements of hot forged samples	129

4.5	Conclusion.....	136
5	Enhancement of measurement precision using sub-pixel analysis	138
5.0	Introduction	138
5.1	Subpixel edge detection.....	139
5.1.1	Curve-fitting methods	141
5.1.2	Moment-based methods	141
5.1.3	Reconstructive methods	142
5.2	Comparative analysis	143
5.3	Problem definition	147
5.4	Experiments and analyses at subpixel level.....	148
5.4.1	Results of diameter length measurements of heated samples	148
5.4.2	Results of diameter & length measurements of forged samples (heated)	156
5.5	Analysis and comparison of proposed system measurement at pixel and subpixel level..	164
5.6	Conclusion.....	166
6	Conclusion and future recommendations	169
6.0	Conclusion.....	169
6.1	Contribution to knowledge	170
6.2	Future research directions.....	171
	References	173
	Appendices.....	179

Figures

Figure 2-1 Process tolerance vs. feature size [13]	20
Figure 2-2 Comparison of temperature, shapes and materials	23
Figure 2-3 Traditional manual measurement of large hot forgings[24]	31
Figure 2-4 Hardware setup for an image acquisition system[26]	32
Figure 2-5 Typical forging image, originally in colour [27].....	33
Figure 2-6 Thermocouple photographed at various temperature [28]	33
Figure 2-7 The low-cost 3D scanner developed at CNR, based on structured light and consumer electronic technology [28]	34
Figure 2-8 Working principle of TOF measurement technique[45].....	39
Figure 2-9 Setup for LaCam® Forge measuring system [15]	39
Figure 2-10 Scheme diagram of single-point scanning device for forged parts geometry [31]	40
Figure 2-11 Measurement principle diagram [31].....	40
Figure 2-12 Mechanism of dual PRRR measurement robot [37]	41
Figure 2-13 Measurement robot setup [37]	42
Figure 2-14 Key components and assembled configuration of the high-temperature measurement system [49].....	43
Figure 2-15 Basic principle of laser triangulation [45]	46
Figure 2-16 Experimental results for building model a) method of topological transformation, b) method of feature recognition[59].....	47
Figure 2-17 Photo of the CMS installed at the forging plant of Pietro Rosa TBM Srl [60].....	48
Figure 2-18 Differential Imaging Technique for High-Temperature Measurement [62].....	49
Figure 2-19 The measurement system[62]	50
Figure 3-1 The principle of fringe projection technique [77].....	62
Figure 3-2 GOM ATOS Scanner working principle [78]	63
Figure 3-3 3D scanning of heated part with GOM ATOS showing infrared glaring	69
Figure 3-4 Comparative analysis of diameter measurements between CMM and GOM ATOS systems	72
Figure 3-5 Diameter measurement error comparison of GOM ATOS and CMM at elevated temperature.....	73
Figure 3-6 Diameter measurement percentage error comparison of GOM ATOS and CMM at elevated temperature.....	74
Figure 3-7 Experiment setup; (a) Camera on tripod and hot workpiece, (b) Hot workpiece on ceramic bricks.....	78
Figure 3-8 Steel cylindrical part mild steel sample	78
Figure 3-9 Molten metal piece handling at a furnace.....	79
Figure 3-10 High-temperature sample image captured using Nikon D3100 with infrared filter and optimized settings.....	81
Figure 3-11 Block diagram illustrating the workflow of the proposed algorithm for high-temperature dimensional measurement	82
Figure 3-12 Camera calibration device[84].....	84

Figure 3-13 Camera calibration setup.....	86
Figure 3-14 Image thresholding at elevated temperature	89
Figure 3-15 Picture taken with Nikon D-3100 (I-R filter); a) aperture= F5.6, temperature=1100°C, b) aperture= F5, temperature=900°C c) aperture= F5.6 , temperature=850°C.....	90
Figure 3-16 A picture captured with I-R filter (monochrome).....	91
Figure 3-17 Threshold IR image	91
Figure 3-18 Image clarity at different temperatures with and without IR filter.....	93
Figure 3-19 Image segmentation process and results of image segmentation	97
Figure 3-20 Diameter measuring results of workpiece at elevated temperature	100
Figure 3-21 Length measuring results of workpiece at elevated temperature	100
Figure 4-1 Quality control setup during hot forging	107
Figure 4-2 Configuration of the system proposed for the measurement of symmetrical forgings....	110
Figure 4-3 Image distortion correction[95].....	111
Figure 4-4 Black background with workpiece shown by white pixels	114
Figure 4-5 Forged workpiece and background segmentation	115
Figure 4-6 Extraction of heated part geometry	116
Figure 4-7 Image processing for noise reduction; a) Raw image of heated sample with noise, b) Processed image through image segmentation	117
Figure 4-8 Interface for proposed dimensional measurement system	118
Figure 4-9 Proposed algorithm	119
Figure 4-10 Statistical analysis results of heated samples dimensional measurement at pixel level before forging	128
Figure 4-11 Descriptive analysis of heated samples dimensional measurement at pixel level during forging.....	136
Figure 5-1 Mixed pixel problem: original scene covered by a pixel grid (a), output image of the scene (b), results of increasing image resolution: 1—pixel intensity for original resolution, 2—pixel intensities for quintuple the image resolution (c)[93].....	139
Figure 5-2 The flow chart of our sub-pixel measurement algorithm[107].	140
Figure 5-3 Subpixel edge detection using curve fitting: input image (a), curve fitted into a properly detected edge (b), curve fitted into an edge with a badly defined edge pixel (c)[95].	141
Figure 5-4 Lyvers' edge model [21].....	142
Figure 5-5 Accuracy comparison of subpixel-level image processing algorithms	144
Figure 5-6 Processing time comparison of subpixel-level image processing algorithms	145
Figure 5-7 Aura surrounding the specimen	147
Figure 5-8 Descriptive analysis of heated samples at subpixel level before forging	156
Figure 5-9 Descriptive analysis of heated samples at subpixel level during hot forging	163
Figure 5-10 Comparison of proposed system for heated samples diameter at pixel and subpixel level	164
Figure 5-11 Comparison of proposed system for heated samples lengths measurement at pixel and subpixel level.....	165
Figure 5-12 Comparison of the proposed system for heated samples diameter measurement at the pixel and subpixel level.....	166

Tables

Table 2-1 Approximate values of dimensional accuracies achievable in various manufacturing process [5].	19
Table 2-2 Values of standard tolerance grades for nominal sizes up to 3 - 3150mm[15].	22
Table 2-3 Comparison of common forging process characteristics [3]	25
Table 2-4 Advantages and disadvantages of cold, warm and hot forging [18]	27
Table 2-5 Examples of warm forgeable steels [19].	29
Table 2-6 Forging temperature (preheat) ranges of stainless steels [11]	30
Table 2-7 Comparison of the actual application of TOF	45
Table 2-8 Comparing measuring quality of laser triangulation.	51
Table 3-1 GOM ATOS technical data sheet [76]	61
Table 3-2 Paired sample test scores between measurements of sample diameters through GOM ATOS and CMM in repetitions	66
Table 3-3 Reliability statistics.	67
Table 3-4 Summary of dimensional measurement results and statistical analysis.	72
Table 3-5 Threshold levels for image segmentation.	88
Table 4-1 Diameter measurements of heated samples before forging (pPixel level)	121
Table 4-2 Diameter measurements of heated samples before forging (pixel level)	122
Table 4-3 Paired sample test scores between diameter measurements of heated samples before forging through (pixels) proposed system and GOM ATOS in repetitions	123
Table 4-4 Reliability statistics.	124
Table 4-5 Length measurements of heated samples before forging (pixel level)	124
Table 4-6 Length measurements of heated samples before forging (pixel level)	125
Table 4-7 Paired sample test scores between length measurements of heated samples before forging through (pixels) proposed system and the GOM ATOS in repetitions	127
Table 4-8 Reliability statistics.	127
Table 4-9 Diameter measurements of heated samples during forging (pixel level)	129
Table 4-10 Diameter measurements of heated samples during forging (pixel level).	130
Table 4-11 Paired sample test scores between diameter measurements of heated samples during forging through (pixels) proposed system and GOM ATOS in repetitions	131
Table 4-12 Reliability statistics.	131
Table 4-13 Length measurements of heated samples during forging (pixel level)	132
Table 4-14 Length measurements of heated samples during forging (pixel level)	133
Table 4-15 Paired sample test scores between length measurements of heated samples before forging through (pixels) proposed system and GOM ATOS in repetitions	134
Table 4-16 Reliability statistics.	135
Table 5-1 Diameter measurements of first eight heated samples before forging	149
Table 5-2 Diameter measurements of remaining eight heated samples before forging	150
Table 5-3 .Paired sample test scores between diameter measurements of heated samples before forging through (sub-pixels) proposed system and GOM ATOS in repetitions	151
Table 5-4 Reliability statistics.	152
Table 5-5 Length measurements of first eight heated samples before forging	152
Table 5-6 Length measurements of last eight heated samples before forging	153
Table 5-7 Paired sample test scores between length measurements of heated samples before forging through (sub-pixels) proposed system and GOM ATOS in repetitions.	154

Table 5-8 Reliability statistics.....	155
Table 5-9 Diameter measurements of first eight heated samples after forging	156
Table 5-10 Diameter measurements of remaining eight heated samples after forging	157
Table 5-11 Paired sample test scores between diameter measurements of heated samples after forging through (sub-pixels) proposed system and GOM ATOS in repetitions	158
Table 5-12 Reliability statistics.....	159
Table 5-13 Length measurements of first eight heated samples after forging	159
Table 5-14 Length measurements of remaining eight heated samples after forging	160
Table 5-15 Paired sample test scores between length measurements of heated samples after forging through (sub-pixels) proposed system and GOM ATOS in repetitions.....	161
Table 5-16 Reliability statistics.....	163

1 Introduction

1.0 Background

It has been 7000 years since metal forming technology was in the world, counting from when the first ornaments and tools were carved by blacksmiths and armourer until to date with mass production in rolling mills and presses [1]. This progress, which has been aided by simultaneous advances in the science of plasticity [2] and the knowledge and prediction of product attributes such as part geometry [3], has resulted in enormous global benefit. The global industrial system today generates 200 kg of steel [4] and 7 kg of aluminium [5] per person per year and transforms them into universally recognised buildings, vehicles, equipment and finished commodities [6] at a relatively low price. The qualities of metal components, unlike ceramic or composite materials, are a result of both their composition and the history of the thermo-mechanical processing employed to convert the raw materials into its final form [3]. The technological advancements that led to today's production have made it possible to quickly and precisely apply deformation and temperature change for metal workpieces [7].

The more accurate control of material composition, temperature history, and geometry has eliminated variability and increased the pace of manufacturing of highly specified components. Metal forming tolerances have decreased over the years, becoming more sensitive to minor uncertainties like contact surfaces, post-processing, as-cast microstructures that are beyond the grasp of even the most advanced production processes are in control now [8] .

Metal forming inaccuracies degrade product quality, necessitating additional downstream manufacturing, which raises costs and reduces efficiency. This is especially relevant in small batch runs, which have the highest levels of uncertainty and where the cost of correcting for such uncertainties cannot be spread out over a long production cycle [9]. Furthermore, as the science of predicting product property advances with the expansion in the spectrum of actuation and sensing for metal forming, there is an increased opportunity for adding more value to metal forming, allowing the tailoring of more accurate product features [3]. Metal forming methods can now seek to produce other specified product qualities such as

component geometry. On the other hand, unexpected processing pauses can cause the final shape of workpieces to deviate from their expected state, especially for forming processes that operate above ambient temperature, such as hot forming.

Dimensional measurement is crucial in metal-forming processes because it ensures that the metal components have the required tolerances and specifications. Any minor dimensional variation in the manufacturing process can affect the accuracy and precision of the final product. Dimensional measurement can help to detect any deviation early in the process so that corrective measures can be taken and the final product can be ensured to have the desired quality level. Additionally, dimensional measurement provides valuable data for process control and optimization, enabling manufacturers to continuously improve their metal forming processes and produce higher quality products. Several distinct techniques for on-line monitoring of the metal forming process have been studied based on information from characteristic signals of the process. These studies have shown that it is difficult to use process monitoring and control systems accurately and reliably to detect process faults and component defects during the production process.

1.1 Problem statement

Obtaining accurate dimensional measurement in high-temperature metal forming processes, e.g., hot forging, continues to be one of the big challenges in today's manufacturing practice. The intersection of thermal expansion, deformation behaviour, and post-process shrinkage creates measurement uncertainties that directly affect product quality, material utilization and consistency of the process. Conventional post-process inspection equipment, such as CMMs and callipers require workpieces to be permitted to cool prior to being measured, thereby inducing delays, increased scrap rates, and defect detection inefficiencies. While state-of-the-art optical measuring systems, like the GOM ATOS, achieve high-precision 3D scanning, they are not suited for continuous, real-time monitoring in the high-temperature forging process environment. This research discusses the critical requirement of non-contact measurement systems that function efficiently in harsh thermal conditions and provide real-time information with the aim of process optimization.

1.1.1 Key challenges

1. Limitations of Post-Process Measurement Methods

- Conventional measurement techniques consist of cooling the workpiece before inspection, which prevents manufacturers from implementing real-time process adjustments.
- Defect detection time lags cause additional material waste, rework, and added production cost.

2. Inadequacies of Current In-Process Optical Measurement Systems

- Hot environments create difficulties such as heat-caused distortions, glare, and material reflectivity, which compromise the accuracy of conventional optical measurement systems.
- Industrial optical systems like the GOM ATOS, although highly accurate, are costly and not suited for real-time dimensional monitoring of forging operations.

3. Impact on Process Efficiency and Industry 4.0 Integration

- Inefficiencies in the process and lack of consistency in quality are caused by the lack of a real-time feedback system.
- As manufacturing moves towards Industry 4.0 and smart manufacturing, there is a growing need for automated, in-line measurement technology that is integrated with digital manufacturing platforms for data-driven process control.

Based on discussion, the present study investigates the capabilities and limitations of contact-based and non-contact-based inspection methods for real time dimensional measurements at elevated temperatures. The main goal is to study and evaluate how effective these techniques are in detecting real-time shape dimensional accuracy. Moreover, identification of faults and defects of the part surface is also required, which can be accomplished using cost-effective non-contact-based part inspection techniques. This study will employ the system based on these techniques for improving the part quality through in-process dimensional measurements of metal components during the forming process at elevated temperatures.

1.2 Research aim and objectives

The overall aim of this research is to create a real-time, non-contact dimensional measurement system specifically for high-temperature metal forming processes, with a focus on hot forging. In this research, the problem of constraints faced by conventional post-process and in-process measurement methodologies is tackled by using the latest optical measurement methods, image processing techniques and intelligent manufacturing principles, thereby enabling accurate and reliable dimensional measurement in adverse thermal conditions. The research objectives are outlined below.

1. **To assess the shortcomings of existing dimensional measurement techniques in high-temperature forging**
 - Conduct a comprehensive review of relevant literature for conventional and emerging measurement techniques used in hot forging, including contact-based techniques (CMM, callipers) and optical systems (GOM ATOS, laser scanning, fringe projection techniques).
 - Identify the key problems associated with high-temperature dimensional measurements, including thermal distortions, measurement deviation, and process inefficiencies.
 - Establish the scientific and industrial need for a measurement solution carried out among processes that enhances accuracy, repeatability and the potential for real-time process control.

2. **To develop a novel real-time dimensional measurement system specifically applied to hot forging processes.**
 - Suggest a non-contact method of measurement incorporating photogrammetry and machine vision algorithms to enable accurate dimensional assessment of forged parts.
 - Develop adaptive image processing algorithms that excel at reducing thermal distortions, glare caused by heat, and material reflectivity variations.
 - Establish a rigorous non-contact dimensional measurement system to ensure high precision and traceability of measurements in real-time industrial conditions.

3. **To empirically validate the accuracy, repeatability and robustness of the proposed measurement system.**
 - Conduct a set of experiments in hot forgings to verify the dimensional measurement accuracy of the system at the pixel and sub-pixel level.
 - Evaluate the efficiency of the suggested system compared to the GOM ATOS and traditional measurement methods by investigating parameters such as dimensional measurement errors, percentage of errors, and statistical confidence levels.

4. **To conduct statistical analysis and determine the reliability of the suggested system for application in industrial environments.**
 - Apply statistical validation techniques, such as paired sample tests, confidence interval tests and correlation tests, to verify the repeatability and reliability of the system.
 - Examine the ability of the system to detect dimensional variations in the course of repetitive forging operations with consistency.
 - Establish the measurement accuracy of the suggested system and include a comparative analysis with standard commercial systems.

1.3 Thesis organization

This thesis is organized in a systematic way to introduce a thorough analysis of a real-time, non-contact dimensional measuring system for high-temperature metal forming processes, here hot forging. The research is characterized by a sequential process comprising problem definition, review of existing measurement methods, presentation of an innovative solution, empirical validation and discussion, embedding in the Industry 4.0 concept. Every chapter is designed to contribute to the overall research objective by laying down a strong basis, a common approach, and an in-depth examination of the experimental outcomes. The six chapters comprising this thesis are as follows.

Chapter 1: Introduction

This chapter describes the research motivation, with an emphasis on difficulties involved in dimensional accuracy in hot forging and the limitations of current measuring techniques.

Chapter 2: Literature review

This chapter provides a comprehensive review of existing dimensional measuring techniques, appraising contact and non-contact against the backdrop of real-time dimensional measurements of metal parts and integration into Industry 4.0. Additionally, state-of-the-art optical techniques such as laser scanning, structured light projection, photogrammetry and the GOM ATOS systems are analysed.

Chapter 3: Proposed methodology and preliminary studies

This chapter presents the scientific principles, system design, and empirical validation of the proposed real-time, non-contact dimensional measurement system for high-temperature forging operations.

Chapter 4: Photogrammetry system evaluation

This chapter gives a comprehensive comparative analysis of the suggested real-time dimensional measurement system in the context of its accuracy and precision compared to accepted reference technologies like the GOM ATOS.

Chapter 5: Enhancement of measurement precision using sub-pixel analysis

This chapter presents a comparative analysis of the proposed system with current industrial measurement technology, its merits, demerits and areas of possible improvement such as coping with aura affecting measurement accuracy due to the heated profile of metal parts.

Chapter 6: Conclusion and future research

The concluding chapter synthesizes the primary research findings, recapitulating how the research has responded to the problem statement and research objectives as well as the technical difficulties of real-time dimensional measurement in hot forging. It underscores the scientific breakthroughs in high-temperature optical metrology and the ensuing practical implications for manufacturing industries.

2 Literature review

2.0 Introduction

Manufacturing processes can be broadly classified into five major groups: primary shaping, metal forming, metal cutting, metal treatment and joining. Metal forming processes are forging, stamping and bending, which result in parts having superior mechanical properties with little material waste. Consequently, it is a vital technique in key industries such as automotive, aerospace, and nuclear power, where strength, precision and consistency are needed [10].

This chapter reviews the literature with respect to the methodologies of metal forming, especially forging, as a basic manufacturing process in producing high-strength components. Different forging techniques based on die and part temperature play an essential role in the production of components that have to meet a set of strict requirements, both in mechanical and dimensional terms [11]. The increasing demands to continually push the boundaries of material efficiency and accuracy have called for an ability to measure and control forged element dimensions in real-time. The literature reviewed gives an insight into some of the state-of-the-art techniques and technologies for dimensional assessment in forging, from conventional methods like laser triangulation to advanced ones such as Time-of-flight.

2.1 Quality control in the forging process

The forming processes are indispensable to industries like automotive, aerospace, nuclear and others because there is a need for parts that possess improved strength with reliable mechanical properties. Table 2.1 depicts the dimensional accuracies achievable by some forming processes to ISO quality scale [7].

Table 2.1 presents a comparative view of the dimensional accuracies achievable across various manufacturing processes, with a focus on forging. The table references the ISO 286-1:1998 standard, which defines the ISO quality scale through International Tolerance (IT) grades ranging from IT1 (the most precise) to IT18 (the least precise). The ISO quality level defines a standard basis for the classification and evaluation of tolerances inherent in manufacturing operations. In the field of metal forming, the forging process is typically

allocated tolerances rated IT14, which refers to a relatively wide band of dimensional accuracy. Such a level of accuracy is suitable for applications where the qualities of mechanical strength and durability are of greater importance than precise dimensional accuracy. In contrast, processes of higher accuracy, like cold forging or machining, can achieve IT grades from IT7 to IT10, reflecting finer tolerances. The ISO quality scale is a valuable tool for engineers to choose manufacturing processes that meet specific application needs. For example, parts that require high precision may need additional finishing operations after forging or other production processes. Through a consistent grading of tolerances, the ISO quality scale optimizes production planning, essentially balancing cost, precision, and performance to meet industrial needs [12].

Table 2-1 Approximate values of dimensional accuracies achievable in various manufacturing process [5].

ISO quality \ Process	5	6	7	8	9	10	11	12	13	14	15	16
Die forging					-----	-----						
Precision die forging		-----	-----	-----								
Cold extrusion		-----	-----	-----	-----	-----						
Rolling (thickness)			-----	-----	-----	-----						
Finish rolling (thickness)	-----	-----	-----	-----								
Finish coining (thickness)			-----	-----	-----	-----						
Deep drawing						-----	-----	-----				
Ironing	-----	-----	-----	-----	-----	-----						
Tube and wire drawing					-----	-----	-----					
Shearing/blanking				-----	-----	-----	-----	-----	-----			
Fine blanking	-----	-----	-----	-----	-----	-----						
Turning			-----	-----	-----	-----						
Cylindrical grinding	-----	-----	-----	-----								

Figure 2.1 demonstrates the relationship between process tolerances and dimension sizes of different manufacturing processes, hence giving valuable insights into the general trend where larger dimension sizes correlate with wider allowable tolerances. The trend best works in large-scale processes, i.e., those involving inherent factors of material deformity and heat expansion, affecting dimension accuracy. Processes defined as large-scale, including

processes of hot forging, mostly register wider tolerances, in accordance with their classification under coarse ISO grades, i.e., IT14, defined under ISO 286-1. Processes including precise machining and cold forging achieve higher accuracy when it comes to tolerances, hence being applicable for smaller dimensioned components with more complex dimension requirements.

While the graph successfully portrays these trends, it lacks contextual data; for example, it fails to consider variations according to material types or effects of process parameters like tool wear or die degradation. Additionally, the lack of error bars or confidence intervals reduces its ability to convey the variability or uncertainties that are inherent to various manufacturing configurations. Finally, the representation fails to differentiate between different forging methods (e.g., hot, warm, or cold forging) and fails to include developments like precision forging, which can potentially enhance tolerances for specific geometries.

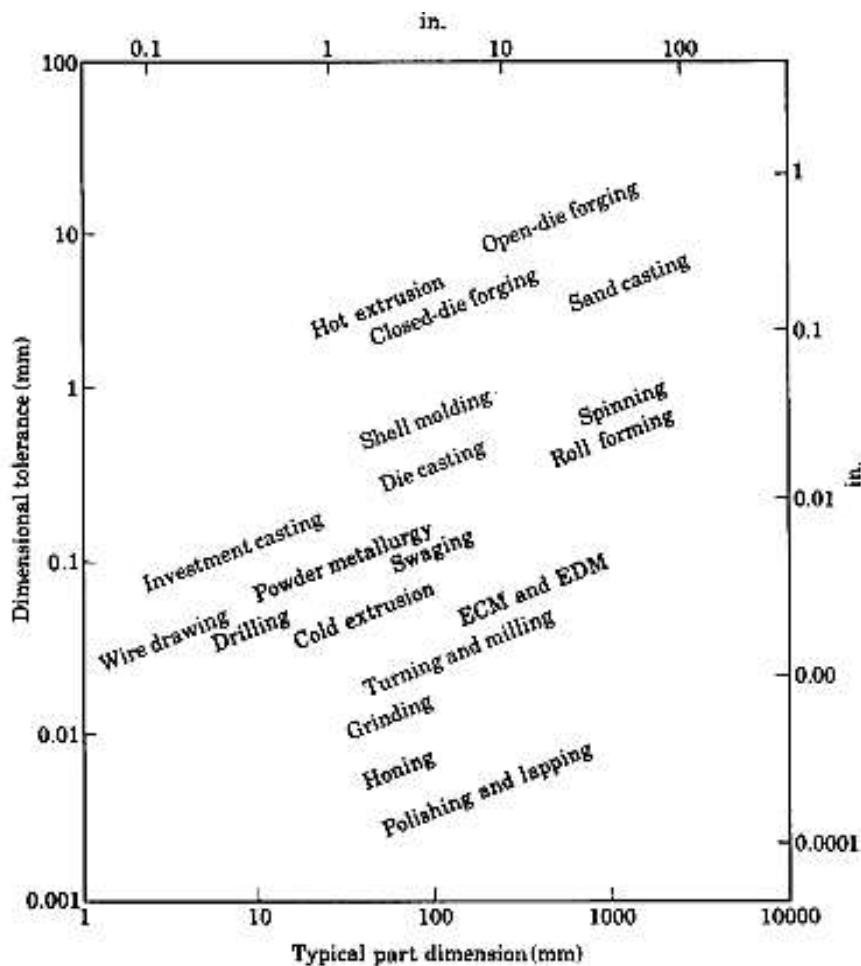


Figure 2-1 Process tolerance vs. feature size [13]

While useful, the figure's simplicity runs the risk of oversimplifying the tolerance-size relationship by ignoring the impact of complex geometries and modern process advances, such as sophisticated metrology equipment and process control methods that could stretch the boundaries of traditional manufacturing limitations. This attribute is particularly important in industries like aerospace and automotive, where tight dimensional tolerances require sophisticated manufacturing processes [14].

Table 2.2 presents standard tolerance grades as defined by ISO 286-1 for workpiece sizes ranging from 3 mm to 3150 mm, serving as a critical reference for determining dimensional tolerances in different manufacturing processes, and particularly hot forging. The table highlights the typical tolerance grades achievable, often falling within IT14 or similar ranges for hot-forged components. This reflects the relatively coarse tolerances inherent to the process, which result from the high temperatures (900°C to 1200°C for steels) and material flow dynamics during forging. For example, for a nominal size of 100 mm, the IT14 tolerance grade permits a total deviation of 0.87 mm, equating to ± 0.435 mm around the nominal size. These tolerances are designed to accommodate the natural variability in hot forging due to factors such as thermal expansion, material flow inconsistencies, and die wear [15].

High temperatures introduce challenges such as thermal radiations and material deformation, which can lead to dimensional inaccuracies during parts manufacturing. The table 2.2 emphasizes the importance of precise dimensional measurement to minimize these deviations. For instance, ensuring consistent forging temperatures and proper die alignment is critical to maintaining tolerances within acceptable range. However, even with careful control, the intrinsic characteristics of hot forging often necessitate additional finishing operations, such as machining, to achieve tighter tolerances.

Table 2-2 Values of standard tolerance grades for nominal sizes up to 3 - 3150mm[15].

Nominal size mm		Standard tolerance grades																			
		IT01	IT0	IT1	IT2	IT3	IT4	IT5	IT6	IT7	IT8	IT9	IT10	IT11	IT12	IT13	IT14	IT15	IT16	IT17	IT18
Above	Up to and including	Standard tolerance values																			
		μm												mm							
—	3	0,3	0,5	0,8	1,2	2	3	4	6	10	14	25	40	60	0,1	0,14	0,25	0,4	0,6	1	1,4
3	6	0,4	0,6	1	1,5	2,5	4	5	8	12	18	30	48	75	0,12	0,18	0,3	0,48	0,75	1,2	1,8
6	10	0,4	0,6	1	1,5	2,5	4	6	9	15	22	36	58	90	0,15	0,22	0,36	0,58	0,9	1,5	2,2
10	18	0,5	0,8	1,2	2	3	5	8	11	18	27	43	70	110	0,18	0,27	0,43	0,7	1,1	1,8	2,7
18	30	0,6	1	1,5	2,5	4	6	9	13	21	33	52	84	130	0,21	0,33	0,52	0,84	1,3	2,1	3,3
30	50	0,6	1	1,5	2,5	4	7	11	16	25	39	62	100	160	0,25	0,39	0,62	1	1,6	2,5	3,9
50	80	0,8	1,2	2	3	5	8	13	19	30	46	74	120	190	0,3	0,46	0,74	1,2	1,9	3	4,6
80	120	1	1,5	2,5	4	6	10	15	22	35	54	87	140	220	0,35	0,54	0,87	1,4	2,2	3,5	5,4
120	180	1,2	2	3,5	5	8	12	18	25	40	63	100	160	250	0,4	0,63	1	1,6	2,5	4	6,3
180	250	2	3	4,5	7	10	14	20	29	46	72	115	185	290	0,46	0,72	1,15	1,85	2,9	4,6	7,2
250	315	2,5	4	6	8	12	16	23	32	52	81	130	210	320	0,52	0,81	1,3	2,1	3,2	5,2	8,1
315	400	3	5	7	9	13	18	25	36	57	89	140	230	360	0,57	0,89	1,4	2,3	3,6	5,7	8,9
400	500	4	6	8	10	15	20	27	40	63	97	155	250	400	0,63	0,97	1,55	2,5	4	6,3	9,7
500	630			9	11	16	22	32	44	70	110	175	280	440	0,7	1,1	1,75	2,8	4,4	7	11
630	800			10	13	18	25	36	50	80	125	200	320	500	0,8	1,25	2	3,2	5	8	12,5
800	1 000			11	15	21	28	40	56	90	140	230	360	560	0,9	1,4	2,3	3,6	5,6	9	14
1 000	1 250			13	18	24	33	47	66	105	165	260	420	660	1,05	1,65	2,6	4,2	6,6	10,5	16,5
1 250	1 600			15	21	29	39	55	78	125	195	310	500	780	1,25	1,95	3,1	5	7,8	12,5	19,5
1 600	2 000			18	25	35	46	65	92	150	230	370	600	920	1,5	2,3	3,7	6	9,2	15	23
2 000	2 500			22	30	41	55	78	110	175	280	440	700	1 100	1,75	2,8	4,4	7	11	17,5	28
2 500	3 150			26	36	50	68	96	135	210	330	540	860	1 350	2,1	3,3	5,4	8,6	13,5	21	33

The table also serves as a practical guide for engineers during the design and manufacturing phases. By analysing the tolerance grade applicable to a specific nominal size, engineers can determine whether the hot forging process alone can meet the dimensional requirements or if supplementary processes are required. This is particularly relevant for components with

strict dimensional specifications, where additional machining may be necessary to refine tolerances beyond the standard allowances for hot forging.

The relatively high tolerances of hot forging are intended to ensure cost-effectiveness, since tighter tolerances would require drastically higher production costs and an increased level of process complexity. This balance makes hot forging an attractive choice for the production of high-strength parts, where mechanical performance is more important than precise dimensional accuracy.

In conclusion, Table 2.2 provides valuable information to understand the realistic tolerances achievable in hot forging, helping to set practical expectations for dimensional measurement accuracy. It highlights the importance of tolerance grades, such as IT14, for balancing functional requirements, process limitations, and cost-effectiveness. By leveraging this understanding, engineers can design and manufacture high-performance hot-forged parts, incorporating appropriate finishing processes when necessary to meet stringent dimensional specifications.

The temperature classifications—cold, warm, and hot—for steel forging are shown in Figure 2.2 [16].

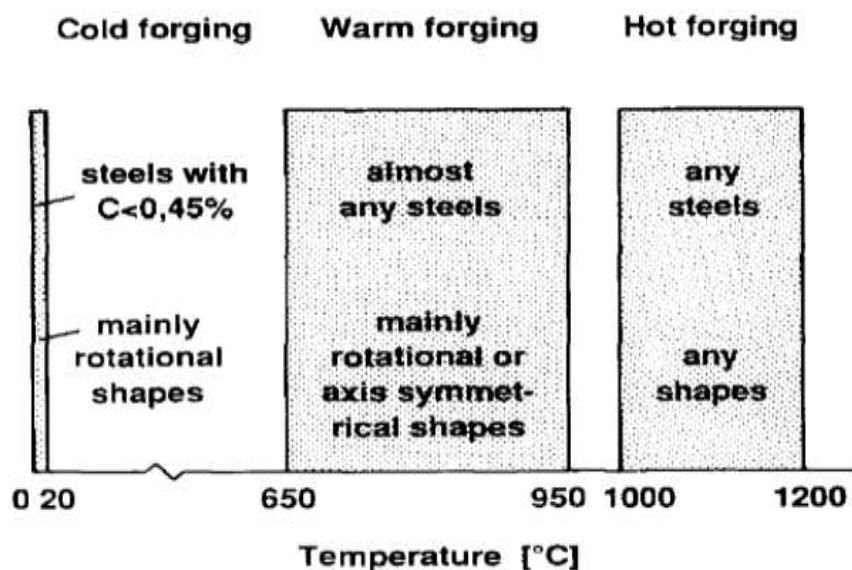


Figure 2-2 Comparison of temperature, shapes and materials between cold, warm and hot forging [16]

Table 2.3 summarises the essential concepts, requirements, and results of the hot, cold, and warm forging processes. It should be noted that the values shown are merely guidelines displaying different tendencies; therefore, they should not be considered absolute statements. Considering the technical and economic aspects of all three strategies (cold, warm, and hot forging), their goals are described as follows:

1. Hot forging can produce components of varying complexities, such as shafts, gears, turbine blades and connecting rods. Typical part sizes can range from a few millimetres to several metres, with part weights from a few grams to over 500 kilograms, depending on the capacity of the forging equipment. For hot forging, dimensional tolerances are generally classified around IT13 to IT16 under the ISO 286-1 standard, depending on part size and forging conditions. For instance, a 100 mm nominal size part forged under IT14 would have a total tolerance of 0.87 mm, as discussed earlier, translating to ± 0.435 mm.
2. The cold forging process is only suitable for lower alloy steel grades and simple and more compact geometries with outstanding and accurate surface quality. In these cases development costs are often high. Thus, there must be sufficient total lifetime production volume per component to amortise the tool's costs.
3. Of the three, warm forging is the most difficult technique, yet it combines the benefits of both hot (excellent formability with tight tolerance) and cold forging (outstanding surface characteristics), thus making it a very promising technology. However, the development cost of its die set is much higher than that of a cold or hot forging die set. The goal of warm forging is to manufacture high-volume precision parts from steel grades that cannot be cold forged.

To identify typical examples of pieces with their geometric requirements and tolerances in the context of hot forming, it is enlightening to study typical examples in industries such as automotive and aerospace. A typical example of such a piece is a gear made from automotive forgings, with a typical nominal dimension of 150 mm and a shape with its circumference covered with teeth. The typical material for this piece is high-carbon steel, with examples being AISI 4140. The related grade of tolerance for this piece generally classifies under IT14,

with a complete tolerance of 1.3 mm (allowable deviation of ± 0.65 mm). In addition, the roundness of the piece is generally kept under 0.2 mm limit for assuring the gear's functioning.

A further example refers to a forged connecting rod made of alloy steel, with typical measurements of 50 mm width and 200 mm in terms of overall length. The alloy steel, such as AISI 4340, has a typical flat rating of IT13, and this defines the overall tolerance of 0.6 mm (within the range of ± 0.3 mm). The flat measurement of the I-beam shape stands at 0.3 mm for its flat sides, and this becomes a decisive factor for its performance quality in engine processes.

Table 2-3 Comparison of common forging process characteristics [3]

Characteristic	Hot Forging (Die Forging)	Warm Forging	Cold Forging (Extrusion)
Shape spectrum	Arbitrary	Rotationally symmetrical if possible	Mainly rotationally symmetrical
Use steel quality	Arbitrary	Arbitrary	Low alloyed steels C<0.45%
Economic lot size	>500 parts	>10,000 parts	>30,000 parts
Initial treatment of billets and slugs	Generally none	Generally none or a graphite layer	Annealing/phosphating
Intermediate treatment	None	Generally none	Annealing/phosphating
Tool materials	Hot work tool steels	Hot work tool steels, high speed steels, hard metals	Cold work tool steels, high speed steels, hard metals
Typical tool life	5,000 – 10,000 parts	10,000 – 20,000 parts	20,000 – 50,000 parts
Material utilization	60-80%	Approximately 85%	85-90%
Energy required per Kg gross of forging.	460-490J	400-420J	400-420J

Within the aerospace industry, a forged shaft with a nominal length of 250 mm and a diameter of 100 mm is often made from titanium alloys like Ti-6Al-4V. The general classification of this standard for tolerance is commonly identified as IT12, with general tolerance of 0.5 mm

(which has a range of ± 0.25 mm). In addition, straightness tolerance generally has a limit of 0.2 mm on the axis of the shaft, and finishing requirements for keyway and bearing faces are generally defined with a roughness average (Ra) of ≤ 1.6 μm for optimal performance. A forged aircraft turbine blade, commonly made from a high-performance alloy, i.e., Inconel 718, commonly has a 500-mm nominal dimension and maximum width of 200 mm. The thin and complex curved sections of aircraft turbine blades commonly are assigned a grade of IT15, with maximum allowance of 1.0 mm (which has a range of ± 0.5 mm). Since the critical finishing of the surface must be achieved, requirements may call for a roughness average (Ra) of ≤ 2.5 μm for maximum aerodynamics, and allowable curve deformations are limited to a maximum of 0.3 mm. The above examples present typical geometric specifications and tolerances for use with commonly employed hot-formed pieces of different industries. Hot forming processes result in higher material and strength properties, but they commonly leave wider tolerances compared with other precise forming processes, with more finishing processes being necessary for achieving more stringent specifications [17].

The selection of the most suitable manufacturing technique can be adopted by making a criterion for component geometry, the quantity of material manufacturing and the precision of parts. The industry uses warm forging and cold forging techniques to achieve better dimensional tolerances [18].

Table 2-4 Advantages and disadvantages of cold, warm and hot forging [18]

COLD	WARM	HOT
<u>Advantages</u>	<u>Advantages</u>	<u>Advantages</u>
Precision Process (Tight Tolerances)	Combines Advantages of cold & hot forging	Can forge complex shapes
Improved part strength	Better formability	Good formability
Better surface finish	Lower forming pressures	Lowest forming pressures
Material conservation	Higher deformation ratio	Can forge parts of higher weight & volume
	No annealing required	
<u>Disadvantages</u>	<u>Disadvantages</u>	<u>Disadvantages</u>
High forming pressures	High tooling costs	Formation of scale
Several pre-forming steps needed	Tooling must withstand forming pressures as well as high temperatures	Decreased accuracy (Larger tolerances)
Annealing steps may be required during process		
Low formability		

Cold forging, warm forging, and hot forging all share different advantages and drawbacks, mainly related to dimension accuracy, material flow behavior, and overall process efficiency. Cold forging stands out for its ability to attain very precise dimensions, generally between the range of IT7 and IT10, with possible tolerances of up to ± 0.1 mm for small pieces. Also, this process yields pieces with very smooth surface finishes, with dimension variations generally not more than 0.05 mm, and hence this process is best for use where precision and quality of the surface are of paramount importance. Another advantage of this process is its low heat demand, which leads to savings of energy and reduces waste of material. Also, cold forging has very high rates of output, from 30 up to 120 individual pieces per minute, depending on the size of the piece and on the capacity of the press being used. There are, however, some drawbacks. Its use for ductile materials, for example, such as for use with mild steels, and for larger pieces is limited. The problem of forming pieces larger than 100 mm in dimension is

compounded by material flow stress, and tooling for the process of cold forming can be very expensive, mainly for complex geometric pieces (Table 2.4).

Warm forging is a process that harmoniously unites the flow properties of the material with techniques of cold forging. The process works between 650°C and 950°C, with the result being enhanced ductility of the material and low probability of cracking and failure of the material when undergoing deformation. The process works for moderately complex forms and can achieve tolerances between IT12 and IT14 with variations between ± 0.5 mm and ± 1.0 mm, depending on complexity and the dimension of the part. Though more precise and ductile compared to hot forming, the process of warm forging does not yield stringent tolerances commonly linked with processes of cold forming. A major limitation of this process of warm forging is its higher cost of production; the need for heating of the material and precise temperature control are contributory factors for its complexity and higher economic significance.

In contrast, the hot forging process best suits the manufacturing of larger parts with a wide range of material usage, such as with high-strength steels and alloyed materials not applicable for use with cold and warm forging methods. Hot forging can accommodate pieces with diameters larger than 100 mm and weighing up to several hundreds of kilograms. Hot forging generally occurs between 900°C and 1200°C, enabling greater material flow and more precise and controlled deformations of heavy pieces. The technique, however, loses accuracy. The normal tolerances of pieces made from hot forming range from IT14 up to IT16, with overall larger pieces' tolerances, such as pieces with a 300 mm diameter, from ± 1.0 up to ± 2.0 mm. The quality of the finishing of pieces made from hot forming also has a relatively coarse surface when compared with pieces made from cold forming, with measurement deviations of around ± 1.5 mm, and may need additional finishing processes for smoother finishing [19].

Hot forging is an acceptable method for various metal alloys, including multiple grades of steel and other non-ferrous metal alloys. To apply hot forging, it is recommended that the metal be used in the as-received hot rolled or drawn condition at temperatures of 900 °C or above. If a lower processing temperature is necessary, annealing is often employed as an advantageous heat treatment to enhance material properties and facilitate subsequent forming or machining operations. In contrast, the working temperature is different for

different steel classes, which helps in selecting the method of forging [11]. Sheliaskov classified hot-forging workpiece steels into unalloyed, low-alloy cementation, superficial hardening, heat-treatable, ball-bearing and stainless [20]. Some examples of these materials are given in Table 2.5.

Table 2-5 Examples of warm forgeable steels [19]

Cementation Steels	Ck10(AISI1010), Ck15(AISI1015), 15CrNi6(AISI4320), 16MnCr5(AISI 5117), 20MnCr5(AISI 5120)
Heat-treatable Steels	Ck35(AISI 1035), Ck45(AISI 1045), Ck60(AISI1060), 34Cr4(AISI 5132), 34CrMo4(AISI 4137), 42CrMo4 (AISI 4140), 50CrV4(AISI6150).
Superficial hardening steels	Cf53 (AISI 1053)
Ball-bearing steels	100Cr6 (AISI E52100).
Stainless steels (General)	X5CrNi189(AISI 304L), X10CrNiMo 17 12 (AISI 316)
a) Austenitic	Cr18Ni9Ti
b) Martensitic	2Cr13, 4Cr13 and Cr17Ni2
c) Precipitation Hardening	Cr12Mn5Ni4Mo3Al

2.2 Forging temperature range

Hot forging is usually performed on metals because it allows easier material deformation and smoother flow. After hot forging, the material must be protected from moisture or cold air, which means a uniform cooling process is required; the cooling process depends on the finishing temperature—that is, the temperature of the metal after hot forging [7].

The steel class determines the temperature, which can influence their use in the forging process. The billet is used at room temperature in cold forging, but the material is heated to a temperature below the material's recrystallization temperature in hot forging. Different types of steel need different temperatures for the forging process. The types of steel and their required temperature are as follows and shown in Table 2.6.

- Carbon Steels: This steel type needs a forging temperature above 600°C to significantly reduce flow stress; below this temperature, from 200°C to 550°C, the steel could become brittle.

- Alloy Steel: This type of steel can be hot forged at elevated temperature because the flow stress decreases with an increase in temperature, which means that temperature increase has a reciprocal relation with the flow stress of the steel.
- Austenitic Stainless Steel: This type of steel frequently requires a forging temperature of 200°C to 300°C because its flow stress decreases dramatically with a small increase in temperature, though it may strain harden. On hot forging at 900°C to 1200°C, it is not susceptible to intergranular corrosion.

Table 2-6 Forging temperature (preheat) ranges of stainless steels [11]

STAINLESS STEEL TYPE	PREHEAT TEMPERATURE
Cr18Ni9Ti (Austenitic Stainless Steel)	Lower – 200°-3 00°C Higher - 500°-800°C
2Cr13, 4Cr13 and Cr17Ni2 (Martensitic Stainless Steel)	650°- 800°C
Cr12Mn5Ni4Mo3Al (Precipitation Hardening Stainless Steel)	650°-800°C

In general, the temperature range for warm forging (650°C to 950°C) is lower than the hot forging temperature range, i.e. 1000°C to 1200°C [20].

Many variables are involved in the forging process, but the most complex and essential one is the workpiece temperature; hence, it should be carefully monitored where the heating device exists [21].

There are two types of forging: open die and close die. Open die forging is used for simple asymmetric shapes, but for relatively complex shapes like shafts, turbine blades and gears, close die forging is used. For measurement accuracy, open die forging is measured when it is still hot, as the product forged through the open die has large dimensions and has low geometry measurement accuracy at elevated temperatures through basic measuring instruments like callipers. For measuring lengths of large ingots (i.e., many tonnes) while they are hot, the manipulator operator uses a measuring rod with chalk marks at the desired dimensions held in front of the ingot [22].

This method is used when large ingots are required for cutting or forming shoulders [23]. It is a comparative measurement method; hence its precision is restricted. Moreover, while handling the measuring tools, the operator is exposed to the enormous heat of the ingot, as shown in Figure 2.3, but there is limited research on automating dimensional measurement

in high-temperature conditions for open-die forging, highlighting a significant gap in this area[24].

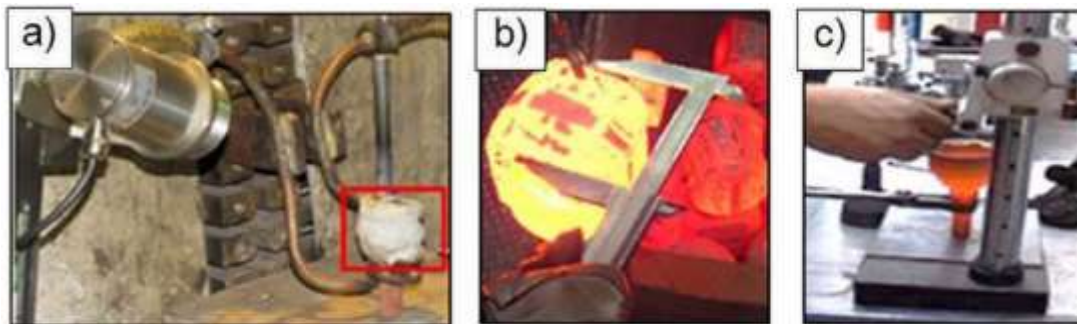


Figure 2-3 Traditional manual measurement of large hot forgings[24]

2.3 Advancements and challenges in vision-based hot forging measurement

It is important to note that automation of contact-based measurements of open die forgings has received little attention. A measurement system described by Siemer et al. [25] consisted of a spring-loaded cable attached to the forging's end. The cable position was measured as the forging was moved back and forth through the press. While effective for obtaining data in a laboratory experiment, the need to link a cable to the forging and the risk of this cable interfering with other process equipment limit the system's applicability. Another contact-based measurement system [22] used the fact that the ingot 'elongates' (i.e., grows in length). At the same time, it is forged, and the manipulator must deflect proportionally to accommodate this elongation. This deflection was monitored in real-time and used to determine elongation by instrumenting the manipulator. This technique was demonstrated to help evaluate some workpiece parameters during forging, but it could not estimate the ingot's overall dimensions. Vision systems have been successfully employed in various sectors of forging to measure the realm of open-die forging. However, the use of vision systems has some limitations, and there are several challenges to overcome, which include creating equipment that can resist the severe environment of the forging process and creating a reliable image of hot incandescent parts in a complicated picture.

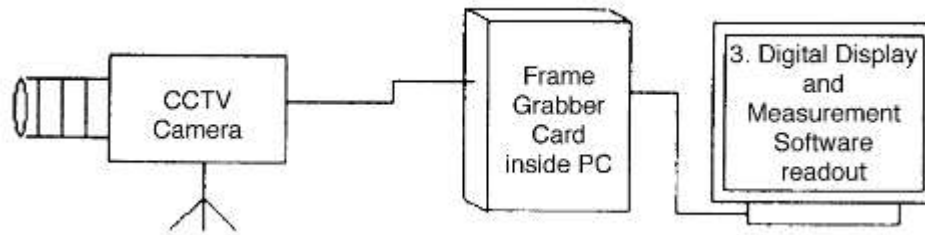


Figure 2-4 Hardware setup for an image acquisition system[26]

In an automated open die forging cell, a vision system described by Wright et al. [27] was deployed as a separate machine integrated with the cell (Figure 2.4). Before measurements could be made, components had to be removed from the forging process and transported to a separate machine. Parts were photographed against a lighted background to create a silhouette image, but the problem of that research was regarding the unaddressed issue of imaging hot parts. The reason was its size, as these parts were turbine blade precursors with a very tiny mass and would not be incandescent when measured. One of the challenges in monitoring hot items like forgings is that their temperature causes them to emit significant amounts of infrared (IR) energy. A notable disadvantage in using vision-based methods for hot-forged component dimensional testing is related to radiation and aura phenomena caused at increased temperatures and leading to object edge distortion. The heat-induced visual distortion is known as aura and is represented as a measurable irregularity surrounding a heated object resulting from temperature variations in surrounding air, leading in turn to refractive index variations. Optical distortion in this manner yields incorrect object edge recognition since optical measuring systems can detect an elongated or blurred shape instead of actual geometrical borders. To meet that challenge, CCD cameras are helpful as they are

sensitive to both visible and near-IR light, although lenses focus differently depending on the wavelength of light.

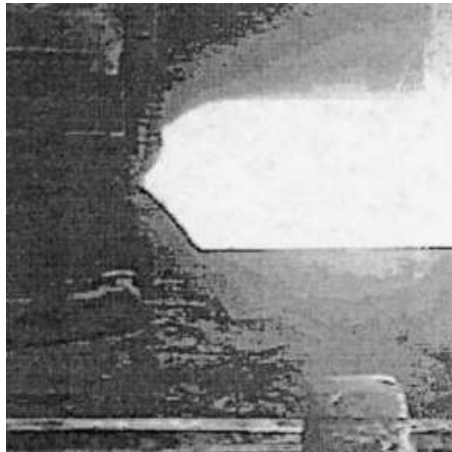


Figure 2-5 Typical forging image, originally in colour [27]

When viewing a heated item through a CCD lens that is focused on visible light, the IR light will be unfocused when it reaches the CCD element, lowering the resulting image's clarity and quality (Figure 2.5). To mitigate this issue, video camcorders commonly use an IR-blocking filter before the CCD element; however, the IR image can be used to help with image acquisition and processing of hot objects. The image processing of welding pools during arc welding, for example, has been dramatically simplified by noting that the emission spectrum of the weld pool differs significantly from that of the welding arc [26]. A clean image of the weld pool is achieved simply by optically filtering away the spectral components related to the arc.

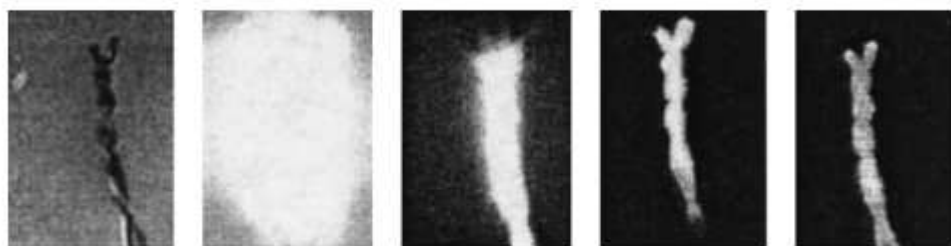


Figure 2-6 Thermocouple photographed at various temperature [28]

Chang et al. [28] recently described a vision system for capturing in-process photos of hot forgings. In one experiment by the researchers, the tip of a thermocouple was imaged with a CCD camera at elevated temperatures of 1100°C, 1350°C (all using a conventional CCD camera), and 1375°C (with their unique technique). While the intricacies of the thermocouple

tip were evident at room temperature and at 1100°C, when viewed with a standard CCD camera, the image of the glowing thermocouple tip at 1350°C lost a lot of clarity and geometry profile (Figure 2.6). However, proprietary image processing technology can mitigate this problem through a high-resolution image of the thermocouple tip at 1375°C. Still, the researchers provided no information about the proprietary image processing technology in their paper. The topic of possible image degradation when viewing hot objects was also missing in this research.

One challenge in using vision systems to measure hot forgings is the need to calculate and match many feature points from the images. This process slows down the measurement because it requires a lot of computation to ensure accuracy. Rocchini et al. [29] reconstructed their projected pattern to obtain the 3D surface of the artwork, but it took too many light patterns to get the entire surface, lowering the system's efficiency (Figure 2.7).



Figure 2-7 The low-cost 3D scanner developed at CNR, based on structured light and consumer electronic technology [28]

Two more models have been used: the blurred edge model and the light stripe model at the sub-pixel level. The former is helpful for components at average temperatures [30], and the latter can be used for hot forgings. Though attempts were made to increase their

measurement precision level by extracting the centre point of light strips at the sub-pixel level, it has the disadvantage of being time-consuming [31].

The literature review has discussed various systems that have been proposed in the domain of measuring workpieces at cold, warm, or hot forgings' geometry. All proposed systems have their advantages and limitations. As this research focuses on measuring the dimensions of workpieces of hot forgings, the discussion regarding cold and warm forging is restricted, and hot forgings are discussed in detail. In this connection, Wright et al. [27] developed a separate machine vision system that measured the part's dimensions after hot parts were transferred from a forging platform. This system showed improved measurement accuracy, but it could not be employed for real-time dimensional measurement of parts due to the time required for the part to transfer from one machine to another for calculations.

The vision system developed by Chang et al. [28] could capture photos of hot forgings using heated thermocouples and an IR filter camera to obtain images at elevated temperatures. However, the limitation of their experiment was that it was conducted in a lab environment with no testing of this system in a natural hot forging setting. Ye et al. [63] developed another system to achieve dimensional measurement of parts with sub-pixel level accuracy. The system was designed as a photogrammetry-based dimensional measurement system capable of attaining sub-pixel level accuracy for dimensional measurement of parts. The system's accuracy was better than that of other proposed systems, as the authors utilized a blur edge model at a sub-pixel level. However, the system required more time to extract geometry for dimensional measurement, and the experimental results of the system at elevated temperatures during hot forging were not presented [30].

The literature review shows that all the discussed systems being used in industrial settings have the problem of accuracy and precision in measuring part geometry in hot forgings, and those that have better accuracy are very time-consuming and unsuitable in industrial settings. Therefore, there is a need for a fast, cost-effective, and reliable measurement system to acquire rapid, real-time dimensional measurements during hot forgings.

2.4 Current dimensional methods for measurement of hot forging

The limitation of the conventional dimensional measurement technique is the belated measurement when the workpiece is cooled to 20°C [32]. Thus, process optimization based on the measured quality parameters cannot be carried out in real-time. Furthermore, during the heating and cooling process stages, geometric imperfections might be generated which are not detected and can impact the final part quality.

Measurements taken during intermittent processes can provide real-time feedback into the manufacturing process. A link between assessed quality features and forging process parameters should be established for this feedback [32, 33].

Process optimization in industrial production faces challenges such as relying on process modifications that are often based on unclear information due to measurement uncertainties and process fluctuations. If these parameters such as part geometry and part size are included, the process can speed up, and process adjustments could also be simplified; for instance a specific stopping criterion based on dimensional measurement could reduce the production cost as there is less wastage and rework needed. For this purpose, a system capable of measuring dimensions at elevated temperatures is required for waste reduction, process optimization and quality control. The next section of this literature review will investigate state-of-the-art measurement systems and their limitations.

2.4.1 Quality control at elevated temperature

In-process measurements performed at high temperatures offer many advantages compared to post-process analysis. Such measurements allow early verification of the workpiece's ultimate geometry and, hence, modifications before the end of the process. Their feasibility can be checked if additional methods are needed, like machining [34, 35].

The establishment of measurements for every step of the process allows for the identification and minimization of errors inherent in every single step. A valid example of measurements performed after forging, but before cooling, can be useful for explaining and measuring the contribution of different process steps. Still, even with the process improvement possibility of this approach, the actual use of in-process measurement systems, defined herein as systems functioning continuously from process beginning, remains rare. The rarity can mainly

be related to harsh working environments typical for forging environments, including extreme temperature fluctuations, heat radiation, and vibration, and hence, complicating installation. Also, the significant cost for developing and implementing such systems limits their use in industrial environments [31].

2.4.2 Parts measurement at elevated temperature

There are both contact-based and non-contact-based measurement systems currently in practice in the forging industry [36, 37]. Contact-based measurement practices can only measure the workpieces when they have cooled. Though some commercial systems are available to measure dimensions of profiles like rods and other regular geometries at high temperatures, these all suffer from limitations [24].

Traditional contact-based methods

Traditional contact-based methods, such as calliper measurements, require operators to be close to the workpiece, where they are subjected to extreme heat. As previously mentioned, a measuring rod with chalk marks is used before the forged part, and its dimensions are compared [38]. This approach is limited in both its precision and accuracy because of the operator influence: it is a subjective perception and there is potential for a parallax effect between the measuring rod and the workpiece. Moreover, traditional contact-based approaches are risky and can result in injuries if considered in the context of the operator's immediate involvement [39, 40].

Traditional defect-detection methods

Before the advent of optical technologies, inline systems based on Eddy-Current Testing (ECT) technology, first developed and applied in the early to mid-20th century, were used to detect defects in work-piece at elevated temperatures, such as hot-rolled bars [41]. There are two solution providers in this case: Institute of Dr Förster GmbH & Co. KG and Prüftechnik Dieter Busch AG, but these are not categorized as measurement systems as they were used to identify flaws in ferromagnetic workpieces indirectly; only an electrical output was detected which fluctuated based on whether flaws were present or not in the workpiece [15].

Optical metrology techniques for dimensional measurement

The basic principle of optical metrology involves the inspection of light interaction with the surface of an object. This methodology generally requires the illumination of the object

through a light source, either a laser beam or a light pattern, followed by the measurement of the reflected or scattered light through sensors like CCD or CMOS cameras.

The collected light is processed by advanced algorithms that seek to replicate the geometric structure under examination. This process begins with a coherent light source that produces a beam or pattern projected onto the surface of the object. When it encounters the surface, the sensor senses the distortions and discrepancies within the reflected pattern. These distortions are then analysed to determine accurate dimensional information, thus enabling an accurate measurement of the object's geometry. Optical metrology plays a vital role in high-temperature forging, where conventional measurement methods face significant challenges. Processes like **Time-of-Flight (TOF)** and **Laser Triangulation** enable non-contact, real-time dimensional measurements in harsh environments. For instance, TOF systems measure distances by calculating the time a laser pulse takes to travel to the object and back to the sensor. This method is particularly effective under high-temperature conditions, as it is unaffected by thermal radiation. Similarly, laser triangulation uses the angle between a laser beam, the object, and a detector to determine the object's dimensions. It provides high-resolution data and is well-suited for capturing detailed surface profiles, even in extreme environments. The following sections present the application of both principles for measuring metal components in high-temperature environments.

Time-of-flight principle

The time-of-flight principle is also known as a fundamental principle of time-of-flight (TOF) or TOF measurement [42-44]. The workings of the principle are shown in Figure 2.8. The measurement system comprises two modules: laser emitter and receiver. The laser emitter generates and directs pulses of light towards the surface of the object being measured. Upon interaction with the object, these laser pulses reflect back to the receiver, which captures the returned light and calculates the distance based on the time delay between emission and reception[45]. The selection of the suitable laser source and wavelength depends on different factors, including the measurement range, environmental conditions and the material of the object. Infrared lasers are suited for forging applications as they block thermal interference and reflective distortions efficiently. By employing high-precision laser emitters and tailored wavelengths, TOF systems provide accurate and precise dimensional measurements, enabling real-time monitoring and optimization even under the challenging conditions of hot forging.

The receiver or sensor receives the continuously emitting laser pulse towards metal parts at high temperatures and reflects it towards the sensor. The receiver module then obtains the distance information, which it converts to information about the coordinates of the feature points on the metal surface via some specific algorithms. In this way, the task of measurement is completed.

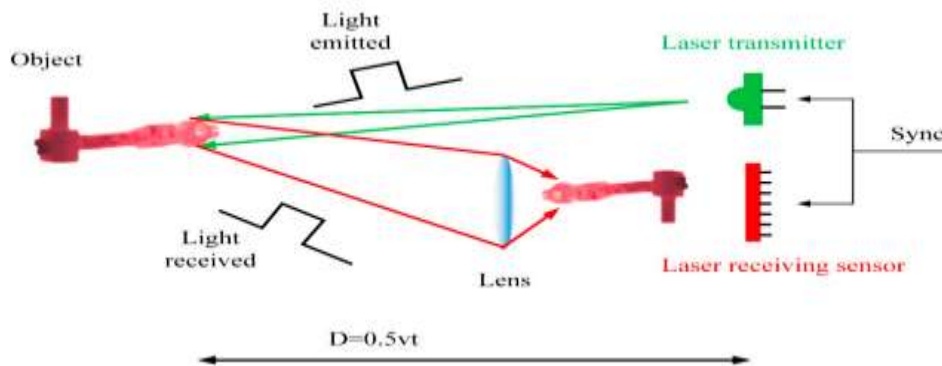


Figure 2-8 Working principle of TOF measurement technique[45].

The LaCam Forge system, developed by Germany Minerals Technologie, is designed to withstand high temperatures and vibrations[15]. Built for use in steel production workshops, it uses range-finding technology and features a laser scanner with a protective cooling shell. This design allows the scanner to be placed close to the forging process, ensuring an effective scanning field. It offers measurement ranges for proper alignment (± 0.5 mm), linearity (± 1 mm per metre), and diameters of metal components (up to 3 metres). Besides that, it can store data and retain it for finite element simulation. However, it needs extra equipment to use in measuring the metal component, which is a particular gripper so that the movement of the metal part can be controlled (Figure 2.9).

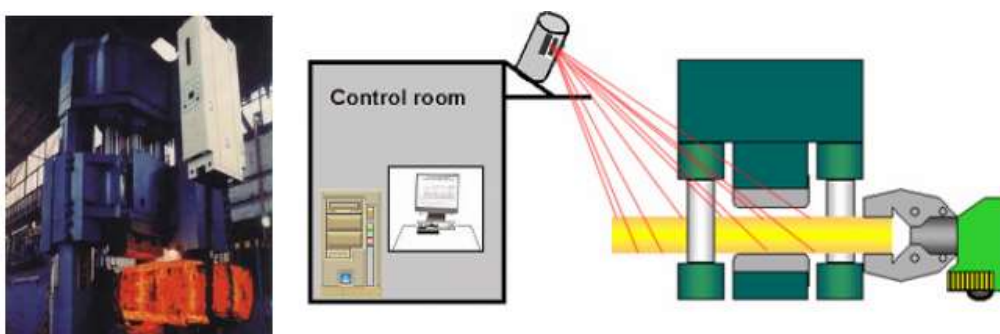


Figure 2-9 Setup for LaCam® Forge measuring system [15]

In the field of forging measurement, another technology was developed by Tian et al. [31], in 2009, based on pulse radar. This technology comprised a single-point scanning device with a 2-DOF spherical parallel mechanism, a pulsed-based TOF laser rangefinder, and two controller-based motors. During the measurement process, continuous rotation of the scanner provides point coordinates of the object being measured (Figure 2.10).

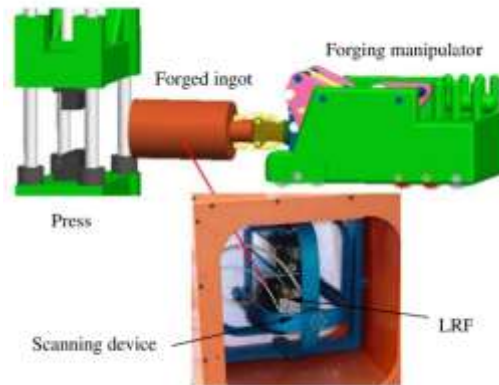


Figure 2-10 Scheme diagram of single-point scanning device for forged parts geometry [31]

The SPM device comprises five space rods, which are used to determine the coordinates of a point ($\varrho \ \alpha \ \beta$) through static motion and sequential rotation of both motors (Figure 2.11).

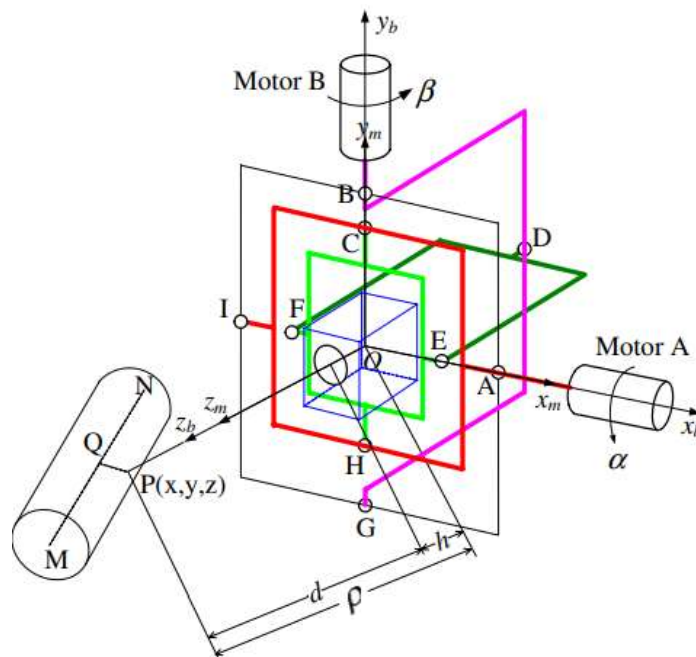


Figure 2-11 Measurement principle diagram [31]

The information on size needs to be obtained by target measurement by fitting the morphology of the target. To obtain the length dimension, two axial scans are required to determine the positions of both end faces of the measured object. In this process, the inertia of moment and vibration is reduced due to the mounting of the motor on a base platform of the system. The drawback of the spherical parallel scanning system is its complexity, which bars its usage in forging workshops on a large scale. The new system was validated by testing in both forging plant and a laboratory demonstrating its capability to measure high-temperature forged components. The length measurement error through this system was reported to be 4.5 mm in the laboratory environment, whereas the actual length was always more than the estimated length of the metal component.

He et al. [37] measured a hot shell using a polar coordinate system installed in a double PRRR robot system with sensors (Figure 2.12). The researchers adjusted the laser scanning plane to be perpendicular, through rotation adjustments, with the cylindrical axis as the system adopted a circular fitting method. The scanning device controlled the laser measurement scanner, which continuously rotated to obtain the polar coordinates of the object. The coordinates were then converted to the Cartesian coordinate system. The optimization of the motion parameters DH matrix was achieved through the joint motion trajectory method [46].

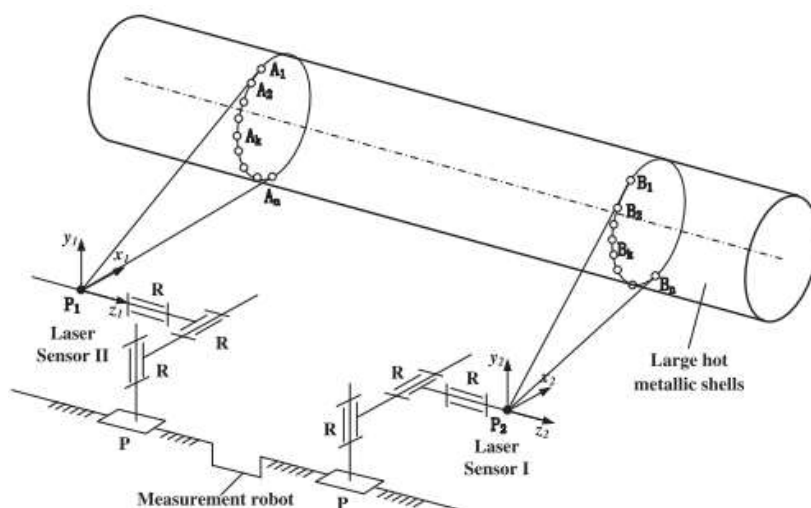


Figure 2-12 Mechanism of dual PRRR measurement robot [37]

This adjustment of parameters for the DH matrix was performed several times so that the rotation axis should constantly be parallel to the metal housing axis (Figure 2.13).

Furthermore, during data processing, the data measurement was made more reliable by using geometric fitting. The percentage of measurement error in the thermal state for the diameters of the right and left cylinder end faces was below 0.205% and 0.235%, respectively. To simplify the measurement process, a complex parallel spherical scanning mechanism was replaced by a PRRR scanning device. In contrast, the adjustment of motion parameters should be made multiple times.

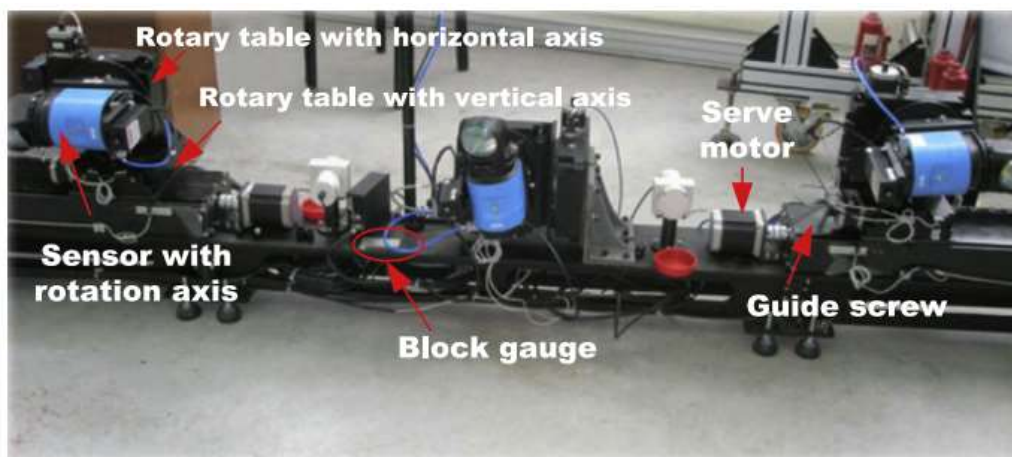


Figure 2-13 Measurement robot setup [37]

In another research study from 2012 by Bokrine et al. [47], the TOF measurement principle was used equipping two TOF laser scanners of the Leica Scan Station [15] for measuring diameters in the high-temperature state (up to 1200°C) of cylindrical metal parts. Simulation software was developed based on a genetic algorithm, and its aim was to determine the laser scanner location to solve the issue of the scanner's perspective as it was typically obstructed in the measurement environment. The collection process required a 120° rotation of the metal component, repeated three times, to obtain the full point cloud. For this purpose, a 3D segmentation method to separate the 3D points from the background of the metal component and to determine the axis of the cylinder's direction under the Gaussian image of the point cloud was used. Finally, the ICP algorithm [48] was used to reconstruct the point cloud. The first experiment of the system was measuring a cooled metal component, which was followed by application to the production line by measuring a hot cylindrical metal component. The system demonstrated high accuracy, with measurement errors of less than 8 mm for high-temperature metal components, which is acceptable given the part size. The process was also efficient, with faster measurement speeds compared to traditional methods.

The system had limitations in measuring cylindrical objects because, for cylindrical objects, the algorithm used in the system could not obtain the point cloud, which means the scope of the application failed.

The measurement of point clouds and extraction of high-temperature objects were studied by a research team of Zhengchun Du [49] in collaboration with Shanghai Machinery-China Ltd (a Shanghai-based heavy machinery manufacturer). They proposed a solution for measuring hot forging in a complex environment. The scanning plane is oriented perpendicular to the main shaft, which is connected to a motor. This setup enables 3D measurements of high-temperature objects, with the measurement points represented in a polar coordinate system (Figure 2.14).



Figure 2-14 Key components and assembled configuration of the high-temperature measurement system [49]

The researchers analysed the point clouds in terms of their distribution characteristics in both the vertical and horizontal directions so that extraction of component point clouds could be

achieved. There were different steps involved in this process. The first step was using distance and angle constraint conditions to remove irrelevant points. The second step involved calculating the curvature to extract the points at the boundary and further clean up by eliminating irrelevant data. The third and last step was analysing hierarchical clustering to remove the points at false boundaries so that point cloud data could be free of interference information. After successfully extracting the point cloud, the reconstruction of the model through the 3D Delaunay triangulation method was undertaken so that the dimension measurements could be realized for the metal components at high temperatures [49]. The 3D Delaunay triangulation method is widely used for the conversion of point cloud data into accurate three-dimensional models. The LaCam Forge is an example of platforms that use this method in order to enable dimensional measurement by reconstructing surfaces, thus avoiding inaccuracies due to faulty boundaries or noise in the data.. The method ensures precise measurements by creating a stable and uniform representation of complex geometries. Its advantages include high accuracy, robustness in handling irregular point distributions, and suitability for large datasets, making it ideal for industrial applications like scanning large forged parts. However, it can be computationally intensive for very large datasets and depends on the quality of the input data, as excessive noise or missing points can affect the triangulation quality. Overall, 3D Delaunay triangulation is a reliable approach for reconstructing 3D models and facilitates precise measurements of metal components in challenging environments. The system took approximately 15 seconds to measure a 3 m extended metal component at high temperature (900–1200 °C) with a dimensional error of less than 2%.

Comparative analysis

Table 2.7 shows the analysis and comparison of research results regarding the TOF method regarding target and measurement equipment with key technologies.

Table 2-7 Comparison of the actual application of TOF

Ref	Detection target	Hardware equipment	Key technologies & algorithms	Measurement accuracy
[50]	Shaft parts (100-400)mm	3D scanner, Laser rangefinder	Cooling protective shell, Wide measurement perspective	Not provided
[31]	Crankshaft (diameter up to 2m)	TOF laser rangefinder, SPM scanning device	Stable scanning system, Measurement self-adaptability	4.5 mm
[37]	Cylindrical metal housing (5m diameter)	PRRR robot, Laser sensor	High precision of scanning system, Optimization of motion parameters	Measurement error is less than 2 mm
[47]	Cylindrical metal housing (3m diameter)	Laser scanner	3D segmentation, ICP algorithm	< 8 mm.
[49]	Large forgings (3-5)m	LMS100 radar, GT-400-SG motion control card	Three-step extraction algorithm, 3D Delaunay triangulation algorithm	1.6 mm

Laser triangulation method

Basic principle

The accuracy and resolution of the obtained 3D information through laser triangulation technology [51-54] are relatively high, and the basic principle is displayed in Figure 2.15. A laser triangulation system typically consists of two main components: a camera and a laser transmitter. The laser emits a line or point onto the high-temperature metal workpiece, enabling measurements to be captured from a specific angle. During this process, a CCD photodetector receives a laser stripe or spot from the surface of the metal part [45]. The change in the position of the laser stripe or laser spot via the camera reflects the change in the morphology and size of the metal component.

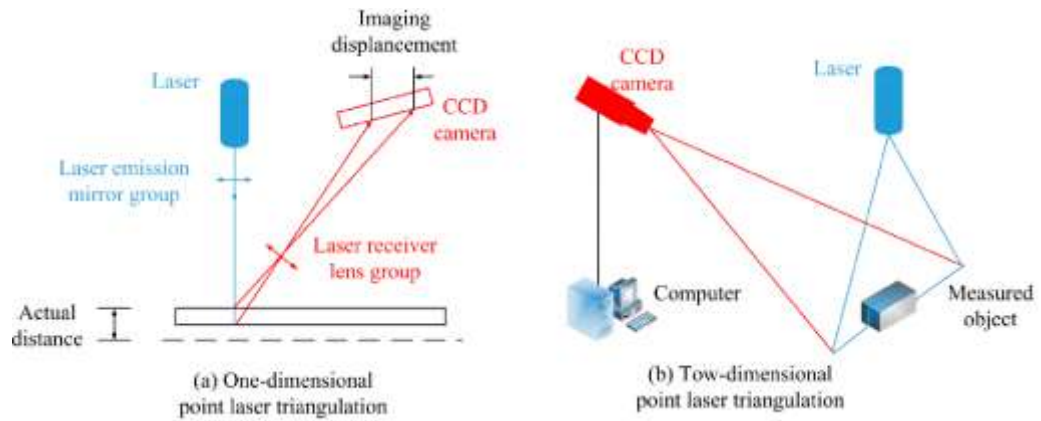


Figure 2-15 Basic principle of laser triangulation [45]

Introduction to specific applications

A research study was conducted in 2014 at Yanshan University regarding the measurement of ring forgings [55, 56]. A team led by Zhang [57] used the laser triangulation principle to measure the diameter of 90–100 mm of cylindrical forgings at elevated temperatures of 900°C–1200°C. They conducted an in-depth study on system calibration by optimizing both camera parameters (internal and external) to improve the system measurement accuracy using the PSO algorithm explained in [57]. The results were found to be an average inaccuracy of less than 0.5 pixels in the horizontal direction and less than 0.25 pixels in the vertical direction, which confirmed the system findings. As the target was a 3D measurement, the measurement error of less than 1 mm was fixed, and the same world coordinate system was obtained by converting scan points using the least squares method to fit the contour of the measured object. Research was carried out in 2017 by Zhang et al [58] in the field of high-temperature-based metal components proposed a method of detection for cylindrical forgings, while the forgings were rotating at a speed of 0.3 m/s. They used a scanner made by an Austrian company, Rieggl, [15] to scan the same sections of forgings multiple times. At the same time, the distance was obtained between the forgings and scanner to convert it into two-dimensional coordinates with a set threshold on the distance size so that the coordinate points could be removed, as they were not part of forging. The least squares method was used to reconstruct the forging contour to fit the circle. As the forging was rotating during the process, the scanner needed to be moved. It is important to note that the system had already been tested by the China First Heavy Industry Group, which stated the measurement error to

be less than 6 mm in the case of the outer diameter of the forging. In order to achieve that an extensive range of scanning was required to ensure that the scanned section was the same during the measurement process, which showed a limitation of this system in practical applications.

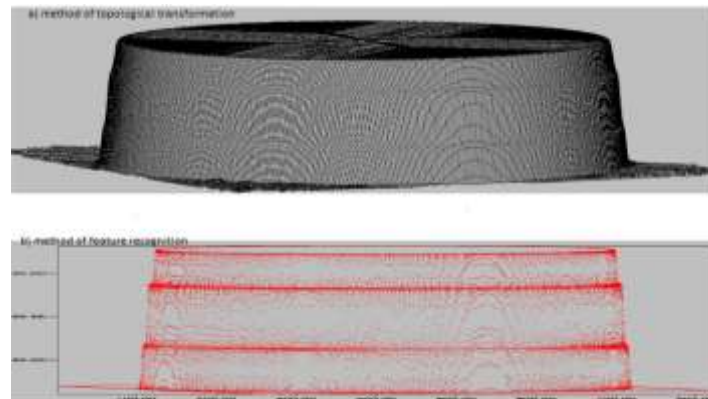


Figure 2-16 Experimental results for building model a) method of topological transformation, b) method of feature recognition[59]

The same team continued their efforts, and in 2018 [59], they started measuring complex annular forgings with free-form surfaces. This time, the system used a top-down approach for laser scanning to obtain cloud data of contour points from the forgings. The contour lines were extracted in a shifting position as the ring diameter increased with the height of the part. Therefore, a suitable filter method, the Kalman time-sharing multiplexing particle filter, was applied to dynamically track the error and noise so that error compensation could be performed on the extracted part cloud data. A smooth surface model was finally obtained via mapping of topological embedding (Figure 2.16). Along with that, the extraction of surface features was completed using the tangent cluster model by topological differential theory. In this way, the designed system measured each step of ring forging for its height to achieve higher accuracy, which was compared with other algorithms to obtain results of less than 1.74 mm for flatness deviation.

Schöch et al. [60] previously developed a CMS (a system), which can be used for 3D measurement of objects with complex surfaces at high temperatures through the support of a hot-gauge. The system has an industrial-level CMOS camera with eight sensors composed of a laser emitter arranged in octagonal morphology for measuring a 2D section of a metal

component (Figure 2.17). The information regarding the direction of the third coordinate was obtained via the movement of the platform. The system used an air cooling system with water pipes to regulate temperature and protective panels with dust control to safeguard the camera's measuring frame. The system measured a 700 mm turbine blade in an experiment to verify its performance, which resulted in a 0.1 mm error range for length measurement and took approximately 4.2 seconds to complete.



Figure 2-17 Photo of the CMS installed at the forging plant of Pietro Rosa TBM Srl [60]

Veitch-Michaelis et al. [61] experimented by combining machine learning with the laser triangulation principle for the measurement of cast steel plates. The project was given the name HTP-C (high-temperature process control). It used a laser transmitter, which emitted a stripe at 405 nm. The camera placement was the same as for conventional systems, placed on the same axis so the laser beam could be attached to the laser beam launching port. To operate effectively in high-temperature environments, the system incorporated a blue filter and cooling housing to minimize environmental impacts. It utilized a detection algorithm based on the centre-of-mass peak to accurately identify laser stripes. Moreover, the same algorithm could accurately extract the laser line while casting metal components was in progress. The system divided the defect detection process into two phases: the first phase used median filtering and morphological edge detection as an image processing algorithm so that detection results could be obtained without false detection. The second phase used training data and an SVM (support vector machine) to obtain accurate defect detection results. An SVM is a supervised machine learning algorithm widely used for classification and regression tasks. It operates by finding the hyperplane that best separates data points into distinct classes in a multidimensional space. The objective of an SVM is to maximize the

margin—the distance between the hyperplane and the nearest data points from each class, known as support vectors. This maximization enhances the model's ability to generalize to unseen data. An increase in the system temperature led to an increase in measurement length due to a change in laser beam quality. Still, while testing the 1970 mm wide slab, the system's behaviour was not normal. In the process, system measurement also required exposure time because its unavailability can produce no detection of minor crack defects.

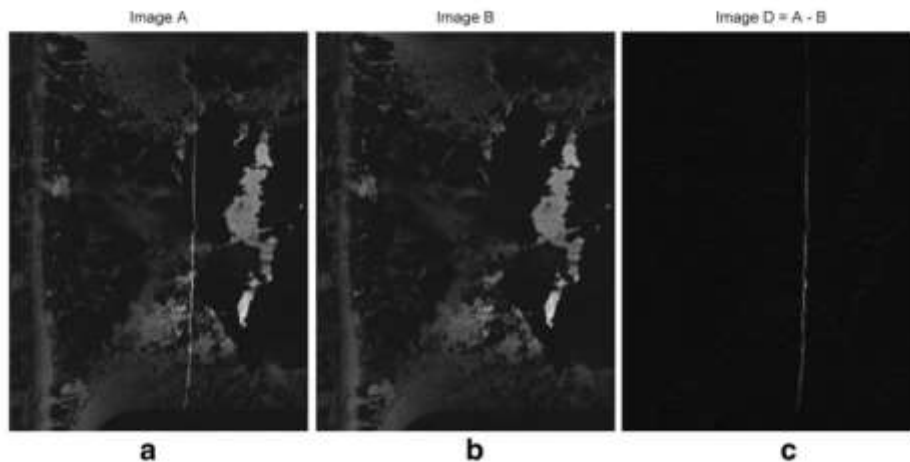


Figure 2-18 Differential Imaging Technique for High-Temperature Measurement [62]

Bracun et al.[62]analysed two-factor interference by using the differential imaging principle for measurements (Figure 2.18). The two factors were a source of light in the environment of measurement and the scale of surface oxide on metal components at high temperatures. The resultant two images, captured from the camera, were used for measurement. The radiation of a laser created the first image, and the second image was not the result of laser radiation. The difference between the images was used to create a third image with a precise laser contour. Median filtering was used to extract the contour with pixel information, which was converted to Cartesian coordinates to obtain accurate measurements. A triangle waveform and the calibration body were used to calibrate the triangle vertex as a point of calibration (Figure 2.19). In this way, the comparison was made between the measurement and output points, and then differential processing was applied to obtain laser fringes; hence, the measurement uncertainty was less than 1 mm. Twenty-five measurements were performed on the 50 images collected in one second with a reduced measurement speed.

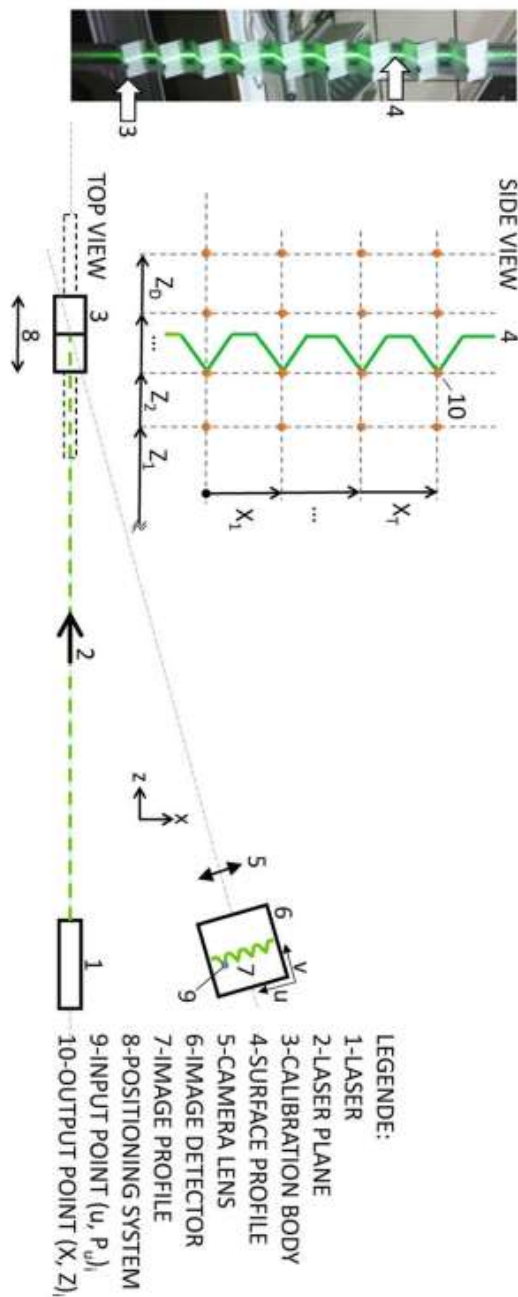


Figure 2-19 The measurement system[62]

Comparative analysis

Table 2.8 shows the analysis and comparison of various research-based results of laser triangulation with a focus on measuring equipment, key technology, and measuring targets.

Table 2-8 Comparing measuring quality of laser triangulation.

Ref	Detection Target	Hardware Equipment	Key Technologies and Algorithms	Measurement Accuracy
[38]	Cylindrical forgings	MV-VE078SM/SC camera, MGL-III laser transmitter (635 nm, red laser)	PSO algorithm	Measurement error is less than 1 mm.
[58]	Cylindrical forgings under rotation	VZ-1000 3D laser scanner, 850 nm near-infrared laser	Least square method, Coordinate rotation processing	Measurement error is less than 6 mm.
[59]	Complex ring forgings	VQ-180 2D laser scanner, 405 nm blue laser	Topological embedding mapping, Topological differential theory	1.74 mm
[60]	Complicated Surface parts such as turbine blades	Mobile platform, SL-405-35-S-C-15.0 laser transmitter (405 nm, blue	Combine eight sensors, Custom meshing algorithm	Length measurement error 0.1 mm.
[61]	Surface defects of cast steel plate	Laser transmitter, UI-3370CPs IDS camera, 635 nm red laser	Centre of mass peak detection algorithm, Deep learning algorithm.	The system performs defect detection in the steel mill.
[63]	Large hot forging.	Camera	Principle of differential imaging	1 mm.

2.4.3 Forging process optimization

This section briefly discusses state-of-the-art in-process optimization methods used in hot forging. The topic is divided into two parts: offline optimization (conducted before the start of actual production), which is based on assumptive models of the process, and online optimization (implemented after the beginning of the actual output), which is also based on assumptive models of the process based on the measurable output of hot forging during the process. The research shows that a lot of scientific effort was put into offline optimization and online optimization was practically ignored while working on offline optimization [19, 64-66].

Offline optimization

Finite element method (FEM) simulations, as an offline optimization method, are commonly used to optimize the forging process. Appropriate approaches are used to find parameter choices that yield the best FEM model in terms of material properties or geometry measurements. Even factors like workpiece geometry that remain stable during production can be considered variable using this method. Practical FEM simulations require data gathered from natural experiments to calibrate FEM simulations, but that is rarely discussed in the literature [64, 66].

Although offline methods have proved their potential to improve forging operations, online process optimization methods offer the advantage of reacting to differences in the production environment, such as environmental disturbances. Although such changes are not directly measured, they can impact the quality features of the workpiece and should, therefore, be considered.

Online optimization and uncertainty errors

A recent assessment of closed-loop control in metal forming [10] noted that real-time dimensional measurement of hot parts has seen limited investigation. In this respect, Recker et al. (2015) [67] provided methods for predicting the part quality of incrementally forged blocks. Their study focused on optimizing the real-time dimensional measurement of metal parts at elevated temperatures during hot forgings. Several identical steel billets were forged at elevated temperatures under the same working conditions, such as background noise and vibration, for which statistical analysis was then carried out to analyse and evaluate the data captured through repeated experiments. In this process, observing and optimizing part temperature is a key factor, which causes measurement uncertainties during in-process dimensional measurements. It is also important to note the high temperature, which can create an aura around the part profile, making it difficult to extract the geometry for real-time dimensional measurement during hot forgings.

In a study by Yan et al., a detailed procedure of geometric error decomposition was developed. The essential purpose of their research was to analyse the measurement uncertainties and variation reduction by using discrete measuring data associated with complex components manufactured through forging processes [68]. Another research study

was carried out by Huang et al. to enhance the precision and output of coordinate measurement gauges [58]. They used a feature-based dimensional error analysis technique to analyse the error that occurs within the geometric shape of the measured parts. In their study, Lira et al. concluded that the sample elongation and reference location cause local displacement uncertainties [69]. Luculno and Lazzari used a vision system to evaluate the measurement uncertainty of optical machines for non-contact 3D measurements [70].

A study was presented by Santo et al. to describe the utilization and evaluation of measurements acquired from digital photos in an industrial context [71]. Spattaro et al. further investigated the measurement uncertainty in virtual instruments. Their research showed a better approach to record measurement uncertainty through numerical simulation methods [72]. One study conducted by Locci discussed the measurement uncertainty method based on a digital signal processing algorithm [73]. They reported that uncertainty analysis could be achieved using Lotus and Excel spreadsheet applications. In contrast, a study conducted by Castrup discussed significant questions about and issues with this method of uncertainty analysis [74], issues which should have been addressed in the study of Locci [73].

2.5 Summary of review

The literature reviewed in this chapter has developed the critical role of dimensional measurement and process control in metal forging, highlighting precisely the challenges and opportunities introduced by real-time measurement in high-temperature environments. For this reason, forging, whether cold, warm, or hot, remains a crucial manufacturing technique in industries such as the automotive, aerospace, and energy sectors, mainly due to its capability to produce high-strength, precise components. However, dimensional accuracy during forging, especially at high temperatures, has become a big challenge for manufacturers.

The review showed that forging methods are available, each having different advantages and disadvantages that suit different needs in the manufacturing industry. While cold forging ensures better surface quality and dimensional accuracy, its limitations also emanate from the material flow stress and geometrical constraints. On the other hand, hot forging enables better flexibility and the possibility of making more large metal components, but this is at the expense of dimensional accuracy and surface quality. Warm forging attempts to compromise

these differences. However, its high development costs and process setup times make it less feasible for widespread industrial use, except in high-volume production where precision and formability are required.

A recurring theme in the literature is that forging processes represent trade-offs between precision, speed and cost. Cold and hot forging have dominated the industry due to their established process efficiencies. Still, one of the significant areas for improvement is the need for real-time measurement and quality control. Without real-time dimensional assessment, manufacturers must focus on post processing measurement, usually after the part has cooled. This dependence results in increased downtime, excessive scrap of materials, and expensive rework. Delays in feedback make process optimization impossible, and the origin of defects also becomes challenging to locate as one is unsure if defects arise from the forging process or subsequent cooling.

A major problem the available literature pointed out is the demand for trustworthy real-time and non-contact measuring systems that operate well at high temperatures. In parallel, conventional methods, like contacting callipers, although easy and inexpensive, are susceptible to human error, risky to safety, and less accurate, mainly when employed on bulky, hot workpieces. None of these systems operate according to the needs of modern industrial practice, whose highest demands are accuracy, speed and safety. This has thrown up non-contact techniques as suitable alternatives, particularly those employing laser technologies of TOF and laser triangulation. However, these systems also face significant challenges in the industry, particularly issues in dealing with thermal distortion, reflective surfaces, and unwanted vibrations, which may affect measurement accuracy.

The literature review has also underlined some of the newest developments in real-time measurement technologies, showing that TOF and laser triangulation-based systems are promising in the lab. At the same time, they still suffer from issues related to robustness, integration and cost that seriously limit their use in real industrial scenarios. Various systems have been tried in controlled conditions; however, they need help when exposed to the extreme conditions typical of actual forging processes: high temperatures, geometries of a complicated nature, and the need for continuous, real-time feedback. These aspects make

the very transfer of such technologies from experimental laboratories to industrial production lines quite formidable.

Most studies have shown that even with enhanced resolution at sub-pixel levels, measuring systems at high temperatures are still crippled by considerable problems regarding uncertainty and repeatable measurements. Measurement surfaces from hot forging-manufactured parts are critical due to various disturbing variables, such as luminous radiative heat, which interfere with determining correct results. Various optical systems have been developed to measure pixel and subpixel levels accurately. Still, their developments have minimally addressed the high-temperature forging environment. This calls for more development of non-contact measurement technologies that can handle this complexity in forging processes with precision and efficiency.

The study identifies the strong impact that real-time, in-process dimensional measurement has on the efficiency of industrial operations. A measurement system that accurately captures a component's dimensions during a forging operation would enable immediate adjustments and lower the incidences of scrap, rework, and material waste. Indeed, such a system would improve the forging process itself by allowing manufacturers to perfect every stage of production in a matter of seconds, thereby improving general output quality while reducing costs.

In other words, while there are significant advances in forging applications through the development of non-contact measurement systems, significant gaps in their usage remain in natural industrial environments. There is a clear need from the literature for a robust, real-time measurement system that can survive the high temperatures and vibrations of the forging environment and deliver the accuracy required for high value-added components. This, in turn, would contribute to reducing waste and improving the productivity and competitiveness of the manufacturing industries dependent on forging technology. Further research should be done to develop these systems' precision, affordability and flexibility so that their integration into the existing industrial setup is smooth and meets the new demands for precision production in the world today.

This literature review forms the basis for the research described in the following chapters. The goal of this research is to develop an original, real-time measurement system designed

to solve a certain number of problems linked to hot forging processes. By linking innovative metrology methods to industrial applications, this work bridges the gap between current limitations and future industrial needs.

2.6 Research gap and Justification of the research project

Contemporary measurement systems used in forging are predominantly set up for ambient temperature testing or require parts to be cooled before accurate dimensional testing. This reliance on post-process testing presents a range of drawbacks. First and foremost, traditional methods introduce significant delays in the feedback cycle, such that defects may only be detected much later in the process, hence creating wastage [7, 16, 20]. Secondly, non-contact measurement technologies, including laser triangulation and Time-of-Flight (TOF) systems, encounter difficulties associated with heat distortion, surface reflections and environmental vibrations despite their potential advantages in high-temperature settings. Such challenges undermine the precision and reliability of the measurements, particularly under the severe conditions characteristic of industrial forging operations [47, 49]. The heat aura is a glow or haze surrounding hot regions due to heat and surface effects. The aura produces a diffused light region in between the part and the background and makes it difficult to view the sharp outlines of the part and results in a significant loss of the edge profile's sharpness. Despite advancements in detail identification and imaging processing, few studies have explored heat distortion and surface reflection as well as how the thermal aura operates in conjunction in real-world production environments. The systems are usually tested under laboratory conditions. True forgings have other complexity factors involved that include heat change situations, vibrations, gases circulating through the system, and irregular surface emissions that have a significant impact on the system's performance [49, 57]. Although there have been certain developments in the measurement accuracy of optical systems, even at pixel and subpixel levels, the repeatability and reliability of the methods during high-temperature forging must be improved for industrial application [67]. These deficiencies indicate the need for novel solution to deliver more accurate, real-time measurements and mitigate challenges resulting from high-temperature environments.

The high value of the components being manufactured makes quality control extremely important. Therefore, real-time dimensional measurement is becoming crucial throughout

the forging process. Current methods, which delay inspection until the component has cooled, are wasteful and lead to higher-than-necessary scrap rates, costly rework and production delay. Establishing a real-time measuring system that works during the hot forging process would eliminate such concerns by providing timely feedback, reducing defects and continuously improving the process.

The measurement at high temperatures presents significant research challenges, particularly in dealing with thermal expansion control, reflectivity of the material, and interference of infrared radiation. The use of advanced image processing techniques like noise reduction and subpixel analysis makes it a multidisciplinary methodology involving aspects drawn from computer vision, manufacturing science, and photogrammetry. The validation in industrial setups for practical use also requires a highly structured experiment and extensive statistical testing for ensuring reproducibility and reliability.

Various pressing industry needs drive this research. First, the availability of instantaneous responses would enable timely adjustments to forging, thus significantly reducing the occurrence of defective parts and minimizing rework and material waste [30]. Secondly, earlier identification of potential dimensionality issues can significantly prevent material wastage in small-lot production with an expensive material, which, when flawed, leads to significant losses [71]. Thirdly, the setup of real-time measurement would increase the overall effectiveness of manufacturing by decreasing the time spent on post-process inspections, thus allowing production lines to run at higher speeds with better confidence in output quality. Lastly, this study aligns well with Industry 4.0 interest, emphasizing the need for intelligent, automated systems capable of real-time monitoring and response [47]. The present work aims to develop a reliable, accurate, and non-contact measurement system, especially for hot forging processes.

2.7 Objective metrics

It is important to determine the metrics on which the development of the system will be based beforehand, to ensure that the proposed system will work effectively in an industrial forging environment. These metrics will give a basis for performance assessment so that the development process stays tuned with practical industrial requirements. The system must achieve dimensional measurement precision within an allowable error range of no more than

± 1 mm during hot forging, depending on the component size and the complexity of its geometry. Such dimensional measurement precision is critical to ensure that the fabricated components meet defined tolerance requirements, thus avoiding rework and minimizing material usage [53].

Another important factor is the capability for real-time feedback. It is expected to provide measurement data within a one-second interval during the forging process. This real-time feedback is crucial for operators because they can make immediate adjustments and prevent defects. Any delays in feedback would compromise the system's efficacy since the real-time optimization of the forging process necessitates an immediate reaction to changes in dimensions [7]. One more critical parameter is the ability of the system to function reliably under high-temperature exposure. The design should be compatible with 1,200°C temperatures developed during a typical forging process. Any loss of shape, distortion or signal deterioration due to temperature would diminish system performance and make it unsuitable for industrial use[16].

Other important factors include the fact that the system is non-contact. The system should have no physical contact with the workpiece, to avoid contamination or damage to the measuring device or the part. Contact methods introduce several risks, especially in extreme temperatures; a non-contact method is much safer and more appropriate [47] . Another important metric is that of integration with current industrial systems.

The system should provide both pixel and subpixel-level measurements, allowing a measurement accuracy of at least ± 1 mm depending on part size and complexity of geometry. The accuracy will be paramount at the subpixel level since minute changes in the parts' dimensions may hardly be noticed with the resolution level at the pixel level. This becomes vital in high-precision forging applications, where even a slight dimensional difference may lead to serious quality issues. The research outlines clear and achievable goals for the system's development by setting these metrics. This means it will align with industry standards regarding accuracy, robustness, and integration.

3 Proposed methodology and preliminary studies

3.0 Introduction

This chapter outlines a detailed analysis of the techniques adopted in the development and verification of a precise real-time non-contact dimensional measurement system for applications in high-temperature forging. The organization of this chapter covers four main stages of the study: identification of measurement techniques used under both room and elevated temperatures, study of the comparative measurement approach, development and evaluation of the new measurement system, and the following optimization and improvement of the system to enhance precision and reliability.

The chapter starts with the evaluation of the effectiveness of existing measurement methods, both contact (for instance, coordinate measuring machines) and non-contact optical (for instance, GOM ATOS), in both normal and high-temperature environments. This includes a critical investigation of their applicability, accuracy, and limitations for use under hot forging environments.

Following the process of verification, a structured approach to the inter-comparability of measurements exists to assess the reliability and agreement between contact and optical systems. Formal analysis techniques are utilized to compare quantitative outputs of the systems through the process of paired sample tests, confidence interval assessment, and correlation analysis and hence provide a critical framework towards the verification of a new system. The proposed metrology system is validated using experimentation in both laboratory environments and real-life industrial forging environments. Tests for measurement accuracy, consistency, and heat resistance are conducted to guarantee that the system meets the accuracy standard of ± 1 mm on both the pixel and sub-pixel scales.

Building on the findings of the proposed system, a more refined version is then developed. Improvements are introduced in areas such as sub-pixel edge detection, glare suppression, and noise filtering. These improvements are validated through another series of experiments targeting more demanding dimensional tolerances under harsher operational conditions. This

version of the system not only provides higher precision but also demonstrates improved adaptability and scalability for broader industrial deployment.

3.1 Preliminary experiments

Measuring real-time data at high temperatures is a challenge in the forging industry compounded by the lack of robust and efficient in-process monitoring and quality control technologies [75]. For this purpose, the researcher carries out trial experiments to measure the diameter of metal parts at standard room temperature (20°C) to establish the measurement accuracy, repeatability and traceability of fringe projection systems in the forging industry.

The main purpose of the preliminary experiments was to better understand the measurement capabilities, repeatability and traceability of a fringe projection scanning system through data analysis of those experiments presented in the current chapter [49] .

3.1.1 Fringe projection system

Fringe projection is the process of projecting structured patterns of alternating light and dark stripes (fringes) onto the surface of an object. The patterns deform according to the geometry of the object, and from several angles, high-resolution cameras capture the deformed fringes. Then, the system reconstructs a detailed 3D model of the object's surface by using advanced triangulation algorithms. Working on this principle, the GOM ATOS system records measurements in real time, assuring quality assurance within the forging process by maintaining continuous control of the process.

Thus, the experiment had to validate the proper geometry of metal parts during the forging process using a non-contact measurement technique that had been validated in advance[76]. A detailed description of the system, prepared based on the manufacturer's datasheet, is presented here, and justification is provided as to why it was chosen for this project. The fringe projection method has also been explained to show how the system works.

3.1.2 Specification of the GOM ATOS system

The structured blue light technology used in the GOM ATOS system allows reconstruction of metal geometry to carry out dimensional measurements. The system is non-contact and thus can scan objects of different sizes and geometries. Table 3.1 provides system specifications.

Table 3-1 GOM ATOS technical data sheet [76]

Specification	Details
Measurement Principle	Structured Blue Light (Fringe Projection)
Measurement Range	38 mm x 29 mm to 2000 mm x 1500 mm (depending on sensor model)
Point Spacing (Resolution)	0.01 mm to 0.5 mm (depending on configuration)
Accuracy	Up to 0.005 mm
Cameras	Dual camera setup with ≥ 5 MP resolution
Light Source	Blue LED fringe projection
Working Distance	490 mm to 2000 mm (depending on sensor setup)
Temperature Range	+5°C to +40°C
Automation Capability	Can be integrated with automated systems for continuous monitoring
Output Formats	Point cloud, mesh data (STL, PLY)
Calibration	Factory pre-calibrated, periodic recalibration available

The resolution, precision and dimensions of the measurements that the GOM ATOS system can provide are very important for its application in this study. High resolution and precision give it the capability to acquire complicated geometries and surface features in detail, which becomes very important when analysing any deviations and defects in forged parts. Similarly, the large measurement range gives flexibility in scanning components of varying dimensions, from small precision to large industrial forgings. Its characteristics explained in Table 3-1 make it suited to address the thesis goals: to create a robust, real-time dimensional measuring system tailored for the challenging environment of hot forging.

A couple of high-resolution cameras in the ATOS system are mounted at different angles relative to the object and projector to capture the deformation of fringe patterns. Two cameras simultaneously capture the deformed patterns from each camera's point of view, generating crucial spatial information about the object's surface. Due to the multi-angle observation of fringe deformation, the system can estimate the amount of surface deviation from the flat plane. The images obtained by the cameras are further processed by the system

software, which resorts to triangulation to establish the precise three-dimensional position of each point on the surface. Triangulation works to build upon the known accurate positions of both the projector and the cameras, in addition to the changes in fringe patterns obtained, to establish depth and distance for each singular surface point (Figure 3.1).

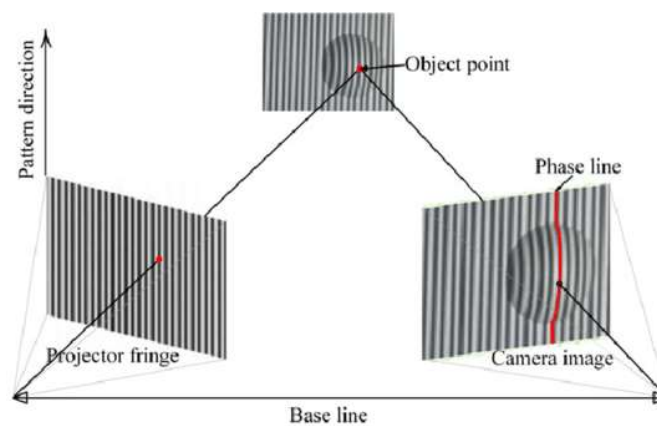


Figure 3-1 The principle of fringe projection technique [77]

Once the triangulation data have been processed, the system outputs a dense 3-D point cloud—a digital model of the whole surface of the object. The point cloud can be converted to a polygon mesh, perhaps forming a basis for further analyses[77]. For instance, this dimensional analysis can be combined with CAD models, geometric tolerances or defect identification. The fringe projection technique is suitable for acquiring complex geometric shapes, like curves, edges and detailed surface features, making it ideal for industrial quality assurance [78].

The fringe projection technique has many advantages over the traditional contact-based measurement methods. Due to the absence of physical contact with the object, damage or alteration to fragile or temperature-sensitive components is avoided. This is particularly critical in very high-temperature applications like hot forging. In addition, since the system uses a blue light source, its performance is less affected due to the wavelength, for instance, by changes in external illumination or temperature, which enables its effective utilization in changing industrial environments.

3.1.3 Justification for selecting the GOM ATOS system

The GOM ATOS system was selected for this study because it aligns with the distinct technical goals and targeted criteria necessary for accurately measuring the dimensions of metal

components throughout hot forging. Since measurements are to be taken at elevated temperatures, a non-contact measurement system is necessary to avoid interference with the workpiece. The fringe projection technique employed by the ATOS system allows accurate measurements from a safe distance without the need for physical contact (Figure 3.2).

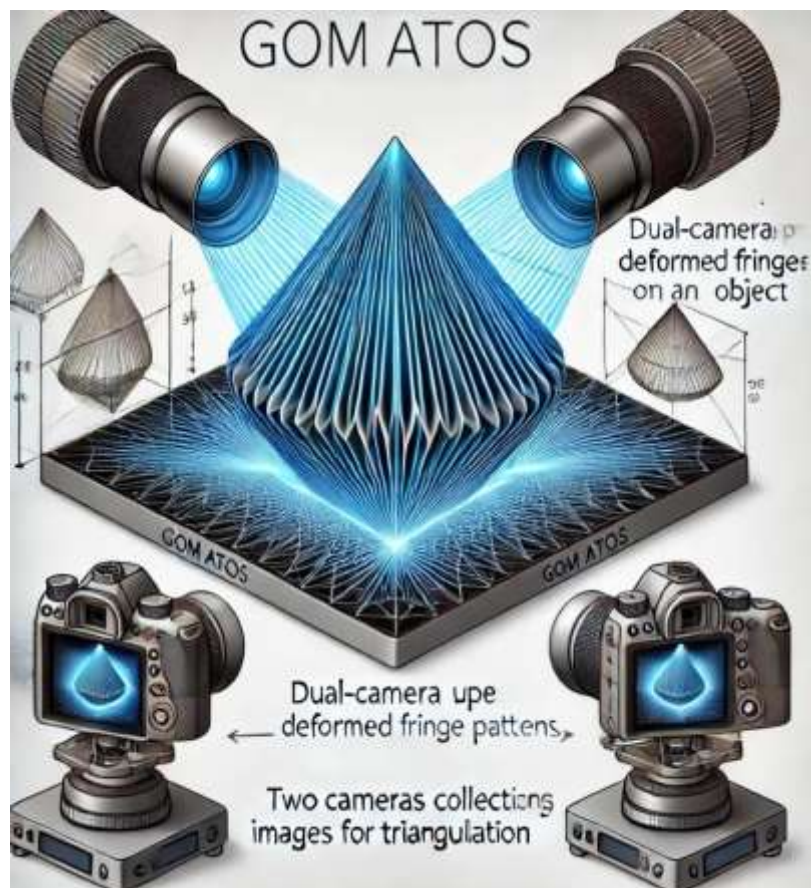


Figure 3-2 GOM ATOS Scanner working principle [78]

The GOM ATOS system has the capability of measuring a wide range of geometries, from small, complex components to large industrial metal parts. It enables detailed comparisons with CAD models, tolerance checks, and statistical analysis, which are crucial in ensuring that parts meet desired specifications. The software also integrates easily into automated processes, allowing continuous monitoring and analysis during the production process.

The GOM ATOS system was selected for this research because it fulfils the critical technical requirements of non-contact dimensional measurements during hot forging processes. Its measurement accuracy and portability make it an ideal tool for dimensional check purposes. The industrial application quality is the reason behind the selection of the measuring system.

The fringe projection technique of the system enables the capturing of complex geometries and fine surface details. It will support the overall research objectives in optimizing production and reducing material waste through dimensional measurement during hot forging through the proposed system. The following section summarizes the performance evaluation of the GOM System at room temperature and at elevated temperature for workpiece dimensional measurements during the trial experiment.

3.2 Preliminary investigation to compare non-contact with contact-based measurement system at room temperature

For the experiment, it was necessary to carry out the dimensional measurements on a metal workpiece with the GOM ATOS system. Although this system is a state-of-the-art scanning system for the dimensional measurement of metal parts, it is still not traceable to the industry ISO standards [79]. It can only be made traceable through calibration against a traceable reference. Hence a coordinate measuring machine (CMM) was used to compare and evaluate the measurement accuracy of the GOM ATOS. The CMM used in the present study is a high-precision device designed to provide accurate measurements of physical geometries. The technical specifications include a touch-trigger probe with a measurement uncertainty of ± 0.005 mm coupled with a working volume of 500 mm \times 500 mm \times 500 mm. This machine has three linear axes: X, Y, and Z; all of them are supported by high-precision bearings to enable smooth and repeatable motions. In addition, there is a programmable control system provided with the CMM, enabling automated sequences of measurements for consistency, with fewer possible operator errors.

The recorded points are processed to calculate dimensions and geometric features such as diameter. A CMM is specially designed to measure the geometries with accuracy and repeatability as per ISO 10360 standards of metal parts measurements during forging applications.

The specifications of the CMM directly support the objectives of this research. High measurement accuracy and repeatability are important for benchmarking the non-contact GOM ATOS system. Using a touch-trigger probe, the CMM takes precise point-based measurements that serve as a standard for evaluating the performance of the GOM ATOS system. The large working volume takes in the cylindrical specimen used in this study, thus

ensuring complete data acquisition from different positions (top, middle and bottom) on the specimen. The precision and flexibility of the CMM make it the ideal reference tool for calibrating the non-contact measurement methods presented in this thesis.

The test specimen was a cylindrical mild steel workpiece with a nominal diameter of 76.08 mm and height of 100 mm. The part geometry was chosen to be of relevance to typical forging applications, to represent common geometries in industrial processes. The workpiece surface was smooth, so as not to incur measurement errors attributed to the presence of unevenness.

An experiment was designed in which a mild steel cylinder diameter was scanned 10 times with the GOM ATOS. The cylinder was scanned 10 times with the GOM ATOS and then with the CMM. The CMM recorded the diameter of the cylinder at the top, bottom and centre (**Appendix 1**). The diameter measurement routine was repeated 10 times on the same sample at room temperature. The mean diameter measurement of each repeated measurement was compared with all the systems (**Appendix 2**).

In the context of this research, length and diameter refer to the primary geometric properties of cylindrical parts. The length is the linear distance from one end of the cylinder to the other, measured along its central axis. This property plays a crucial role in examining an object's general dimensions and geometry in industrial applications such as forging. The diameter of a cylinder, on the other hand, refers to the width across its round cross-section, measured across the centre of its points. In this case, diameter measurements are essential for investigating the roundness of such cylindrical parts so that they can meet the required specifications for usefulness and assembly onto systems during manufacturing.

The diameter measurement is performed in this section using the GOM ATOS system, which captures the complete geometry of the sample through 3D scanning. The principles of the measurement methodology include relevant ISO standards to ensure that precision and traceability are maintained. The length is measured according to ISO 14405-1, which describes the rules for the specification of linear dimensions and their corresponding tolerances, ensuring that the size is consistently measured along the central axis of the cylindrical specimen. The principles of the measurement methodology include ISO 14405-1 to ensure that precision and traceability are maintained. The ISO 14405-1 measures the diameter by

taking measurements at several points around the circumference of the cylinder. This way, any deviation in surface geometry is taken into account to give an accurate calculation of the diameter[80].

The measurements are taken using the GOM ATOS system, which calculates mean values for length and diameter over many data points. This helps to reduce the chances of measurement errors and can thus permit a complete geometric analysis of the object.

Table 3-2 Paired sample test scores between measurements of sample diameters through GOM ATOS and CMM in repetitions

Pair	Items in the Pair	No.	Mean		Std. Deviation	T score	Sig. (2-tailed)
			Single	Overall			
1.	GOM ATOS (mm)-1	5	75.086	.004	.0054	1.526	.202
	CMM (mm)-1	5	75.082				
2.	GOM ATOS (mm)-2	5	75.084	.002	.0055	.735	.503
	CMM (mm)-2	5	75.082				

Table 3.2 shows the statistical analysis of diameter measurement results from the two different measuring systems: GOM ATOS and CMM, based on 10 repetitions. The measurements are divided into two data sets with each set including 5 measurements from the GOM ATOS as well as from the CMM. The average diameters measured by GOM ATOS and CMM are very close to each other in both sets. For Pair 1, the average diameter found by GOM ATOS is 75.086 mm, while the measurement from CMM is 75.082 mm, with a difference of only 0.004 mm. For Pair 2, a similar pattern is observed because the mean diameter obtained through GOM ATOS is 75.084 mm, against a value of 75.082 mm from the CMM, which forms a deviation of only 0.002 mm; in fact, even more surprisingly, the standard deviation values of both pairs are similar, at about 0.0054 mm for GOM ATOS and 0.0055 mm for the CMM. The T-scores, which are used to denote the direction and magnitude of any observed differences, are quite low (1.526 for Pair 1 and 0.735 for Pair 2), thus showing that there are negligible differences between the two systems. The calculated p-values for each of the pairs are above the threshold of 0.05, being 0.202 for Pair 1 and 0.503 for Pair 2. This means that the observed differences in the measurements are not statistically significant. In a nutshell, these results show that the measurements obtained from GOM ATOS and CMM

are very similar, with no significant statistical difference, thereby implying that both systems give similar results when measuring the diameters of the samples at ambient temperature.

Table 3.3 summarizes the reliability statistics for measurements obtained from the GOM ATOS and CMM systems. In this case, the reliability statistics are meant to define the level of consistency and repeatability of the measurement results over a series of trials or iterations. Measurement system studies must include reliability, meaning the stability of performance of the system under similar conditions, and if the results can be considered to be valid representations of true values within acceptable error boundaries.

Table 3-3 Reliability statistics

Cronbach's Alpha^a	Cronbach's Alpha based on standardized items	No. of Items
0.247	0.428	10

The reliability statistics in Table 3.3 are a gauge of how reliable the data to be measured are. This is mostly represented using the metrics Cronbach's Alpha or equivalent measures of relevance with respect to internal consistency. On that note, these statistics were employed in establishing whether results remain stable over numerous repeated measurements while ensuring fluctuations are very minimal and the measuring systems, GOM ATOS and CMM, can produce constant dependable results. High reliability means that the measurement system is consistent and can confidently be used to make exact measurements on different samples or under different conditions. Advanced statistical analyses now allow deeper insight into the precision of measurement systems so that their acceptability for intended applications can better be evaluated.

As Table 3.3 shows, the Cronbach alpha score is 0.247, which indicates moderate reliability between the measurements of sample diameter by GOM ATOS and CMM. The standardised items score is 0.428, which means inter-correlation is good and measurements are accurate. Standardized items are especially helpful in comparing different sets of data or systems that might use different ranges or methods of measurement. This would help to make judgments about the performance of each measuring system more objective; it would help the researcher to identify which system more accurately and reliably measures diameters in samples. The data is standardized, hence allowing the formulation of sound conclusions with

regards to precision and dependability of the measurement systems in place, imperative in retaining the quality and consistency of findings in research.

A detailed statistical analysis was carried out on the above experiment results to evaluate the accuracy, repeatability and intercorrelation of the two measurement systems. Results showed that the GOM ATOS and CMM presented repeatable measurements that showed both systems' measurement accuracy. It is also noticeable that the results of the systems are correlated but have good repeatability at room temperature, which justifies the selection of the GOM ATOS as a benchmark system for dimensional measurements at room temperature. But as this research aims to evaluate the repeatability and accuracy of the proposed system at elevated temperatures during hot forging, it's also essential to carry out an experiment where the sample part is heated at an elevated temperature and then measured with the GOM ATOS at that temperature. However, the GOM ATOS's measurement accuracy at an elevated temperature has still not been evaluated. Thus, the author carried out an experiment to evaluate the measurement capability of the GOM ATOS system at an elevated temperature.

The following section summarises the results of an experiment to measure the diameter of a metal cylinder at an elevated temperature to justify the need for a non-contact proposed system for real-time dimensional measurement of parts during hot forging. The CMM is a very precise system demonstrating good repeatability and that, through calibration, it can be considered accurate. Similarly, the GOM shows good similarity in the average value and repeatability and therefore can be considered a suitable alternative measurement solution.

3.3 Evaluation of the GOM ATOS performance at elevated temperature

Four steel cylindrical billets were measured at both room temperature (20 °C) and an elevated temperature (200 °C). A calibrated CMM machine was used to obtain the reference diameter of samples at room temperature. A total of four samples' diameters were measured in a heated state with the GOM ATOS, and CMM measurements were carried out at room temperature.

3.3.1 Dimensional measurement results of heated samples

The primary purpose of this experiment was to evaluate the accuracy and functionality of the current measurement system, i.e. the GOM ATOS, at an elevated temperature (200 °C for the current experiment). The reconstructed geometry of the heated sample had several hundred missing data points. Large grey areas in the reconstructed three-dimensional geometry are visual indicators of data dropout, particularly around the contours of the sample (Figure 3.3). By carefully considering the reconstruction errors that could be seen in areas where the data was missing, it is possible to estimate visually that about 25–30% of the total data points were lost during the measurement process.

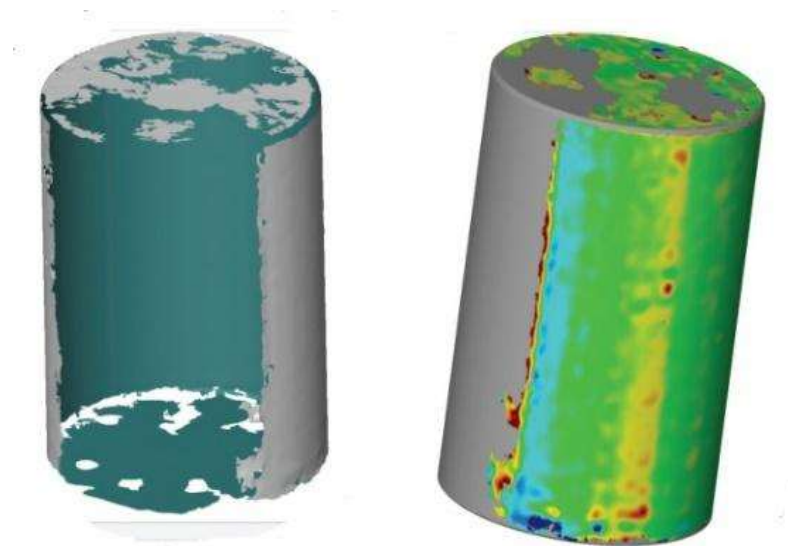


Figure 3-3 3D scanning of heated part with GOM ATOS showing infrared glaring

The percentages of data dropout are the ratio of measurement points that were not recorded successfully during dimensional measurement of the heated samples. The values are calculated by comparing the total number of measurement attempts to the number of successful measurements achieved for each sample.

Here, total measurement attempts is the full set of points or features to be measured in the sample, and failed measurements are those points which could not be correctly recorded or processed. The percentage indicates how much the measurement system has failed in high-temperature conditions.

This metric is critical for the dimensional measurement results of heated specimens, since it gives important information on how the system will perform and its reliability under harsh conditions. Elevated temperatures can cause a change in materials by either thermal expansion or changes in surface reflectivity, together with ambient conditions like air turbulence and thermal radiation that could interfere with the measurement process. A high data dropout rate indicates problems with data acquisition, possibly due to limitations of the sensors or the disturbances in the environment. By inspecting such dropout rates, this study evaluates the reliability of measurement systems like the GOM ATOS at elevated temperature, with an emphasis on their limitation and identification of the potentials for improvement to ensure accurate and reliable dimensional measurements also in real high-temperature applications.

The surface glare from the heated metal specimens also produces most of the drops in the data observed. Upon heating, the hot specimens created strong reflections which interfered with the optical sensors of the GOM ATOS system [20]. Such situations resulted in the "blindness" of the system and prevented it from acquiring the surface geometry with high accuracy. This phenomenon could mainly be observed in those regions with curved or angled surfaces, where strong reflections are typical. It contributes approximately 15–20% to the overall loss, being exclusively that part of the data.

Measurement technique is the last thing that contributes to data loss during measurement. The fringe projection technique system may not be capable of handling environmental conditions at high-temperatures, such as heat distortion and increased background noise. Such limitations may not enable the software to process the distorted signals properly and hence contribute to about 5% of the total data dropout.

Samples were measured at 200 °C because obtaining accurate reference measurements using the GOM ATOS was not possible at high temperatures, and no alternative measurement techniques were available for such conditions. CMM is a contact-based measurement system but cannot be deployed near hot metal parts. Hence, the author used thermal expansion formulae for metals to obtain the theoretical reference values from the measurements taken in the unheated state for CMM measurements after the part is unheated.

Most materials expand when heated or contract when cooled as higher temperatures rise and increase atomic vibrations. The thermal expansion process is such that for a given material, its dimensions change with temperature change. The expansion amount depends upon the thermal expansion coefficient of the material under consideration. Metals, for instance, generally have higher CTEs (coefficients of thermal expansion) than ceramics, meaning they expand more for the same temperature increase. When measurements are taken at temperatures other than the reference standard of 20°C, such as at elevated temperatures like 200°C, the object’s dimensions will not reflect its actual size at room temperature. Failure to consider this may result in a faulty conclusion on the compliance of a component with stipulated design specifications.

The formula for thermal expansion is very commonly used. It gives the change in length for any substance as a temperature change [81]. The equation accounts not only for the change in size but also for the final length the substance will have after it has been exposed to heating or cooling.

$$l_1 = l_0(1 + \alpha \cdot \Delta t) \tag{3.1}$$

$$d_1 = d_0(1 + \alpha \cdot \Delta t) \tag{3.2}$$

Here’s a breakdown of each term in (3.1):

l_1 = The final length of the material after the temperature change

l_0 = The initial length of the material at the reference temperature (typically 20°C)

α = Coefficient of linear thermal expansion (a material-specific constant that indicates how much the material expands per degree of temperature increase)

Δt = Change in temperature (final temperature – initial temperature)

Mild steel material was used for the samples. As the literature suggests, 11×10^{-6} [m/(m °C)] is the coefficient of thermal expansion of mild steel. The room temperature was approximately 20°C and 200 °C in a heated state during the experiment. The dimensions of cooled-down samples were measured with the CMM at room temperature. However, the values of diameter after adding thermal expansion values are mentioned in Table 3.4. It must be noted that thermal expansion values were only added to the final measurement values of

CMM. The dimensional measurements of heated samples were carried out with the GOM ATOS system at elevated temperatures; therefore, there was no need to add thermal expansion values to the final results through the GOM ATOS.

Table 3-4 Summary of dimensional measurement results and statistical analysis.

Diameter measurement(mm) of sample part at temperature 200 °C			
GOM ATOS mm	CMM result with calculated thermal expansion (mm)	Measurement error (mm)	Percentage error %
48.77	53.51	4.74	9.72
49.01	53.53	4.52	9.22
50.09	53.54	3.45	6.89
47.09	53.52	6.43	13.65

Table 3.4 shows the diameter measurement at 200°C with two different measuring systems, one from the GOM ATOS and the other from the CMM, compensated for thermal expansion. The table details four measurement samples and the differences between the two systems in measurement and percentage errors. This highlights the potential for significant errors in GOM ATOS measurements when measuring metal parts at elevated temperatures. (Figure 3.4).

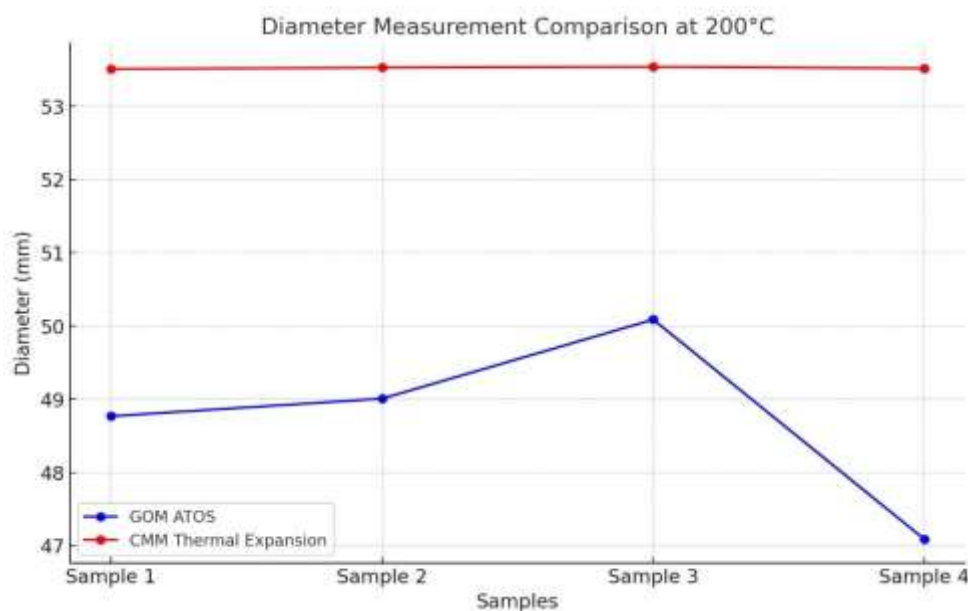


Figure 3-4 Comparative analysis of diameter measurements between CMM and GOM ATOS systems

3.3.2 Comparison of GOM ATOS and CMM at elevated temperature

The difference between the measurements is taken as the measurement error of the CMM and GOM ATOS. In this regard, the range is from 3.45 to 6.43 mm (Figure 3.5). Sample 4 follows with a maximum measurement error of 6.43 mm, suggesting that GOM ATOS grossly underestimates this sample against the thermally corrected CMM. Even the smallest measurement error, 3.45 mm for Sample 3, suggests that GOM ATOS struggles to provide accurate measurements under these conditions. These errors are notable because they reflect considerable deviation from the reference values obtained through the CMM machine, which corrects for thermal expansion, making it more reliable for high-temperature measurements.

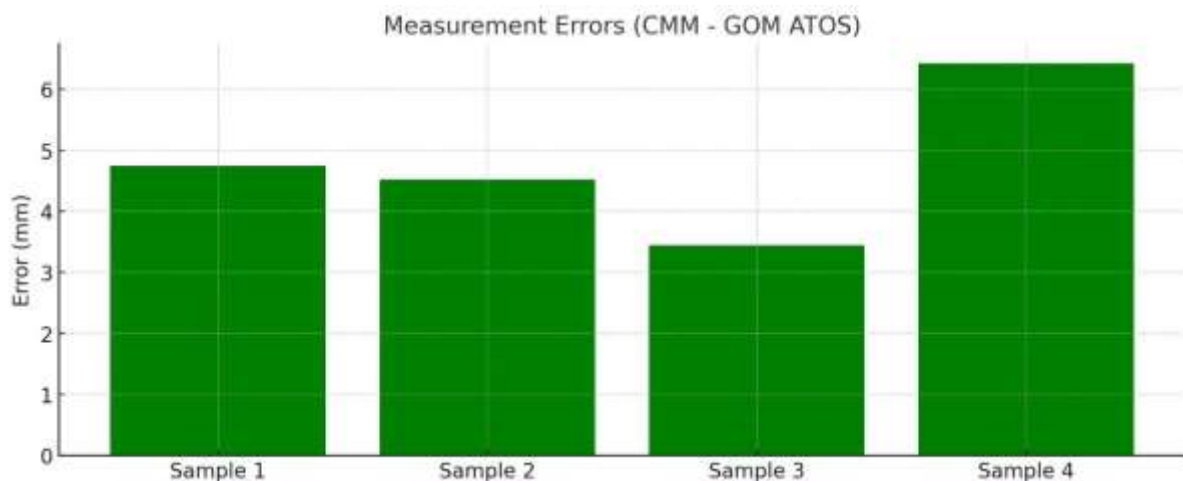


Figure 3-5 Diameter measurement error comparison of GOM ATOS and CMM at elevated temperature

The more extensive temperature condition further exposed the poor performance of the GOM ATMOS system,, with a percentage error ranging between 6.89% and 13.65%, the most significant error belonging to Sample 4. This shows that the GOM ATOS system deviated up to 13.65% from the actual dimensions in some cases, which is a significant deviation for a device mainly required to give results at a very high degree of accuracy (Figure 3.6). Even the most minor percentage error of 6.89% recorded for Sample 3 implies significant discrepancies.

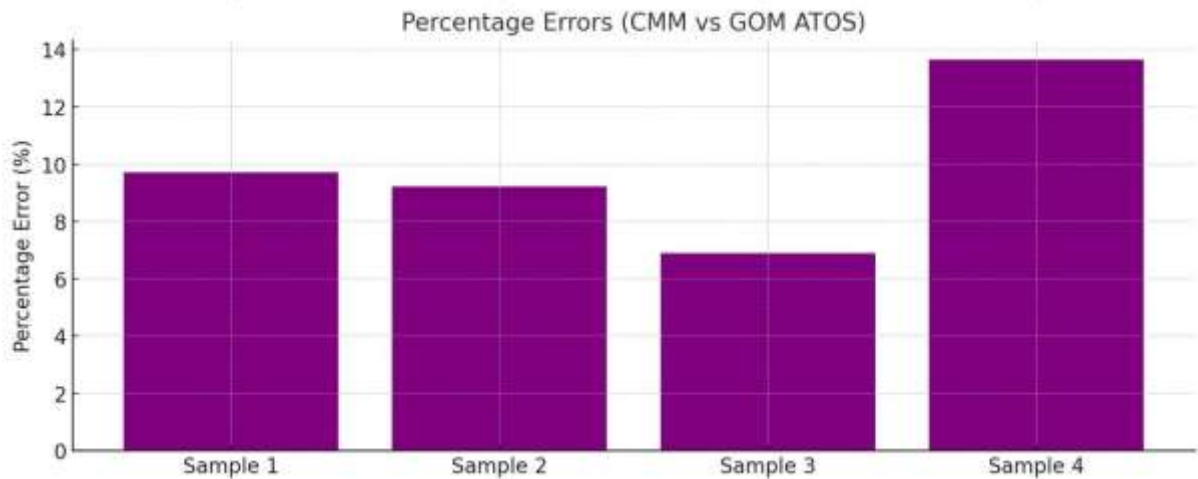


Figure 3-6 Diameter measurement percentage error comparison of GOM ATOS and CMM at elevated temperature

The relatively high percentage of errors further underscores the limitations of the GOM ATOS system in providing precise measurements at elevated temperatures, and they suggest that a more reliable, non-contact, fast and portable measurement system should be used for such applications. The GOM ATOS is quick, portable, and accurate at room temperature; therefore, it is considered a benchmark system for comparing the dimensional measurement results of the proposed system.

3.4 Proposed dimensional measurement system at elevated temperature

Accurate dimensional measurement in high-temperature environments is a unique challenge in forging processes. The extreme environment—meaning high temperatures, strong radiation of heat, and rapid deformation of the material—rules out traditional measurement methods. The industry requires a system that can perform exact measurements using a non-contact method under these harsh conditions with immediate feedback to optimize the process for prevention of defects.

A dimensional measurement system for hot forging should address the following requirements to take advantage of modern manufacturing demands, especially in the fields of automotive, aerospace, and energy.

High precision: The system should achieve a dimensional measurement error of not worse than ± 1 mm, independent of the size and complexity of the component. It is necessary that this level of accuracy is achieved to ensure the manufactured parts meet tight tolerance requirements, thereby reducing costly rework.

Real time feedback: Measurements have to be taken and analysed quickly, within seconds, so that any adjustments that are needed in the forging process can be implemented. Real-time data plays a critical role in the minimization of waste, improvement of efficiency, and continuity in production.

Temperature resistance: The system should be able of providing dependable consistency at up to 1200°C and be sufficiently capable of overcoming thermal distortion, heat radiation, and outside vibrations, which may disturb the accuracy of measurement.

Non-contact operation: In such high temperatures, it is impossible to maintain contact with the workpiece continuously; this will tend to destroy either the measuring equipment or the component being measured. A non-contact method eliminates such dangers and simultaneously maintains the integrity of measurements.

Integration capability: The system has to seamlessly integrate into existing industrial installations and workflows. Compatibility with Industry 4.0 standards like automation and intelligent data exchange, among other things, definitely counts in its favour.

The proposed measurement solution fits closely within the objectives of the current research study to overcome the deficiencies inherent in the measurement techniques presently adopted in high-temperature forging environments. Traditional methods largely rely on contact measurements or assessments after the process, which lack direct feedback, although direct feedback is very instrumental in improving the operations of the processes. In addition, the techniques create delays, increase material waste, and lower the potential for finding and eliminating manufacturing process defects.

The proposed non-contact optical metrology system provides an innovative approach to performing real-time dimensional measurements. This overcomes several key issues, such as thermal distortion and interference caused by reflective surfaces, to provide a reliable and accurate measurement in the most extreme conditions—importantly, it has the ability to

underpin the goals of the study in waste reduction and rework while offering wide-ranging efficiency in the hot forging process.

Additionally, it is based on more advanced algorithms and hybrid methodologies, emphasizing the key objective of this study: high precision and flexibility. The presented approach not only raises the accuracy of measurement but also enables the design of intelligent, automated systems in line with the principles of Industry 4.0. In this way, the proposed measurement system marks a significant step in closing the gap between innovations prepared in laboratory conditions and their industrial practice, thereby making a vital contribution to the field of forging technology.

In brief, a dimensional measuring system for high temperatures has to meet the challenges in accuracy, speed, and reliability under extreme forging conditions. The proposed measurement system forms the technological foundation for a reliable, non-contact solution. Its aim will be to incorporate advanced principles to meet industrial demands, improve production processes and hold on to consistent quality control.

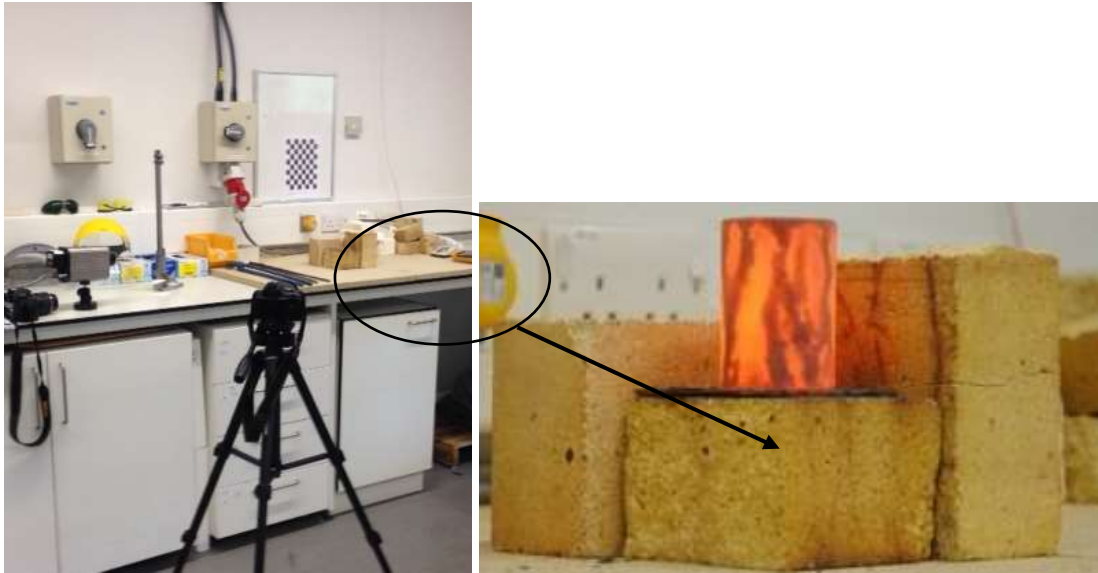
The proposed system integrates machine vision and photogrammetry techniques since both are robust, capture large areas and allow real-time analysis. A CCD camera was used to capture images from hot metal samples, while an image segmentation algorithm was developed to extract the geometry profile from high-resolution images. There is an example of using a similar system by researcher Fabijańska for carrying out an experiment to extract the hot metal parts geometry from images captured at elevated temperatures. Still, in that study, the limitation was that it was not explicitly used in hot forging applications [82]. In the current research, the experiments were carried out in a hot forging workshop for dimensional measurement of hot forged metal parts. This measurement is a pattern analysis task that, in general, is difficult to complete because component features must be retrieved from an image before measurements can be taken. Image processing techniques, including image segmentation, were performed to eliminate superfluous picture data and considerably simplify the analysis effort by using the luminance of the hot part. Furthermore, a novel algorithm was developed to achieve the pixel-level measurements of geometry during image processing, shape extraction, and elimination of glow around the part, which were the issues noted during the experiment. It is also worth noting that the CCD camera utilised in this study

has an automated gain feature that tries to change the gain dynamically to maximise image exposure. The automated gain feature adjusts the amplification of the camera's signal in response to the brightness of the scene being captured to maximise the exposure of the resulting image. Here "gain" refers to the amplification of the signal received by the CCD camera.

In principle, gain represents the level at which the strength of the signal is increased by electronic components inside the camera before processing and being converted into an image. The camera's automatic gain adjustment allows adaptation to the surrounding light conditions and provides well-exposed photos with good contrast and detailed information. The work may be extended by developing a vision-based dimensional measurement system that includes camera gain control in various ways or by using alternative filters, such as IR bandpass.

3.4.1 Experimental setup

The experiments were designed to determine the ability of initial equipment configuration. Therefore the same sample of mild steel cylinder was used in the current experiment. A small furnace was used to heat the steel cylindrical part until it reached 1200 °C. The temperature of the furnace was checked using thermocouples, which were placed inside the furnace. It was impossible to measure the internal part temperature as there were no holes on the part to attach the thermocouples so that a confirmed temperature could be measured. An IR camera was placed at a distance from the part to document the temperature degradation of the hot part. The camera recorded the temperature of the part while it was glowing. The experimental setup in which the physical arrangement of the camera on a tripod and hot workpiece used in the experiment are depicted in Figure 3.7.



(a)

(b)

Figure 3-7 Experiment setup; (a) Camera on tripod and hot workpiece, (b) Hot workpiece on ceramic bricks.

3.4.2 Material and part geometry

Material selection was an important step carried out as per the research findings noted in the literature review. The cylindrical samples were manufactured on a lathe machine to the required size (Figure.3.8). Part sizes were selected by considering the constraints such as geometry shape and space constraints (e.g., furnace size). Considering resource constraints, including machine size, surface finish and workspace, a sample part with dimensions of 79.5 mm in height and 53.4 mm in diameter was selected for heating and measurement purposes up to 1200°C. Before heating, the sample's initial dimensions were measured at room temperature (20°C) using a GOM ATOS scanner to establish a baseline for comparison.



Figure 3-8 Steel cylindrical part mild steel sample

3.4.3 Furnace and Camera Specifications

A high-temperature laboratory furnace was used to heat the metal components. A silicon carbide furnace is specifically designed for heating objects to high temperatures, ensuring uniform and consistent heating required for accurate measurements. Its robustness and high-quality construction provide rapid heating and can bear temperatures up to 1400 °C. This furnace has high energy efficiency due to low thermal mass insulation. Its heat-up time is 30 minutes, which makes it a good choice for lab-level experiments. The external and internal dimensions of the furnace are H x W x D (mm), 655 x 435 x 610, and 120 x 120 x 205 respectively [83]. Hence, it is suitable for small metal parts due to its internal size limitation. That is why the appropriate dimension of the selected metal part is a critical element of the experiment. The metal piece was kept inside the heated furnace for an hour. The furnace temperature was set to 1200°C with a 20°C temperature increase per minute (Figure 3.9).

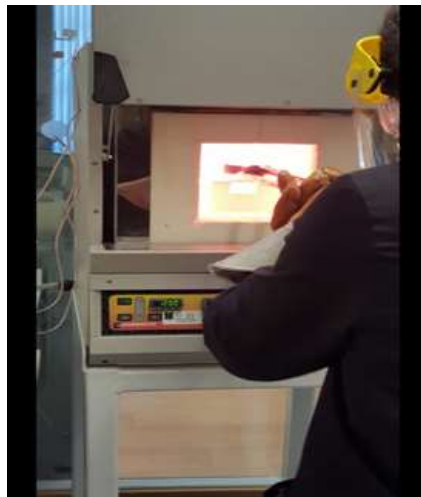


Figure 3-9 Molten metal piece handling at a furnace

After the hot metal piece was removed, it was placed on plain ceramic bricks to protect the laboratory floor. As the glow of the metal was rapidly diminishing with cooling, the camera settings had to be preconfigured to take good images. The settings used with the high-resolution digital camera were F5.6, ISO 1600, and a zoom range of 24-35 mm, which allowed it to get sharp images retaining the geometric details of the sample.

ISO 1600 refers to the sensitivity of the camera's sensor to light. This high ISO setting increases the camera's ability to capture images in low-light conditions, making it ideal for

photographing the cooling steel part as its glow fades. The higher sensitivity compensates for the diminishing light emitted by the metal, ensuring that sufficient detail is captured without requiring additional light sources. But high ISO values are likely to introduce noise into the photographs; however, a balance with the aperture (F5.6) and the infrared filter minimizes this effect, thus yielding clear and feasible pictures.

The camera also contains a special IR filter that helps to reduce thermal radiation interference and allows better differentiation of the geometric features of the sample. The employed IR filter possessed a wavelength spectrum specifically tuned for applications involving elevated temperatures, generally spanning from 700 nm to 1000 nm. This specific range proficiently diminishes the glare generated by the strong luminescence of the heated sample, while simultaneously permitting the camera to concentrate on the emitted infrared radiation, thereby improving image resolution.

The fixed zoom lens proved to be very important in the present study because it provided a controlled field of view and ensured consistent framing of the sample during the rapid cooling process. A fixed focal length, via the fixed zoom lens, decreased potential mechanical errors due to variable zooms and increased the precision of measurements. The compatibility of the system with the infrared filter improved its ability to capture high-resolution images and thus allowed for the accurate measurement of the size and surface geometry of the incandescent steel sample immediately after being taken out from the furnace. The combination of these requirements ensured the relevance of the imaging equipment to the research goal of evaluating the reliability of the intended machine vision system under high-temperature conditions.

The part geometry was captured at an elevated temperature of 1100 °C. Several black patches are noticeable on the surface due to oxidation and an aura effect due to high temperature of object's surface. The metal part was captured with background features, such as the insulation bricks, as depicted in Figure 3.10.

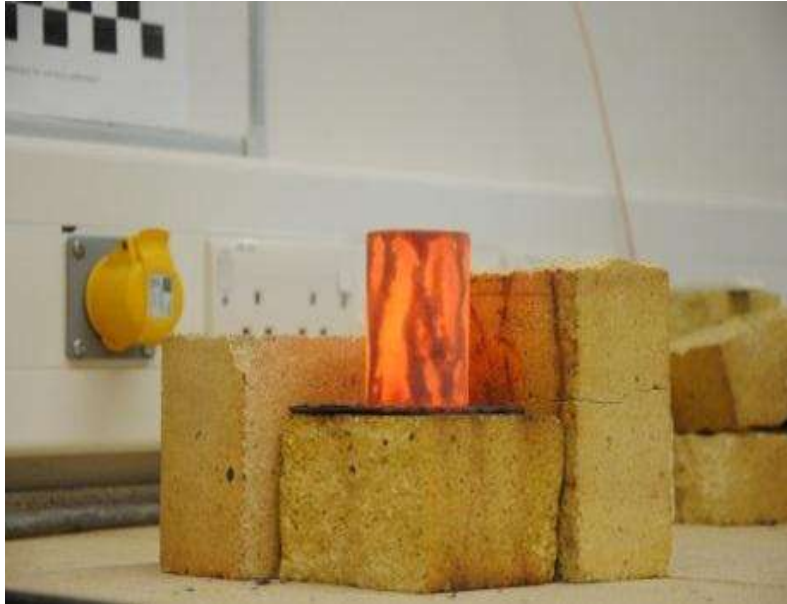


Figure 3-10 High-temperature sample image captured using Nikon D3100 with infrared filter and optimized settings

3.4.4 The dimensional measurement processes

The image processing algorithm performs dimensional measurements based on the specimen's shape analysis. The shape analysis was carried out through image segmentation, which helps to extract the specimen's shape by removing background and image noise. It has three separate regions: base area, background area, and specimen area.

Figure 3.11 presents a block diagram of the steps of a proposed algorithm for dimensional measurements in high-temperature environments. The workflow starts with camera calibration, which is an essential step to ensure that the DSLR camera (Nikon D3100) is set up in such a way that it eliminates distortions and provides accurate image data. In general, the calibration process encompasses intrinsic factors, such as lens distortion and focal length, and extrinsic factors, such as the spatial position of the camera with respect to the object being measured. This ensures that image acquisition, on which measurement depends, is consistent and reliable throughout the process.

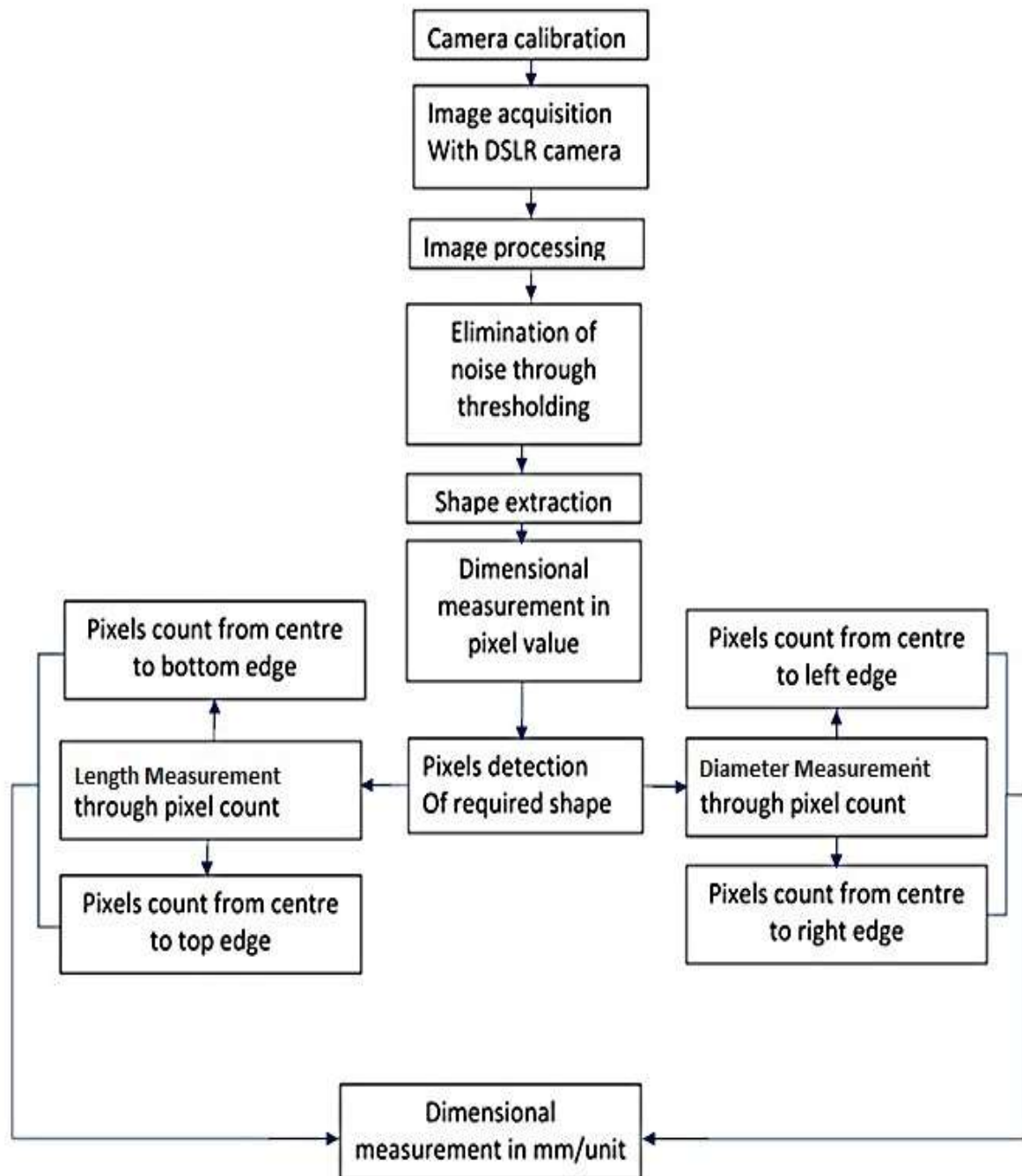


Figure 3-11 Block diagram illustrating the workflow of the proposed algorithm for high-temperature dimensional measurement

The high- resolution DSLR camera, with optimized settings of fixed zoom, set aperture, and an added IR filter, is used to perform This setup is crucial for taking clear images of heated components since glare and thermal radiation might reduce the

visibility of important features. Lastly, these acquired images are processed during the image processing stage, where enhancements are applied to improve their quality.

During the noise reduction process through the thresholding phase, such artifacts as glare and reflections, caused by the high temperature of the components, are removed. This helps to define the shape of the object by highlighting edges and borders, hence preparing the image for the next steps. During the shape extraction phase, analysis of the processed image is done to determine the geometric features of the object, including boundaries and contours. These features are very important for accurate dimensional analysis.

The dimensional measurement process starts with key parameters being calculated in pixel units. In the case of the length measurement, the algorithm counts pixels between the centre of the object and its top and bottom edges. Likewise, for diameter measurement, it counts pixels between the centre and the left and right edges. These pixel-based measurements are then converted into physical dimensions in millimetres or another physical unit through a predetermined calibration factor. The final step makes the dimensional data available in industry-relevant units, which concludes the measurement operation.

The novelty of the algorithm is that it copes with the problems caused by a high-temperature environment. The system incorporates IR filtering to reduce the influence of thermal radiation, which is quite rare in most traditional methods. It also allows for real-time processing to provide rapid feedback, which is necessary in industrial workflows. This algorithm is very important to the study because it deals directly with the need for non-contact, high-precision dimensional measurement in the area of hot forging applications. The real-time feedback contributes to manufacturing efficiency, waste reduction and quality assurance. Moreover, the non-invasive nature of the method provides greater safety and avoids measurement errors often associated with contact-based systems.

3.4.5 Camera calibration

Calibration is integral to image acquisition when undertaking dimensional assessments in machine vision applications. Calibration ensures that images acquired with a camera indicate actual size and geometric relations among real-world objects. Generally, the various calibration routines of cameras involve determining intrinsic and extrinsic parameters.

Intrinsic parameters refer to the internal characteristics of the camera, such as focal length, principal point and lens distortion. Extrinsic parameters describe the camera's position and orientation in relation to a world coordinate system, allowing the reconstruction of 3D relationships between objects.

In the experiment, images of heated metallic components were captured using a Nikon D3100 camera. Calibration was performed using the SpyderLensCal calibration tool (Figure 3.12). The setup for the calibration testing was done by positioning the SpyderLensCal board at a fixed distance of 700 mm from the camera while aligned on the same plane as the camera [15].



Figure 3-12 Camera calibration device[84]

This setup ensured that the board and camera were aligned horizontally, which minimizes the possibility of introducing angular distortions. Imaging was run for a series of 25 images, each focused on the central scale bar of the SpyderLensCal device to measure the precision of camera focus [84]. Some images exhibited front focus, while others displayed back focus. Ultimately, the intrinsic and extrinsic parameters of the camera were calibrated using those images that accurately focused on the middle value of the scale.

The SpyderLensCal tool provided a robust means of detecting camera distortions by comparing the captured image to the calibration grid. The scale values in the figures were used to correct for lens distortions and correctly measure geometric features in the images

obtained. The scale bar on the calibration apparatus ensured that the focus adjustments could be analysed and adjusted quantitatively [85].

Mathematical grounds of camera calibration rely on solving a camera matrix—a camera matrix that maps 3D points in the world to 2D points on the image plane. In the calibration process, correspondences must be established between the known 3D coordinates of points (on the calibration artefact) and their 2D projections in the captured images. These correspondences are then used to solve for the parameters of the camera matrix. A camera calibration matrix is a mathematical model of how a camera maps 3D points in real life onto 2D points on the image plane and includes intrinsic and extrinsic parameters, each of which plays a vital role in the transformations that real-world coordinates undergo to get accurate pixel coordinates for image-based measurements.

The general form of the camera projection matrix, often referred to as P , combines intrinsic and extrinsic parameters and is given by:

$$P = K[R/T] \tag{3.3}$$

where:

- P is the camera projection matrix, combining intrinsic and extrinsic parameters.
- The intrinsic matrix K contains information about the camera's internal characteristics, such as focal length and image centre.
- $[R/T]$ represents the extrinsic parameters: the rotation matrix R and the translation vector T , which define the camera's orientation and position about the world coordinate system.

In practice, calibration will involve minimizing this reprojection error, which is the difference between the ground-truth 2D image points and the reprojection based on the camera matrix. In any case, a calibration algorithm should provide an accurate estimate of the camera's intrinsic and extrinsic parameters by minimizing this reprojection error. Further, these parameters will be used for lens distortion rectification and real-world measurement extraction from the 2D image data [86].

The calibrated camera captured the geometry of heated metal parts, allowing for accurate dimensional measurement. The calibration process's guarantee of lens distortion correction played a key role in achieving reliable measurements. Calibration is essential in applications where high-temperature conditions may introduce optical distortions, as the camera's ability to accurately capture the object's actual dimensions is necessary for validating the dimensional analysis results.

Hence the process of camera calibration, performed with the Spyder-LensCal device and checked by a series of accurate images, provided the accuracy and confidence of the measurements obtained with the machine vision system (Figure 3.13). This step becomes essential for reliable dimensional control, especially when images are taken under adverse conditions such as high temperatures in hot forging.

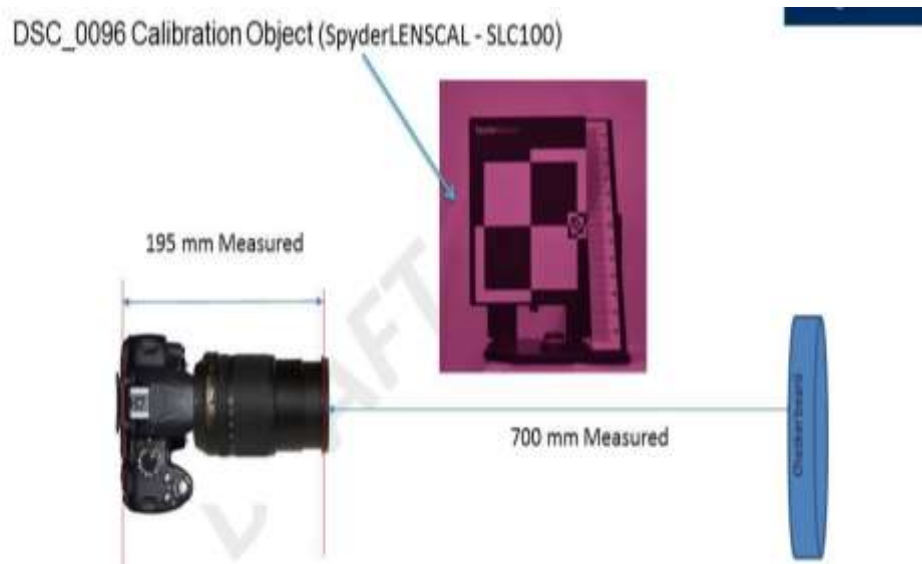


Figure 3-13 Camera calibration setup

The calibration matrix serves as the basis for projecting 3D real-world objects onto 2D images, preserving their spatial relationships. This will also be an essential tool in basic applications involving machine vision or 3D measurements concerning the captured images' reliability and precision. It provides robust dimensional accuracy because mathematical principles involve this process's intrinsic and extrinsic parameters. This is very important in practices like hot forging, where measurement precision may not be ideal.

3.4.6 Image acquisition of hot part

Image capture is the most critical stage in real-time processing. After calibrating and optimizing all the camera parameters, the next stage is to position the heated metal portion in front of the camera. The following parameters determine the distance between the camera lens and the heated metal.

1. The infrared radiation created by the heated metal component due to elevated temperature should not influence the camera lens.
2. During the forging process in the real environment, the camera lens should be kept at a safe distance because when a hot item is forged heavily, particles from the hot object can be spilt into the portion and damage the image-capturing equipment.

Therefore the distance between the camera and the imaging equipment was adjusted to 700 mm. This was the smallest distance between the camera and the hot object that allowed the entire experiment to run correctly without harming the instrumentation devices or disturbing the image quality. After adjusting all the equipment and metal parts in the appropriate position, the forging was started, and the image of the red-hot item was captured for real-time analysis.

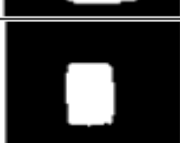
Digital images of the hot object, which is heated to 1100°C, are captured before and after the forging operation to complete real-time dimension measurement after adjusting the camera settings.

3.4.7 Image processing of monochrome image

After capturing the coloured image, it was converted into a greyscale through MATLAB. The image processing algorithms (Figure 3.11) produced good results while working with the greyscale image. Every greyscale image is represented through its pixel values. The computer represents each pixel in numbers ranging from 0 to 255, in which 0 refers to the darkest intensity and 255 represents the brightest intensity in each pixel. After that, image segmentation was carried out at different threshold values (100 to 200 pixels) to find the right threshold level for extracting the required metal piece shape from the image. To achieve good results, a trial experiment was carried out on five images of the same hot part taken during the experiment to optimize the threshold values. Each image had the threshold set at two levels: maximum and minimum. Table 3.5 shows the results of this preliminary experiment.

Results demonstrated that the required shape extraction was successful when the minimal thresholds were below 60 and above 190, and the maximum thresholds were between 120 and 180.

Table 3-5 Threshold levels for image segmentation

Image	Threshold level		Metal part extraction success		Images
	Minimum	Maximum	Minimum	Maximum	
1	60	175	No	Yes	
2	82	210	No	No	
3	124	180	Yes	Yes	
4	155	199	Yes	No	
5	167	190	Yes	No	

Moreover, the hot part was placed on ceramic bricks, and background objects were visible in the image (Figure 3.9). Part reflection was another hurdle to the applied image processing operation due to having the same light colour. The best threshold range acquired from Table 3.5 was then applied to the required image (Figure 3.14) for image processing. The initial test results showed that the thresholding program was not able to eliminate all unnecessary details from the image due to the same light intensities of molten metal ingot and other light sources such as sunlight.



Figure 3-14 Image thresholding at elevated temperature

Therefore, it was postulated that the molten metal exhibited a higher spectral intensity in the red wavelength region than the surrounding objects in the background. As only the workpiece geometry was required for dimensional measurement, unnecessary details such as noise, surface reflection and unwanted information were eliminated from the captured image before processing it for dimensional measurement.

3.4.8 Image processing of I-R image

Hot parts emit an immense amount of radiation in this I-R spectrum range during hot forgings, and common DSLR cameras are normally sensitive to this light, which is near the spectrum range (700 nm-1550 nm) [87].

The infrared filter used in this measuring device has unique transmission characteristics, especially for measuring dimensions at high temperatures. This means that within the visible range, between 400 nm and 790 nm, it should block all wavelengths to ensure any form of visible light, including the reflected rays from the heated component, is well suppressed. This blocking capability ensures that no visible light interferes with the system's efficiency in making accurate measurements. While most filters would block at this critical cut-off point of 790 nm, this filter switches to complete transmission, allowing 100% of light in the infrared spectrum above 790 nm to pass through. This becomes quite important in high-temperature measurements where the system should detect infrared radiation emitted by the hot metal part. It ensures thermal insulation, preventing distortions caused by thermal glare or interference from visible light. It also provides greater measurement accuracy since the filter focuses only on infrared wavelengths and not visible light.

A trial test was performed in a lab to evaluate the effect of an IR filter on image analysis in MATLAB because an IR pass filter could block wavelengths below 790 nanometres. So, a cylindrical metal part was heated up to 1100°C and pictures were taken at different temperatures with the camera having an IR filter attached to the lens (Figure 3.15).

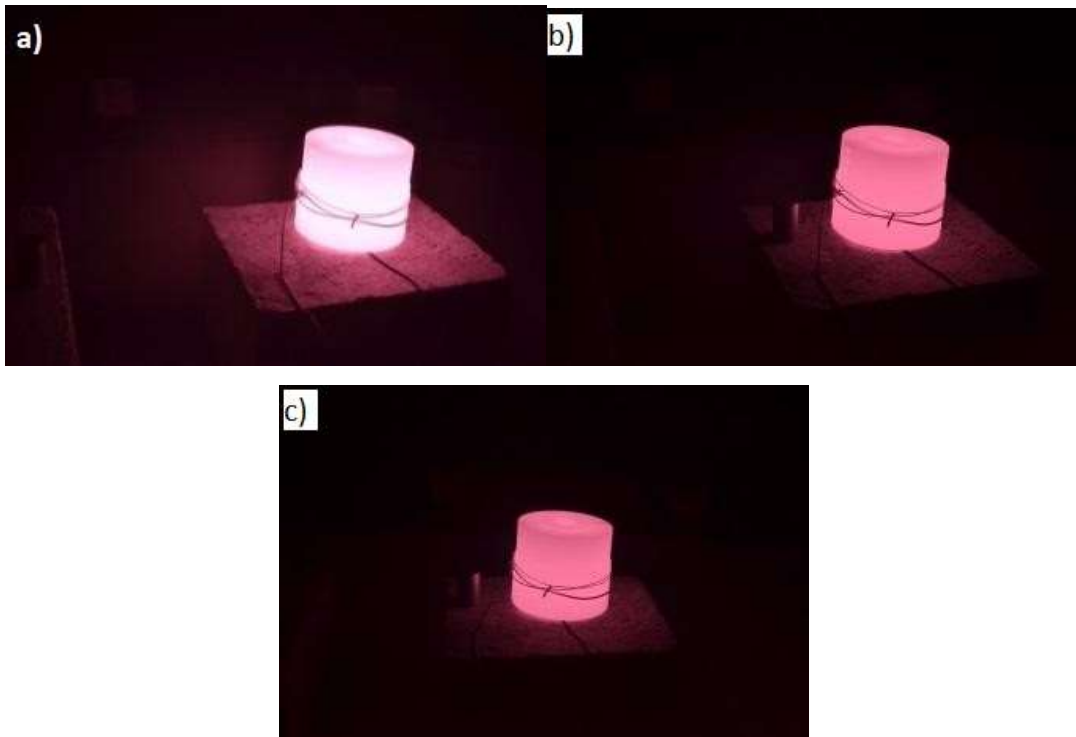


Figure 3-15 Picture taken with Nikon D-3100 (I-R filter); a) aperture= F5.6, temperature=1100°C, b) aperture= F5, temperature=900°C c) aperture= F5.6, temperature=850°C

Black cardboard was used in the background to avoid unnecessary objects and light reflection in the captured image. The camera with an IR filter with a live view was focused on the hot metal part, which can be seen in Figure 3.15a, where the metal object is more focused than in Figure 3.15b and Figure 3.15c. In this process, the I-R filter helped to focus the hot objects by illuminating the light intensities different from the light intensity of the hot objects. Hence images were significantly improved, and geometry was more precise with a dark background compared to the images in Figure 3.16.

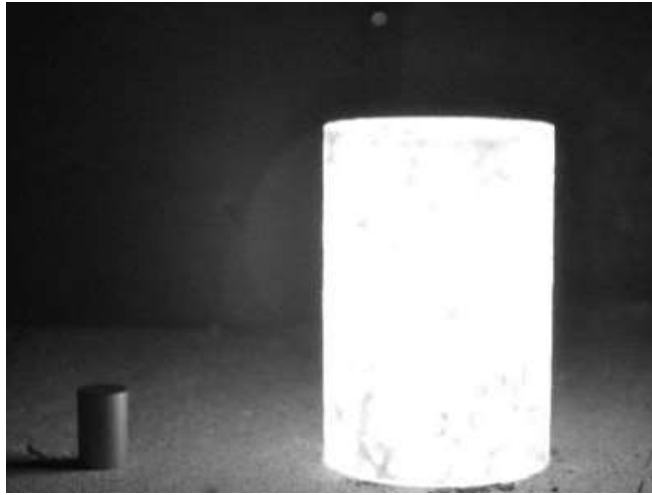


Figure 3-16 A picture captured with I-R filter (monochrome)

The same setup with an IR filter was then applied to capture images of a cylindrical object, and the image with the I-R filter was shown. Image processing operations on the captured image then eliminated unnecessary details, as shown in Figure 3.17.

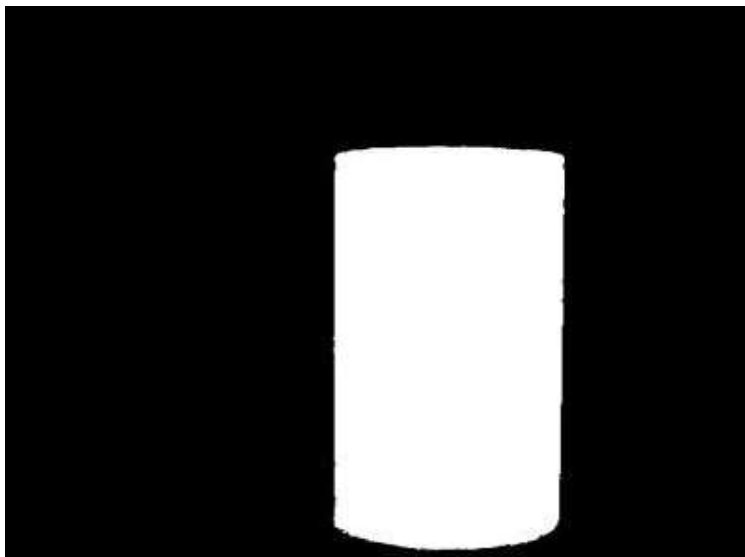


Figure 3-17 Threshold IR image

The threshold image eliminated all the unwanted details, such as part reflection, background noise, and part oxidation marks (Figure 3.17). The experimental result shows that a wide range of threshold values work with I-R images over ambient light conditions. The experimental results regarding geometry recognition are more reliable and accurate, which

can further help increase the robustness of dimensional measurement of hot ingots during forgings.

3.4.9 Physical filtering

The Plank body radiation formula explains that the radiation spectrum of hot metal specimens between 800°C and 1200°C is infrared, in which red solid light with a wavelength could be longer than 600 nm. Hence physical filtering techniques could be suitable for minimising the disturbance of intense visible light during dimensional measurement [40]. Optical filters are highly effective for this purpose, as they enable physical filtering by regulating the light entering through the camera lens. In this way, only the required wave band can enter the lens while others are eliminated. Thus, the image resolution, while imaging hot parts, can be decreased due to high temperature, background noise, and halation around the hot specimen. Hence an infrared filter is mounted on the Nikon D-3100 camera lens to achieve high-quality images by filtering the strong visible light in the I-R band.

The IR filter in the dimensional measuring system is designed to minimize only the impact of glare and interference due to visible light, with particular emphasis on high-temperature levels. This kind of filter cuts off at 790 nm, which means below this limit, all wavelengths of light are blocked, thus effectively eliminating visible light, including bright red light emitted by metallic surfaces when heated [88]. This filter allows only infrared radiation with a wavelength greater than 790 nm to pass through, so the camera focuses only on the relevant infrared information necessary for accurate dimensional measurements.

This filter is made of optical glass that can withstand harsh conditions at high temperatures during the forging process. This long-pass filter is intended to block any shorter wavelengths, such as visible light, yet transmit longer ones in the infrared spectrum. This property contributes to reducing glare, halation, and various forms of noise originating from thermal radiation that could lead to degradation in captured images and diminished accuracy in measurements.

This IR filter mounted on the Nikon D-3100 camera provides better clarity of images and focuses on the hot workpiece for better geometry recognition. This filter finds excellent application in acquiring accurate dimensional data in the temperature range between 850°C

and 1100°C, thus making it an essential component in high-temperature industrial applications where infrared solid emissions greatly impede visibility.

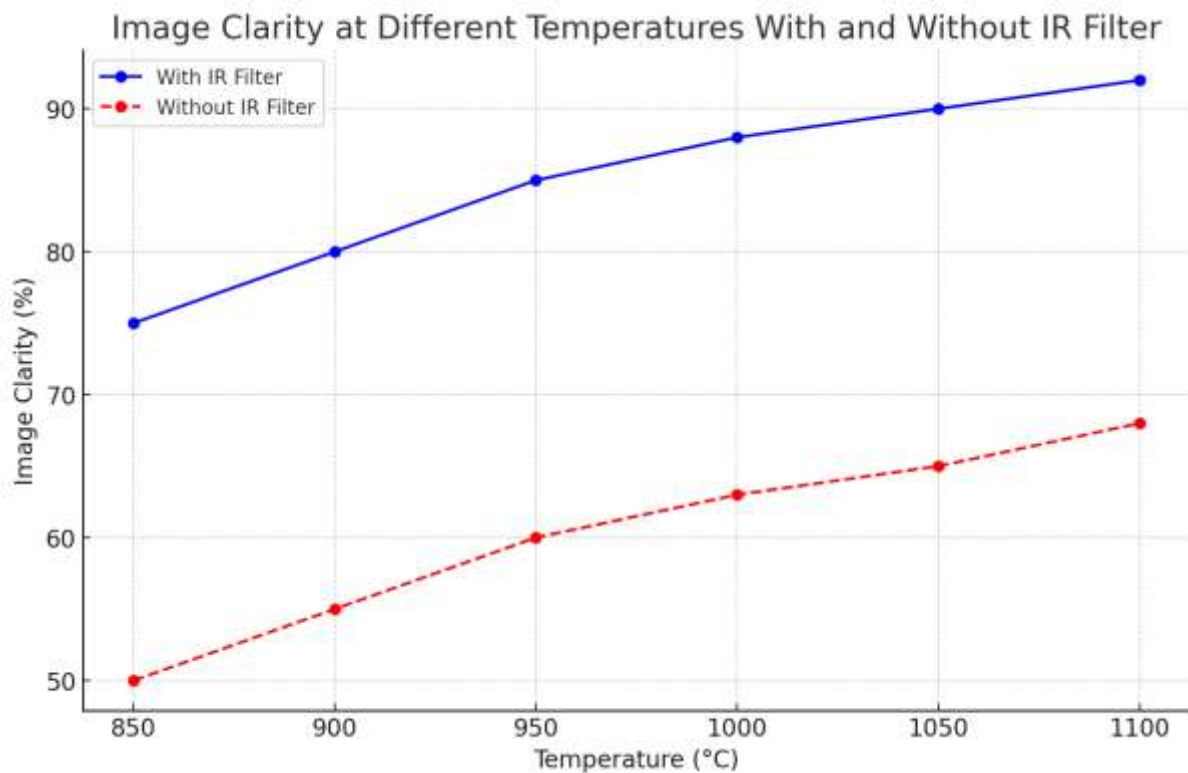


Figure 3-18 Image clarity at different temperatures with and without IR filter

Figure 3.18 shows the contrast in image clarity between using and not using an IR filter for a range of temperatures between 850°C and 1100°C, showing distinct enhancement of image clarity with the use of the IR filter.

With the IR Filter: As the temperature increases from 850°C to 1100°C, the image clarity improves steadily, reaching about 92% clarity at 1100°C. This would suggest that this filter efficiently decreases interference by visible light and halation, providing more transparent images for dimensional measurements at elevated temperature.

Without IR Filter: Without the IR filter, image clarity remains very poor, reaching only about 68% at 1100°C. The absence of the filter does not cut off the visible light, mainly the red light, which distorts the image and lowers the accuracy of geometry recognition.

This is absolute evidence that IR filtering is highly important in ensuring high image clarity in high temperatures and accurate dimensional measurement during the hot forging process.

The filter enables the camera to perceive infrared data relevant to the application while excluding visible light to enhance the performance of the measurement system.

3.4.10 Image de-noising

When images of hot specimens are captured in an uncontrolled environment, the most noticeable factor is image noise, which can bring errors to the results of vision measurement. This noise can be divided into two categories: dark and random noise [89]; hence, in capturing pictures with a CCD, the noise is unavoidable because of making errors (as aforementioned) in the measurement results. As a result, the characteristics of the noise of the CCD need to be calibrated.

When no light arrives at the photosensitive pixels, there is a dark current noise, which shows the output of CCD; to reduce its influence on images, 20 images were captured when the aperture was closed. Their average was used as the evaluation image for the dark current noise. The dark current noise was then restrained when every image was subtracted from this evaluation stage. As for random noise, median filtering and mathematical morphology filtering methods were applied to reduce it, and the distinct edges were sustained simultaneously. The proposed algorithm for dimensional measurement of the hot specimens could perform various important tasks such as camera calibration, image processing, noise removal, shape extraction from the background, dimensional measurement at the pixel level and dimensional measurement at the millimetre scale.

Gradient masks were used to extract the specimen's shape by eliminating the background and noise in the captured image [39]. Gradient masks are important in image processing, especially for edge detection and determining the outlines of an object in complex scenarios that include high-temperature assessment. In the algorithm put forward in this work, gradient masks are used to detect object outlines through noise suppression and segmentation of regions of interest based on intensity gradients.

In image processing, an image's gradient represents some directional change in intensity or colour. In applying this gradient mask, the algorithm picks up significant changes in pixel intensity, which generally occur along the boundaries of an object [90]. The following equation represents the necessary mathematical process underlying the extraction of the gradients:

$$|\nabla L(x,y)| \approx |h_x \otimes L(x,y)| + |h_y \otimes L(x,y)| \quad (3.4)$$

where:

h_x is the horizontal derivative mask,

h_y is the vertical derivative mask,

\otimes represents the convolution operator, and

$L(x,y)$ is the intensity function of the image.

Equation 3.4 approximates the gradient of an image by convolving the intensity function $L(x,y)$ with horizontal and vertical derivative masks. These masks show edges as sites of sharp variation in intensity in the x and y directions in a manner that delineates objects.

A gradient mask is thus applied pixel by pixel to identify an object's shape against the surrounding background. Regions that have lower intensity values, which typically represent the background or noise, are rejected. Pixels with higher intensity levels usually represent the object being studied and will be specifically kept for further evaluation [11]. The **intensity gradient** has long played a crucial role in boundary detection, in which large contrasts between neighbouring pixels are emphasized as part of the image. In this case, the difference is of special concern at locations where the hot temperature metal specimen intersects with the ambient background. To carry out such demarcations, the gradient of the image intensity function, represented as $\nabla L(x,y)$, is determined, as in Equation 3.4.

Once the regions of high intensity are detected, **image segmentation** is carried out to delineate the object from the background. The gradient mask removes pixels with intensities similar to the background while highlighting the ones that represent the heated metallic object. This segmentation process ensures that only the relevant parts of the image are analysed for dimensional measurements (Figure 3.16).

The accuracy of this process is directly related to the pixel size calibration in the experimental setup. The size of a pixel K is determined using a standard calibrated object of known dimensions L_0 . The relationship between pixel count N and the actual size is given by:

$$K = L_0 / N \quad (3.5)$$

Once an equivalent pixel size of a calibrated object is determined, the same experimental setup can be applied to measure the unknown dimensions of a hot specimen through Equation 3-5:

$$L = K x N' \quad (3.6)$$

where:

N' is the number of pixels across the object, and

L is the calculated dimension of the object.

This process ensures that the dimensional measurements are accurate, even when the object is imaged at elevated temperatures where glare and noise could otherwise interfere with the results.

3.4.11 Blob analysis

Blob analysis is one of the more simple methods employed in image processing and involves identifying and computing definite regions within a binary image. In hot forging for dimensional measurement, blobs are the regions identified matching the heated metal objects. The algorithm reads the binary image, which results from converting the greyscale image (Figure 3.19). In the case of this research, the blob analysis is applied to separate the workpiece of the hot-forged material from the image back ground to allow immediate measurements at raised temperatures. [91]

A blob is a connected set of pixels that share similar intensity values. Blob analysis starts by detecting all forms that can be present in the image - the so-called "blobs" - and then removes those smaller ones that are less relevant. Therefore, the most crucial goal is to detect the biggest blob, representing the object under study, and remove smaller blobs coming from noisy signals, reflection, or another type of interference. From the mathematical point of view, the algorithm segments the binary image $g(x,y)$ by labelling distinct regions using Equation 3-7:

$$g(x,y) = \begin{cases} 1, & \text{if } f(x,y) > T \\ 0, & \text{if } f(x,y) \leq T \end{cases} \quad (3.7)$$

where:

$g(x,y)$ is the output binary image,

$f(x,y)$ is the input grayscale image, and

T is a threshold value that distinguishes the object from the background.

After removing the noise, blob analysis was performed on the target object with a well-defined boundary. This was calculated using the computer vision toolbox in MATLAB.



Figure 3-19 Image segmentation process and results of image segmentation

Blob study is a machine vision approach focused on analysing consistent image regions, in which an area is any subset of image pixels. It is the most basic method of image processing to examine the shape features of an object, such as the presence, number, area, position, length, and direction of lumps. The statistics of the labelled region in the binary image were computed using this approach. The Blob analysis solution consisted of the following steps:

- a. Extraction: After using image thresholding algorithms, the item's target region (the hot part in the image) was examined.
- b. Refinement: The extracted region was improved utilizing region transformation techniques throughout the refining phase.
- c. Analysis: The refined region was measured in the final phase, and the final findings were calculated.

The blob analysis algorithm was used to find and count objects and to measure their characteristics based on their regions.

The segmentation approach discussed in the dimensional measurement process primarily focuses on separating the hot metal part from the background in images. However, this measurement approach does not consider any sample tilt or misalignment. It assumes that the component is correctly aligned in front of the camera when it comes to extracting actual dimensions.

Accounting for tilt or misalignment is critical in some applications because such factors can lead to inaccuracies in the measured dimensions. For instance, in a tilted sample, the geometry projected will result in a distorted shape; the computed dimensions, such as length or diameter, will not give the actual dimensions. In this case, a calibration technique or correction algorithm must be applied to get accurate dimensional measurements, regardless of any misalignment.

Tilt correction is not required in the present application since the setting and nature of the measurements are controlled. The heated object is systematically placed on a flat surface, such as ceramic bricks, so that the camera can capture the geometry under consideration without significant tilt or misalignment. The controlled experimental parameters and camera setup—dimmed with a precise alignment at a constant 700 mm distance from the heated object—reduce to a minimum the occurrence of tilt, which can greatly affect the output.

The system is fundamentally designed to be repeatable and reliable in an environment with minimal possibility of tilt or misalignment. Therefore, complicated compensation techniques that might account for misalignment are not required since the setup provides consistent and reliable measurements without additional correction algorithms.

3.5 Validation of proposed system

For validation, the diameter and length of a mild steel cylinder are measured at ambient temperature using a CMM and at elevated temperature through the proposed measurement setup. Since the CMM is a highly accurate and repeatable device, it was used as a reference to check the accuracy of the proposed measurement setup.

3.5.1 Part measurement at room temperature using a CMM

The cylinder's diameter and length were measured by a CMM using a calibrated probing system to obtain highly accurate readings. Diameter measurements were taken across the

point of the circular cross-section, while length measurements were taken from the top to the bottom surfaces.

At room temperature, the cylinder's diameter was 53.4 mm, and its length was 79.5 mm. These measurements were used as reference values for subsequent comparisons with the proposed system and during heated conditions.

3.5.2 Elevated temperature measurements using proposed system

The mild steel cylinder was heated to 1100°C and placed at a distance of 700 mm from the infrared-modified camera in the proposed system. Several images were captured, and the most suitable image was processed using a custom image processing algorithm developed in MATLAB.

The proposed system calculates the number of pixels corresponding to the object's dimensions, which are then converted into millimetre values. This pixel-to-millimetre conversion allows for accurate geometric measurements of the heated part.

Figures 3.20 and 3.21 illustrate the results of the diameter and length diameter measurement (Figure 3.20). The nominal diameter of the cylinder at room temperature was 53.4 mm. The proposed system measured the diameter at elevated temperatures within a range of 53 mm \pm 0.5 mm. This indicates a measurement error of less than 1 mm, which is within acceptable limits for industrial applications requiring real-time monitoring during hot forging. At room temperature, the cylindrical specimen was measured to have a length of 79.5 mm. Under elevated temperatures, the measurement system recorded the length as 79.0 mm with a tolerance of \pm 0.5 mm. The observed measurement error remained below 1 mm, demonstrating the system's ability to accurately measure the component under high-temperature conditions (Figure 3.21).

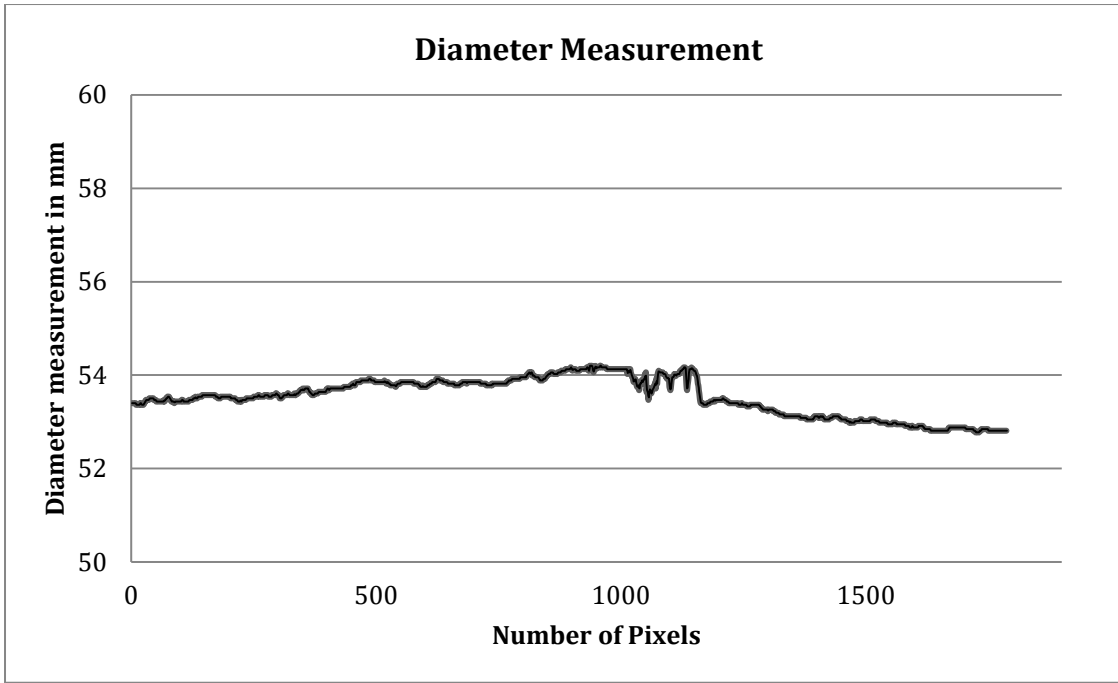


Figure 3-20 Diameter measuring results of workpiece at elevated temperature

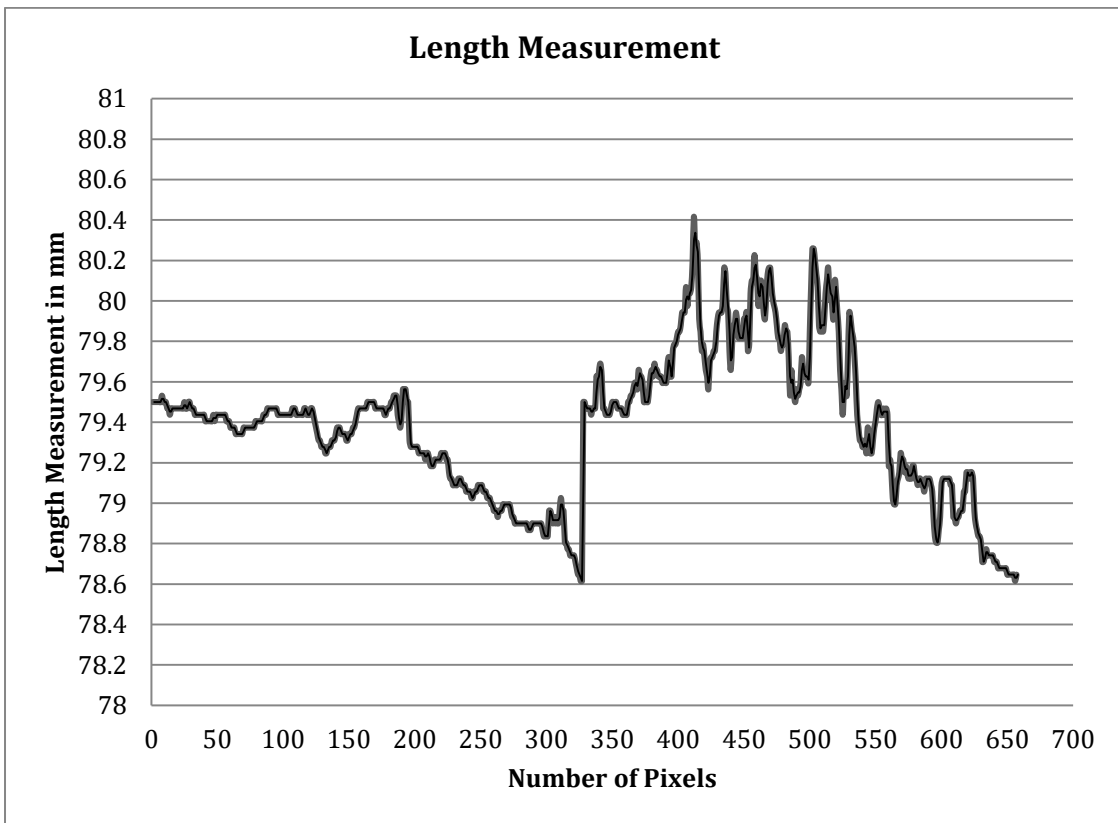


Figure 3-21 Length measuring results of workpiece at elevated temperature

3.5.3 Justification of proposed system in current research

This system also demonstrates its capability of measuring the diameter and length at higher temperatures with a minimum deviation within ± 0.5 mm, which is sufficient for on-the-spot dimensional measurement in hot forging processes. Furthermore, this system's capability of measuring dimensions without contact makes it highly suitable for high-temperature conditions where earlier conventional systems of contact-based measurement, such as coordinate measuring machines, may be inefficient or dangerous.

3.6 Conclusion

This chapter has provided an in-depth exploration of the experimental methodologies used to evaluate the dimensional measurement capabilities of non-contact optical systems, particularly the GOM ATOS fringe projection system, in the context of hot forging applications. Through a series of preliminary experiments and comparative analyses, several critical insights into the system's performance, strengths and limitations have been uncovered.

The first part of the chapter focused on understanding the limitations of traditional contact-based measurement systems, such as Coordinate Measuring Machines (CMMs), which, while highly accurate, are unsuitable for real-time measurements during high-temperature processes due to their contact-based nature and inability to function safely in extreme heat environments. In response to these limitations, the GOM ATOS system was selected for this research based on its ability to perform non-contact, high-precision measurements using the fringe projection technique. This technique allowed for the detailed capture of complex geometries by projecting structured blue light onto the surface of the workpiece, with deviations in the fringe patterns providing the necessary data to reconstruct the object's three-dimensional geometry.

The chapter outlined the system's technical specifications and explained the fringe projection technique in detail. The GOM ATOS system demonstrated excellent accuracy, with its structured light approach proving particularly effective for measuring parts at room temperature. However, when tested at elevated temperatures, significant challenges were encountered. These included data dropout due to glare from the heated surface, spectral interference from infrared radiation and software limitations in handling high-temperature conditions. Despite these issues, the system proved effective at room temperature and for

lower-temperature applications, where its non-contact capabilities provide clear advantages over traditional methods.

To assess the system's accuracy and reliability, the GOM ATOS measurements were compared with those obtained using a CMM. The results showed that the GOM ATOS system can perform accurate dimensional measurements at room temperature, with minimal deviation from the reference values obtained via the CMM. However, as the temperature increased to 200°C, the accuracy of the GOM ATOS system decreased significantly, with measurement errors ranging from 6.89% to 13.65%. These findings indicate that while the GOM ATOS system is highly suitable for room temperature measurements, its current configuration is not optimal for high-temperature applications due to the interference of thermal effects on optical sensors.

To address the challenges associated with measuring hot forged components, a novel non-contact dimensional measurement system was proposed, integrating machine vision and photogrammetry techniques. The system was designed to capture the geometry of metal parts at elevated temperatures using a CCD camera and advanced image processing algorithms. Initial trials of the proposed system demonstrated promising results, with the system achieving accurate geometric measurements within ± 0.5 mm at temperatures up to 1100°C. The system's ability to perform non-invasive, real-time measurements without physical contact makes it an ideal candidate for high-temperature industrial applications, where traditional methods fall short.

In conclusion, the experimental findings presented in this chapter highlight both the potential and the limitations of current non-contact optical measurement systems, particularly the GOM ATOS, in high-temperature environments. While the GOM ATOS system excels in room temperature conditions, its performance at elevated temperatures is compromised by factors such as infrared interference and data loss. The proposed system, however, shows great potential for overcoming these limitations, offering a reliable and accurate alternative for real-time dimensional measurement during hot forging processes.

The work presented in this chapter provides a critical foundation for future research, which will focus on further refining the proposed measurement system to improve its robustness and accuracy in high-temperature applications. By addressing the challenges identified in this

study, the proposed system can potentially revolutionize the way dimensional measurements are performed in the forging industry, contributing to enhance process control, reduced material waste and improved product quality.

4 Photogrammetry system evaluation

4.0 Introduction

In recent years, the demand for high-precision dimensional measurements in industrial forging processes has highlighted the limitations of traditional contact-based measurement methods, particularly in high-temperature environments [92]. Accurate, real-time measurement of parts during hot forging not only ensures quality control but also enables immediate corrective actions that can prevent costly rework and material waste. In such a scenario, non-contact measurement systems offer a viable option; however, they face significant challenges because of high temperatures and other environmental conditions common in the forging environment. Chapter 4 discusses the assessment and characterization of a proposed non-contact dimensional measurement system, which has been specially designed to overcome such challenges, thus allowing accurate, real-time data acquisition under challenging industrial conditions.

Building on the initial experiments and findings from Chapter 3, this chapter examines the performance of the proposed system in an industrially realistic environment, with temperature ranges extending from 1000 °C to 1250 °C. Unlike the controlled laboratory environment used in preliminary testing, this setting introduces additional complexities such as thermal radiation, heat-induced distortions and variations in part alignment. The main goal of this extensive research is to critically evaluate the ability of the system to provide accurate and reliable measurements across different stages of the hot forging process, and to analyze its viability for maintaining reliability in real-world applications.

To assess the effectiveness of the system, a comprehensive testing methodology was formulated, involving three main phases: pre-forging, forging, and post-forging. During the pre-forging phase, mild steel samples—selected due to their mechanical properties at high temperatures—are machined to precise specifications in preparation for the ensuing heating process. Subsequent to this, the samples are heated at the set forging temperatures, the beginning of the forging phase; during this, high-resolution images are recorded to enable real-time dimensional measurement. This phase is of crucial importance, as it involves the most challenging conditions in which the accuracy of measurements as well as the system's

ability to withstand extreme thermal environments are tested. The post-forging phase involves cooling of the samples to room temperature, following which the specimens are scanned using the GOM ATOS 3D scanner. This scanning device is a reference system, providing a baseline against which measurements obtained by the proposed system during the forging phase are compared and validated.

A significant aspect of this study is the analysis of dimensional stability and repeatability across multiple sample sets. Sixteen cylindrical mild steel samples were prepared to allow for a statistically robust comparison of measurements taken under different conditions. The samples were selected with varying nominal diameters to test the ability of the system to measure components of different sizes accurately. The technique not only tests the precision of the system but also checks its flexibility and versatility over a range of dimensions, a crucial feature for industrial use involving size and shape variations. In addition, the intentional use of mild steel was driven by its thermal expansion properties, which allow for even dimensional changes that enable systematic measurement and analysis.

This chapter also explores the general goals of data reliability and stability in the manufacturing industry. A structured testing method is utilized to compare results based on the proposed system with results based on the GOM ATOS reference system using statistical methods to assess precision and accuracy. Confidence interval analyses, standard deviations, and paired-sample tests provide extensive information regarding the system's performance, comparing its adherence to industry standards for precision in dimensional measurement. This comparative analysis highlights the proposed system's ability to perform real-time, contactless measurements at high temperatures and its potential integration into quality control processes in hot forging applications.

Ultimately, this chapter aims to substantiate the feasibility of the proposed measurement system in an industrial environment, emphasizing the potential for enhanced productivity, precision, and quality assurance in hot forging. Through a rigorous experimental framework and comprehensive data analysis, this chapter contributes valuable insights into the application of non-contact measurement technologies in high-temperature settings, paving the way for future advancements in real-time dimensional control within manufacturing.

4.1 Part specifications, scanning methodology, and calibration process

4.1.1 Overview of experimental samples and preparation

The samples selected for this study were cylindrical mild steel components, chosen due to their robust mechanical properties and suitability for high-temperature measurement in forging. These samples were machined to stringent tolerances of ± 0.05 mm, ensuring dimensional consistency. Sample dimensions were determined based on equipment constraints, particularly the size of the forging machine and hammer. A set of sixteen samples was prepared to facilitate statistically robust measurement comparisons across various conditions. Each sample's initial dimensions were verified using the GOM ATOS scanner before hot-forging trials.

Figure 4.1 shows the quality control configuration used in hot forging, with a focus on real-time dimensional monitoring and inspection of heated components. The configuration uses proposed non-contact dimensional measurement that capture the geometry of components at high temperatures. The process ensures that measurements are precise as regards exact dimensions and then checked against stipulated tolerances. In doing this, real-time feedback allows quick adjustment to the forging process, eliminates material wastage to a significant extent, and produces parts that can reach industrial standards. This arrangement points out the importance of quality control in ensuring accuracy, efficiency and reliability in the forging industry.

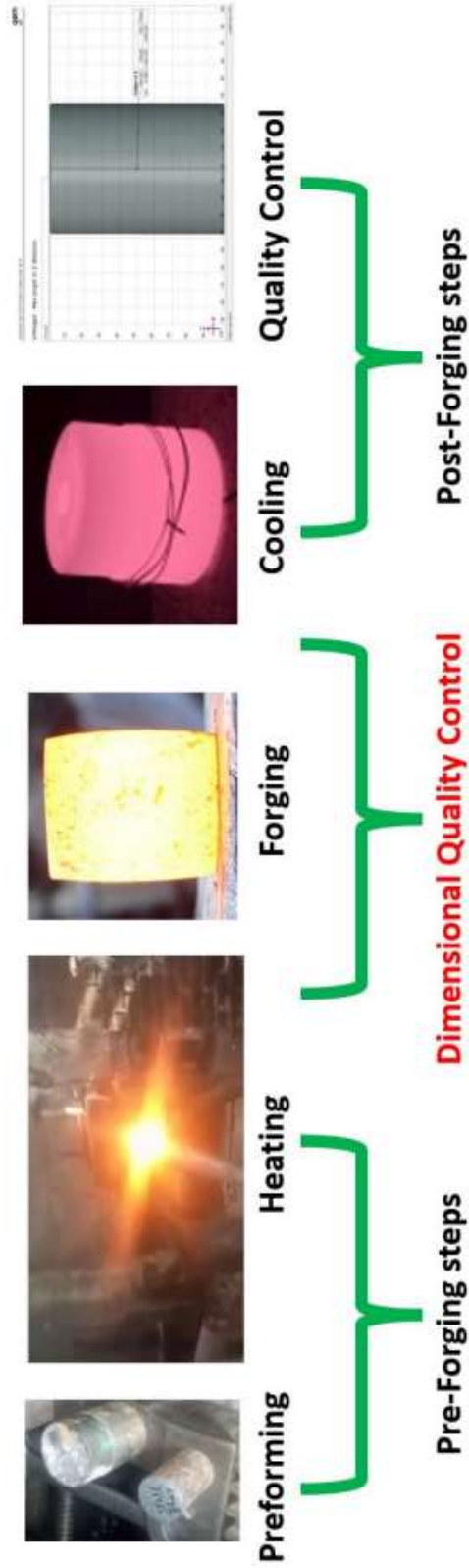


Figure 4-1 Quality control setup during hot forging

4.1.2 Scanning methodology using the GOM ATOS system

The GOM ATOS system employs structured blue light projection for non-contact surface measurement and two cameras to capture geometry photos simultaneously, producing a high-resolution 3D point cloud. Each sample was scanned in full 360° using a rotational stage with reference markers, allowing complete surface geometry to be captured. Although telecentric lenses can reduce perspective distortion by maintaining constant magnification regardless of sample distance, a non-telecentric lens was chosen for this setup due to its operational flexibility, cost-effectiveness and compatibility with the study's required range of distances and sample sizes [93].

4.1.3 Calibration of the GOM ATOS scanner

A rigorous two-part calibration was performed on the GOM ATOS system to ensure dimensional accuracy:

Intrinsic calibration: Intrinsic calibration was performed through standardized calibration panel, to correct for any optical distortion within the lens. This step aligned the focal and optical properties of the camera, achieving accurate pixel-to-distance conversion factors.

Extrinsic calibration: External calibration allowed the spatial reference points of the scanner to be aligned with the sample by using reference markers. This is necessary for creating a consistent coordinate system between various samples and avoiding errors due to positional differences. Reference objects with known sizes were also scanned to check the calibration accuracy, which was achieved successfully within the ± 0.1 mm tolerance set by the GOM ATOS.

4.1.4 Justification for using a non-telecentric lens system

While telecentric lenses excel in eliminating distance-related magnification errors, they come with limitations that impacted the decision to use a non-telecentric lens for this experimental setup. The primary reasons include [94]:

Flexibility across variable distances and sizes: Telecentric lenses are intended to operate at fixed, pre-determined distances, thus limiting their range of operation. In the current research, samples of different sizes were measured at different stages during the forging process. A non-telecentric lens offered the required flexibility to adapt to these variations,

allowing easy adjustments without the need for recalibration for every change in distance or sample size. This working flexibility was especially beneficial given the variable conditions inherent in the hot-forging process, where specimens can undergo slight displacements as a result of handling.

Cost-effectiveness: Telecentric lenses are defined by their high accuracy; however, they are costly and often require additional equipment to maintain a constant working distance. Non-telecentric lenses significantly reduce equipment costs and simplify the configuration process, while at the same time allowing for accurate measurements through controlled positioning and calibration. This cost-effective approach has made it possible to replicate the experimental setup in an industrial environment with low cost.

Compatible accuracy for required tolerance levels: While telecentric lenses minimize magnification variation, non-telecentric lenses can achieve high accuracy when used with careful calibration and positioning. In this study, the required measurement tolerance was achieved by controlling sample positioning relative to the camera and through rigorous calibration routines. The calibration protocol established repeatable positioning parameters, effectively mitigating the distance-related magnification errors common in non-telecentric systems.

4.1.5 Analysis of distance-related magnification error and mitigation techniques

The use of a non-telecentric lens can cause potential measurement inaccuracies due to differences in magnification as the distance between the sample and the camera changes. This effect is most significant in cylindrical samples, in which even small changes can greatly affect dimensional accuracy. However, these problems were overcome by adopting certain measures:

Fixed mounting and consistent calibration: To minimize positional deviation, the camera was mounted on a sturdy tripod, and sample placement was standardized. Consistent sample positioning relative to the camera reduced potential distance fluctuations. Calibration was repeated regularly to ensure that any potential shifts were identified and corrected.

Image processing and distance corrections: Advanced image-processing algorithms were applied to compensate for minor distance-related variations. Edge detection and depth correction techniques were implemented to reduce the effects of magnification variation on the measured dimensions. By incorporating these software-based adjustments, distance-related magnification errors could be controlled effectively, allowing the non-telecentric lens system to achieve reliable accuracy in measurements.

4.2 Measurement approach and system setup

The proposed measuring technique assumed that the actual shape of these geometrically basic objects may be determined (in the simplest instance) from boundary curves that are perpendicular to each other and detecting the edges of the forging in a photo can yield the boundary curves. Figure 4.2 depicts the system's layout with a camera, where measurements of forgings are achieved by using a camera in a parallel arrangement to the metal part placed in a hot forging die.

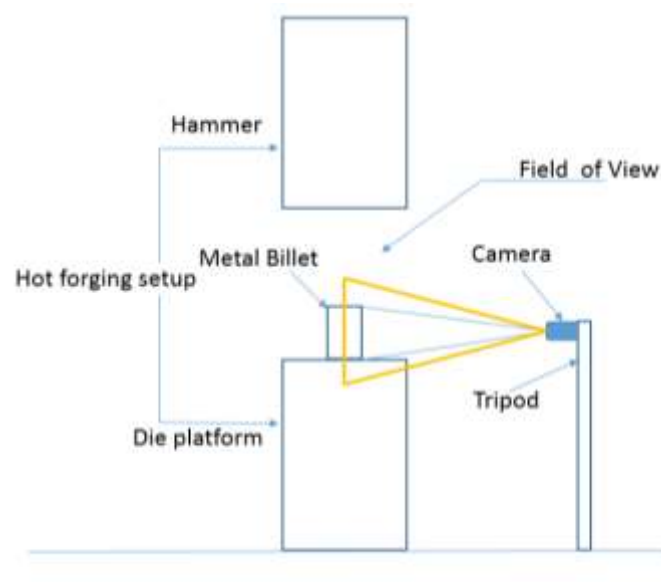


Figure 4-2 Configuration of the system proposed for the measurement of symmetrical forgings

A fixed focal lens can capture an image at a fixed distance from the metal sample without varying the lens resolution, so, a Nikon D3100 fixed zoom single-lens of 80mm reflex camera with a resolution of 15.1 megapixel was used in the current experiment, which can reduce background environment distortions while taking pictures of metal parts at high temperature. This algorithm is intended to provide a clear and concise representation of how the software operates, highlighting the key steps and processes involved in its functioning.

4.2.1 Camera calibration of proposed system

The correction of radial distortion in photographs is the first stage and was adapted and obtained from MATLAB's central database [95]. Metal parts geometries were captured with a fixed-lens camera. However, the distortion of the lens due to the heated metal caused problems with object detection due to the distorted proportions and coordinates of the image. This rendered the images unfeasible and decreased the precision of the system. One solution to the problem is to incorporate distortion correction techniques to acquire the most precise position of an object where a parallel grid structure considered as a base for correction, as shown in Figure 4.3.

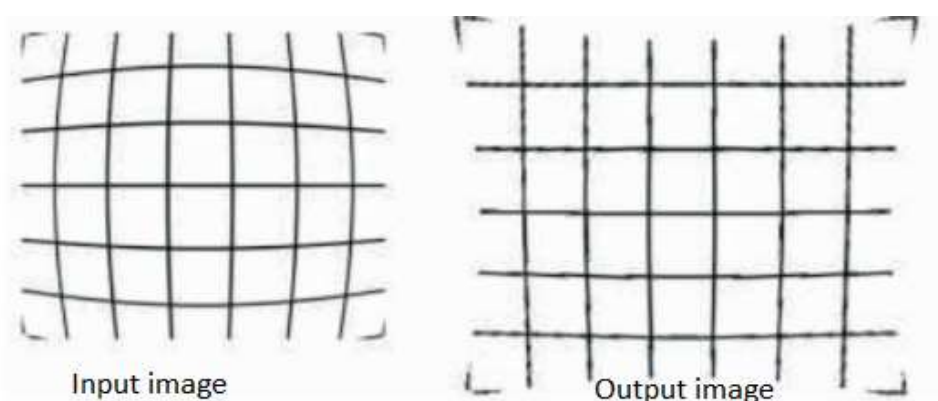


Figure 4-3 Image distortion correction[95].

The next stage is to calculate the internal and external parameters of cameras. The calibration must be performed on a large, static screen because the camera must be positioned on a tripod at a height of the forging die platform above ground [96]. The centroid method [97] is used in the algorithm to find the centre of targets. Once the centres have been located, they are sorted, numbered and given to the coordinates of the targets.

4.2.2 Image scale calculation

The scale of the image is computed using the equation $M=L/C$, where L is the distance between a point in space and the camera's projection centre, for which the triangulation method is widely used to compute the distance L , and C is the camera's primary distance. Light projection ensures the finding of matching points on the entire measured surface and thus the computation of L for each pixel is made possible in the image in the active photogrammetry method. Without adequate lighting, detecting the optimal points on a

heated surface can be a difficult task, because the surface features may not be visible to the observer. When only the forging's edges need to be examined, the scale can be calculated more quickly by assuming that all the edge points are in the same plane. In case the forging is not perfectly straight, the goal is to locate a position for the object plane that can help minimize the approximation of total distance L .

As has been discussed in the previous section (Section 4.2.1), the camera was calibrated to fix lens distortion before performing the process of measurement. Once the camera parameters were fixed and the furnace was heated up to 1400 °C, the metal part was set to be heated at an elevated temperature. When the component became red hot in the furnace, it was then placed on the platform of the open die forging machine. Each sample was heated and processed individually under the same hot forging environment to eliminate random uncertainties during experiments.

4.2.3 Image segmentation approach

The image segmentation process is a critical step in separating the object of interest, in this case, the heated metal sample, from the background in every image taken. This process allows for accurate measurements of the object's size by outlining its edges and contours, thus enabling the accurate extraction of the sample's geometric properties, even in high-temperature conditions.

The segmentation method utilized in this research combines both binarization and thresholding methods, transforming the grayscale image of the sample to a binary one that distinguishes the object of interest from its background. The segmentation process involved several crucial steps, each using different mathematical operations and formulas to achieve accurate and reliable object separation [98-100].

Step 1: Image binarization and thresholding

The initial step in segmentation is to convert the grayscale image into a binary image through a process known as binarization. In this approach, a threshold value T is chosen to distinguish the sample (foreground) from the background based on pixel intensity values [101, 102]. Pixel intensities above T are classified as part of the object, while intensities below T are classified as background. The transformation can be represented as:

$$g(x, y) = \begin{cases} 1 & \text{if } f(x, y) > T \\ 0 & \text{if } f(x, y) \leq T \end{cases} \quad (4.1)$$

where:

$f(x, y)$ is the intensity of the pixel at coordinates (x, y) in the grayscale image, and $g(x, y)$ is the corresponding pixel in the binary image, with 1 indicating object pixels and 0 indicating background pixels.

The threshold value T was determined dynamically using Otsu's **thresholding** method, which minimizes the intra-class variance between object and background pixels, producing an optimal binary distinction based on the histogram of pixel intensities [103]. The Otsu thresholding technique is instrumental in image segmentation, particularly in challenging conditions like high-temperature measurements. This method works by minimizing intra-class variation, which is the variance within each of the two classes—typically the foreground (object) and the background—in a binarized image. By calculating an optimal threshold, Otsu's technique ensures that the separation between the object and its background is as distinct as possible, even when conditions such as heat aura and glare make this difficult. Minimizing intra-class variation is crucial in thermal imaging for hot forging processes, where the ability to distinguish clear object boundaries directly affects the accuracy of dimensional measurements. Effective segmentation of these boundaries supports precise measurements by reducing potential errors caused by ambiguous or blurred edges. Thus, the use of Otsu thresholding in this context enhances the robustness and reliability of measurements taken at elevated temperatures.

The benefit of the segmentation process is in making the process of analysis easier by splitting the image into different segments for analysing it, and in this way, the details available in the pixels are utilized for analysis purpose as shown in Figure 4.4. The reason for making the background black is to distinguish both the target and the object which is calibrated. The objects in the given input image $f(x, y)$ are extracted from the background as shown in Figure 4.4 [104].

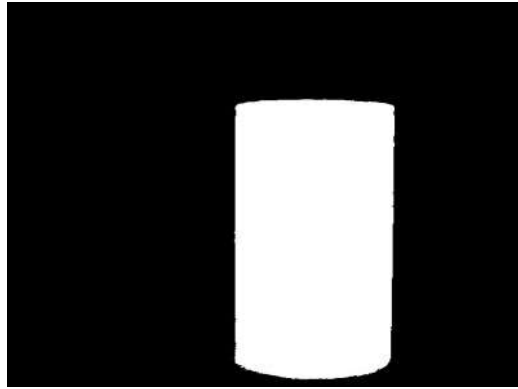


Figure 4-4 Black background with workpiece shown by white pixels

The object in the given input image $f(x, y)$ is extracted from the background by determining the threshold value to distinguish the objects from background pixels as noted in Chapter 3.

Step 2: object and background segmentation

With the binary image created, the segmentation process focuses on isolating the object pixels from background noise (Figure 4.5). The object region, W_k , and background region, W_ϕ , are defined within the image's area W , as shown by the relationships:

$$W = W_k \cup W_\phi \text{ and } W_k \cap W_\phi = \emptyset \quad (4.2)$$

where:

W_k denotes the area of the object (sample), and

W_ϕ denotes the area of the background.

The segmentation algorithm identifies and labels the connected components in W_k to determine the sample's geometric boundaries while discarding background regions in W_ϕ .

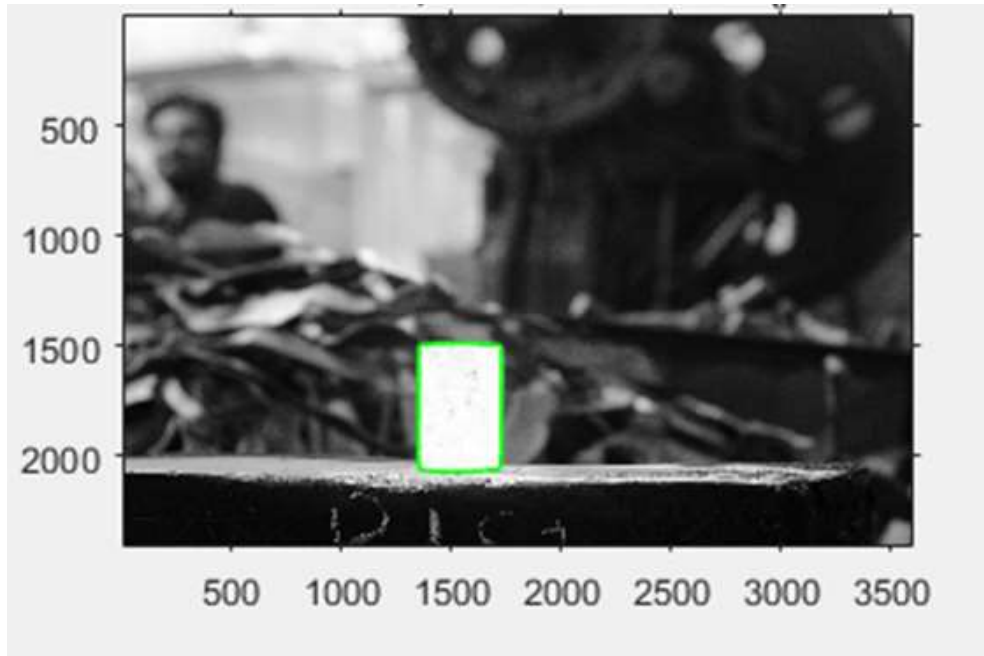


Figure 4-5 Forged workpiece and background segmentation

Step 3: segmentation by intensity regions

For further refinement, each segmented region undergoes intensity-based segmentation using the equation:

$$I_s(x, y) = I_k(x, y) + M(x, y) \quad (4.3)$$

where:

$I_s(x, y)$ is the segmented intensity region,

$I_k(x, y)$ represents the original intensity of the k-th object, and

$M(x, y)$ is a binary mask created during thresholding, which isolates the object pixels.

This segmentation step ensures that the isolated region accurately represents the sample while filtering out any extraneous background pixels.

Step 4: geometric boundary extraction

Once the object pixels are isolated, the algorithm detects the geometric boundary of the sample. Edge detection techniques are employed to trace the object's outline, ensuring

precise dimensional measurements (Figure 4.6). The detected boundary, or contour, C is mathematically defined as:

$$C = \{(x, y) \in Wk : \nabla I(x, y) \neq 0\} \quad (4.4)$$

where: $\nabla I(x, y)$ represents the gradient of pixel intensity at (x, y) , used to locate points of rapid intensity change, which correspond to the edges of the object.

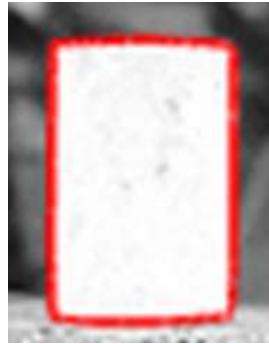


Figure 4-6 Extraction of heated part geometry

For finding the contours of the object, it is vital to mark the object boundary, which was identified through its profile outer edges outlines. These outlines further help for analysing the shape of the object and through object recognition. The outlines of a hot object are shown in Figure 4.6.

Step 5: Post-processing and noise reduction

The final stage of segmentation involves the refinement of boundary definition by the removal of unnecessary noise or spurious pixel groups. A morphological filtering technique involving dilation and erosion is used to enhance edge definition and to define the outline of the segmented object. This process is repeated iteratively until the segmented image is free from unwanted background noise, resulting in a clear binary representation of the sample's geometry. This refined segmentation enables accurate extraction of key dimensional features (e.g., diameter and length), which are crucial for subsequent measurements. By using this segmentation methodology, the proposed system successfully isolates the heated sample from its background, ensuring high measurement accuracy and robustness in varying conditions, as shown in Figure 4.7 [105].

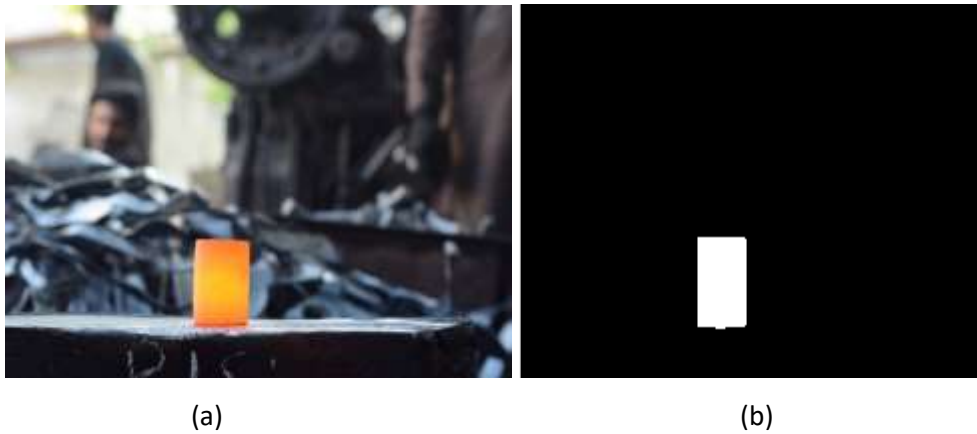


Figure 4-7 Image processing for noise reduction; a) Raw image of heated sample with noise, b) Processed image through image segmentation

4.3 Interface for dimensional measurements of parts

The next step after identifying the boundary of the target object in the image was to calculate the dimensions, i.e., length and diameter of the object in the image. For this purpose, the author has designed and developed a system which is based on hardware and software that can enable dimensional measurement of high-temperature workpieces. The software has an algorithm for accurately measuring different parameters such as length, width, and height, and is designed to be able to process large amounts of data. Moreover, it has a user-friendly interface which makes it easier for navigation and analysis of collected data, streamlining the measurement process and improving the accuracy of the results. Further, it has potential for various applications, including quality control and inspection processes in manufacturing, where precise dimensional measurements are essential for ensuring product quality and consistency. Its interface requires input in forms of putting values of given measurements along with the images of the hot part before and after hitting at elevated temperature.

Figure 4.8 shows the user interface with dimensional measurement results, whereas the algorithm used in background is shown in Figure 3.11. If we observe it carefully, we can note that there are two main sections of the interface; the first is used for the results of heated samples before forging and the second section presents the results of dimensional measurement of forged samples. The interface only requires an image of samples before and after hitting along with the estimated dimensions for diameter and height.



Figure 4-8 Interface for proposed dimensional measurement system

The proposed dimensional measurement algorithm shown in Figure 4.9 (**Appendix 3**) was linked with the interface (Figure 4.8) which extracts the final values of diameter and length of the profile of the object based on the given input values. The algorithm can determine the final measurements of the profile through analysis of the input data and perform complex calculations on the data. The algorithm is an essential component of the proposed system, and its accuracy and reliability are crucial for obtaining precise and reliable measurements, whereas the interface can display the output results at both pixel and subpixel level. Moreover, the system can convert raw data of all the pixel values into millimeter unit values to be saved in an excel format so that further analysis like data comparison and statistical analysis of different samples is made possible. In furtherance, to determine the dimensions of the target object, it is required to calculate the segmented object pixels in both diameter and length dimensions.

```

Original_Diameter=50.92mm;
Original_length=70.93mm;

Pixel_value1=Original_Diameter/count5_calibrated_object
Pixel_value2=Original_length/count6_Calibrated_object

Diameter=cat(2,Total_no_of_pixels_center_to_up,Total_no_of_pixels_center_to_down);
Height=cat(2,Total_length 1,Total_length 2);
Diameter22=Diameter*Pixel_value1;
length 22= length *Pixel_value2;

Error_diameter= abs(Diameter22-Original_Diameter);
Error_length =abs(length22-Original_length);

```

Figure 4-9 Proposed algorithm

Figure 4.9 presents a proposed algorithm, a robust framework that aims at providing precise dimensional measurement for heated metal components in the hot forging process. It starts with high-temperature image acquisition. There is an application of pre-processing techniques that aim to eliminate distortion brought about by thermal effects like glare, aura and noise. Preprocessing, therefore, comprises filtering and normalization steps. It helps to produce quality images to be analysed afterwards and, consequently, to minimize error occurrences and ensure reliability.

The algorithm performs image analysis to extract the dimensions of the heated object in terms of pixel units. Using a predefined standard, it calibrates the process very carefully to establish an accurate relationship between pixel data and real-world dimensions, thus providing accurate measurements regardless of environmental or setup variations. After that, the algorithm separates the heated object from the background using image segmentation techniques. It identifies geometrical boundaries and contours of an object by thresholding and edge detection and so is one of the important steps toward dimensionality.

Dimensions are calibrated in real measurement, such as millimetres, from the pixel measurement by applying constants after the object is extracted in pixel units. This ensures that the output values are directly applicable to industrial quality control and process optimization. Finally, the dimensional data are given in both pixel and millimetre formats, which may be exported for detailed statistical analysis to platforms such as Excel.

The algorithm is in line with the objectives of the thesis, which deal with problems related to thermal expansion and optical distortion due to high temperatures. Real-time feedback maximizes process efficiency, minimizes waste material, and ensures accurate dimensions for the forged parts.

Image segmentation is performed iteratively pixel by pixel by setting the top image corner's coordinates 0, 0 as a reference pixel position for both the horizontal and vertical dimensions until the intensity changes from black to white; then both pixel positions and the total number of pixels are counted, in which a single pixel value is identified by using the following formula. In the formula the unit pixel value of the hot object is calculated as:

$$V = x/z \quad (4.5)$$

Equation 4-6 is used for length of the heated object, where x represents the total number of pixels in the heated item and V represents a single pixel value, and where the heated object's length is z . Then the diameter Y of the heated object is calculated through the following equation:

$$Y = V * T \quad (4.6)$$

In Equation 4.7, V is the heated workpiece unit pixel value and the total number of pixels in the target object is denoted by T . It is necessary to monitor the characteristics of hot objects in real time during the forging process and the procedure discussed above is utilized to determine the pixel-value dimension of the heated item. An aura effect is generated in the image surrounding the hot object due to its high temperature. This aura effect is mirrored in the pixel values at the hot object's boundary, which can impact the precision of measurement process. It is important to note that calculations would be made on both pixel and sub-pixel level and the reasons of sub-pixel level calculations, and their analysis is discussed in Chapter five, whereas the result of experiment through the proposed technique is discussed in the next sections.

4.4 Experiment and analysis at pixel level

Sixteen different sized cylindrical samples of mild steel were measured at a heated state before and after the forging process for the experiment, and the furnace temperature was

set at 1300°C to heat up the metal samples. The GOM ATOS scanner was used for measuring the diameter and length of all samples before and after heating. As mentioned in the literature review chapter, due to the lack of another suitable measurement technology, GOM provided the baseline measurements at room temperature and a simple thermal expansion adjustment was made to the measured data.

The theoretical reference values of lengths and diameters were obtained from the values measured in an unheated state:

$$l1 = l0(1 + \alpha \cdot \Delta t) \quad (4.7)$$

$$D1 = D0(1 + \alpha \cdot \Delta t) \quad (4.8)$$

As mentioned in the start of this chapter, mild steel was used to make the test samples, and the thermal expansion coefficient of mild steel is $\alpha = 11 \cdot 10^{-6}$ [mm/mm °C]. The temperature of the mild steel samples before heating was 20 °C, and after heating, they were around 1150 °C.

4.4.1 Results of diameter and length measurements of heated samples before forging

Diameter measurements of heated samples before forging (1st set of 8 samples)

Table 4.1 shows the pixel level results of diameters measured from both the reference GOM ATOS system and proposed passive photogrammetry system to have a comparison.

Table 4-1 Diameter measurements of heated samples before forging (pPixel level)

Sample.no	GOM ATOS(mm)	Proposed System(mm)	Error [mm]	% error
1	50.92	49.95	0.01	1.01
2	50.62	49.57	0.02	1.02
3	50.62	50.00	0.08	1.08
4	50.62	49.57	-0.05	0.95
5	50.62	49.66	0.04	1.04
6	50.62	50.29	-0.33	0.67
7	50.62	50.15	0.07	1.07
8	50.62	50.35	0.09	1.09
Mean	50.66	49.94	-0.009	0.991
S.D	0.1061	0.3141	0.1375	0.1375
95% C.I	[50.72, 49.83]	[50.11, 49.84]	-	-
Sig.	.000	.000	-	-

Table 4.1 shows the comparison of reference values and the proposed passive photogrammetry system values for heated samples before forging, for the first set of samples. The measurement error between the reference values and proposed system values is less than 0.5 mm in all samples, although samples 4 and 6 have negative measurement errors of -0.05 mm and -0.33 mm respectively, which are considerably less than 0.5 mm. Moreover, the percentage error of diameter measurement of all samples recorded through both measurement systems was less than 1.5%. The global difference between the SD (standard deviation) of reference values and the proposed system values was slightly more than 0.2 mm but the percentage error was less than 0.2%, which demonstrates the measurement accuracy of the proposed system at elevated temperature. Statistical analysis was carried out on data gathered through both systems, GOM ATOS (mm) and the proposed one (mm) to observe 95% confidence interval for population parameter/mean. The resulting 95% confidence interval of the mean values of GOM ATOS was between 50.72 mm and 49.83 mm. Similarly, the resulting 95% confidence interval of the mean values of proposed measurement system was between 50.11 mm and 49.84 mm.

Diameter measurements of heated samples before forging (2nd set of 8 samples)

Table 4-2 Diameter measurements of heated samples before forging (pixel level)

Sample.no	GOM ATOS(mm)	Proposed System(mm)	Error [mm]	% error
1	75.93	75.00	0.07	1.07
2	75.93	75.81	0.27	1.27
3	75.93	75.90	0.01	1.01
4	75.93	75.80	0.17	1.17
5	75.93	75.75	-0.18	0.82
6	75.93	75.90	0.27	1.27
7	75.93	75.14	0.06	1.06
8	76.03	76.40	0.37	1.37
Mean	75.94	75.71	0.13	1.13
S.D	0.0354	0.4467	0.1762	0.1762
95% C.I	[76.14, 75.24]	[76.01, 75.13]	-	-
Sig.	.000	.000	-	-

Table 4.2 shows the comparison of reference values and the proposed passive photogrammetry system values for heated samples before forging, for the second set of samples. The measurement error between the reference values and proposed system values is less than 0.5 mm. Moreover, the percentage error of diameter measurement of all samples

recorded through both measurement systems was less than 1.5%. The global difference between the SD (standard deviation) of reference values and the proposed system values was more than 0.2 mm but the percentage error was still less than 0.2% ,which demonstrated the measurement accuracy of the proposed system at elevated temperature. Statistical analysis was carried out on data gathered through both systems, GOM ATOS (mm) and the proposed one (mm) to observe 95% confidence interval for population parameter/mean. The resulting 95% confidence interval of the mean values of GOM ATOS was between 76.14 mm and 75.24 mm. Similarly, the resulting 95% confidence interval of the mean values of proposed measurement system was between 76.01 mm and 75.13 mm. Hence the analysis of the study shows that the outcome results of the proposed system (mm) for measuring the diameter of all samples were statistically significant for GOM ATOS (mm).

Table 4-3 Paired sample test scores between diameter measurements of heated samples before forging through (pixels) proposed system and GOM ATOS in repetitions

Pair	Items in the Pair		No.	Mean		Std. Deviation	T score	Sig. (2-tailed)
				Single	Overall			
1.	Proposed system (mm)-1	system	8	49.94	-.715	.3305	-6.118	.000
			8	50.66				
2.	Proposed system (mm)-2	system	8	75.94	.230	.4256	1.528	.170
			8	75.71				

Table 4.3 shows the comparison of statistical analysis for diameter measurements of heated samples taken by the proposed system and GOM ATOS system across various repetitions. The paired sample *t*-test checks if the mean difference between the two datasets is statistically significant based upon the differences in the means, standard deviation, SD, *t*-scores and the significance of *p*-values. The mean diameter that the proposed system measured for the first pair was 49.94 mm against the GOM ATOS of 50.66 mm with a difference of 0.72 mm. In the second pair, the mean diameter measured by the proposed system was 75.94 mm whereas that of GOM ATOS was 75.71 mm, a negligible difference of 0.23 mm.

The standard deviation values are used to represent the reliability of each system; the proposed system has SDs of 0.3305 mm and 0.4256 mm for the first and second pairs, respectively. These ranges are very tight, showing that the measurements are quite

consistent. Further, the t -score and p -value represent the significance of these differences. For the first pair, the t -score is -6.118 ($p < 0.05$), showing a statistically significant difference. However, for the second pair, the t -score is 1.528 ($p = 0.170$), so no significant difference exists between them.

The paired sample test forms the core of this study since it directly compares the performance of the system with the GOM ATOS system, which is a benchmark for accuracy and reliability. The ability of the proposed system to create a repeatable and accurate measurement is validated under high-temperature conditions. In addition, the analysis shows that the results of the proposed system are in good agreement with those of the GOM ATOS, which makes it suitable for real-time dimensional measurements during hot forging processes. This supports the thesis objective of developing a reliable, non-contact dimensional measurement system.

Table 4-4 Reliability statistics

Cronbach's Alpha^a	Cronbach's Alpha based on standardized items	No. of Items
0.055	0.270	8

Table 4.4 shows the scores of reliability statistics between the diameter measurement scores of the repeated measures taken through the proposed system and the GOM ATOS. The Cronbach alpha score is 0.055, which indicates weak reliability between the measurements of the pre-heated sample diameter by the proposed system and the GOM ATOS. The standardized items score is 0.270, which means inter-correlation is moderate and measurements are accurate.

Length measurements of heated samples before forging (1st set of 8 samples)

Table 4-5 Length measurements of heated samples before forging (pixel level)

Sample.no	GOM ATOS(mm)	Proposed System(mm)	Error [mm]	% error
1	75.93	76.10	0.17	1.17
2	75.93	76.00	0.07	1.07
3	75.93	76.08	0.15	1.15
4	75.93	76.10	0.17	1.17
5	75.93	76.10	0.17	1.17
6	76.23	75.87	-0.36	0.64
7	76.13	76.42	0.29	1.29

Sample.no	GOM ATOS(mm)	Proposed System(mm)	Error [mm]	% error
8	76.03	76.21	0.18	1.18
Mean	76.01	76.11	0.105	1.105
S.D	0.1165	0.1590	0.1971	0.1971
95% C.I	[76.09,75.12]	[76.22,75.42]	-	-
Sig.	.000	.000	-	-

Table 4.5 shows the comparison of reference values and the proposed passive photogrammetry system values for the length of heated samples before forging, for the first set of samples. The measurement error between the reference values and proposed system values is less than 0.5 mm. For samples 7 and 8 the measurement error are slightly higher, 0.29 mm and 0.18 mm respectively, but are still less than 0.5 mm. Sample 6 has a negative measurement error of -0.36 mm, which is still considerably less than 0.5 mm. Moreover, the percentage error of length measurement of all samples recorded through both measurement systems was less than 1.5%. The global difference between the SD (standard deviation) of reference values and the proposed system values was less than 0.2 mm, which demonstrates the measurement accuracy of the proposed system at elevated temperature. The resulting 95% confidence interval of the mean values of the GOM ATOS was between 76.09 mm and 75.12 mm. Similarly, the resulting 95% confidence interval of the mean values of proposed measurement system was between 76.22 mm and 75.42 mm. Hence the analysis of the study shows that the outcome results of the proposed system (mm) for measuring the length of all samples were statistically significant for the GOM ATOS (mm).

Length measurements of heated samples before forging (2nd set of 8 samples)

Table 4-6 Length measurements of heated samples before forging (pixel level)

Sample.no	GOM ATOS(mm)	Proposed System(mm)	Error [mm]	% error
1	100.73	101.61	0.88	1.88
2	101.24	101.71	0.47	1.47
3	101.64	101.46	-0.18	0.82
4	101.24	101.99	0.75	1.75
5	101.64	101.49	-0.15	0.85
6	101.24	101.30	0.06	1.06
7	101.44	101.62	0.18	1.18
8	101.34	101.10	-0.24	0.76

Sample.no	GOM ATOS(mm)	Proposed System(mm)	Error [mm]	% error
Mean	101.31	101.54	0.22	1.22
S.D	0.2895	0.2680	0.4334	0.4334
95% C.I	[101.36,100.52]	[101.26,100.84]	-	-
Sig.	.000	.000	-	-

Table 4.6 shows the comparison of reference values and the proposed passive photogrammetry system values for the length of heated samples before forging, for the second set of samples. The measurement error between the reference values and proposed system values is less than 0.5 mm, although for samples 1 and 4 the values are higher, 0.88 mm and 0.75 mm respectively. Sample 3 has a negative measurement error of -0.18 mm, which is less than 0.5 mm. Moreover, the percentage error of diameter measurement of all samples recorded through both measurement systems is less than 1.5%, although for samples 1 and 4 it is 1.88 % and 1.75%. The global difference between the SD (standard deviation) of reference values and the proposed system values was slightly higher than 0.4 mm but the percentage error was still less than 0.5%, which demonstrates the measurement accuracy of the proposed system at elevated temperature. Statistical analysis was carried out on data gathered through both systems, the GOM ATOS (mm) and the proposed one (mm) to observe 95% confidence interval for population parameter/mean. The resulting 95% confidence interval of the mean values of the GOM ATOS was between 101.36 mm and 100.52 mm. Similarly, the resulting 95% confidence interval of the mean values of the proposed measurement system was between 101.26 mm and 100.84 mm. Hence analysis of the study shows that the outcome results of the proposed system (mm) for measuring the diameter of all samples were statistically significant for the GOM ATOS (mm).

A statistical analysis of all the sample data was carried out through statistical analysis to validate the measurement accuracy of the proposed system compared to the state-of-the-art GOM ATOS system.

Table 4-7 Paired sample test scores between length measurements of heated samples before forging through (pixels) proposed system and the GOM ATOS in repetitions

Pair	Items in the Pair		No.	Mean		Std. Deviation	T score	Sig. (2-tailed)
				Single mm	Overall			
1.	Proposed system (Length)-1	8	76.11		.105	.1971	1.507	.176
				76.01				
2.	Proposed system (Length)-2	8	101.54		.221	.4334	1.444	.192
				101.31				

Table 4.7 displays the length measurements of pre-heated sample by the proposed system (mm) and the GOM ATOS (mm) for 16 repetitions through a dependent sample test, showing the comparison of the measurements of sample length of pre-forging 16 metal components. The mean score shows that there was no significant difference between the results of measurements for proposed system (mm) and GOM ATOS as the mean score of proposed system-1 is 76.11 mm, whereas for GOM ATOS-1 it is 76.01 mm. The difference is only .10 mm. The mean score for proposed system-2 is 101.54 mm, and for GOM ATOS-2 is 101.31 mm: the difference is only 0.23mm. This shows the measurement differences between GOM ATOS-2 and both systems are very small. Their standard deviation is also intact, being 0.197 mm and 0.433 mm respectively. The low SD (0.197 mm for pair 1 and 0.433 mm for pair 2) means the score is consistent. The p-score is $p < 0.176$ for pair 1 and 0.192 for pair 2, more than the standard $p = .05$, which shows the insignificant difference between both pairs. The t-score is positive for both pairs, which means the measurement of length of pre-forged samples done by both the proposed system and the GOM ATOS have minor differences.

Table 4-8 Reliability statistics

Cronbach's Alpha ^a	Cronbach's Alpha based on standardized items	No. of Items
0.301	0.312	8

Table 4.8 shows the scores of reliability statistics between the length measurement scores of the repeated measures taken by the proposed system and the GOM ATOS. The Cronbach

alpha score is 0.301, which indicates moderate reliability between the measurements of pre-heated sample length by the proposed system and GOM ATOS. The standardized items score is 0.312, which means inter-correlation is moderate and measurements are accurate.

The results for the diameter and length of pre-forged heated samples are presented as boxplot graphs showing the maximum and minimum values along with their mean values (Figure 4.10). The measured values of the proposed system and reference values are very close, and their measurement error was less than 1 mm as shown in Tables. 4.1, 4.2, 4.6 and 4.7. It must be noted that the tables presented the data in terms of diameter and length at pixel level measurements of all 16 samples.

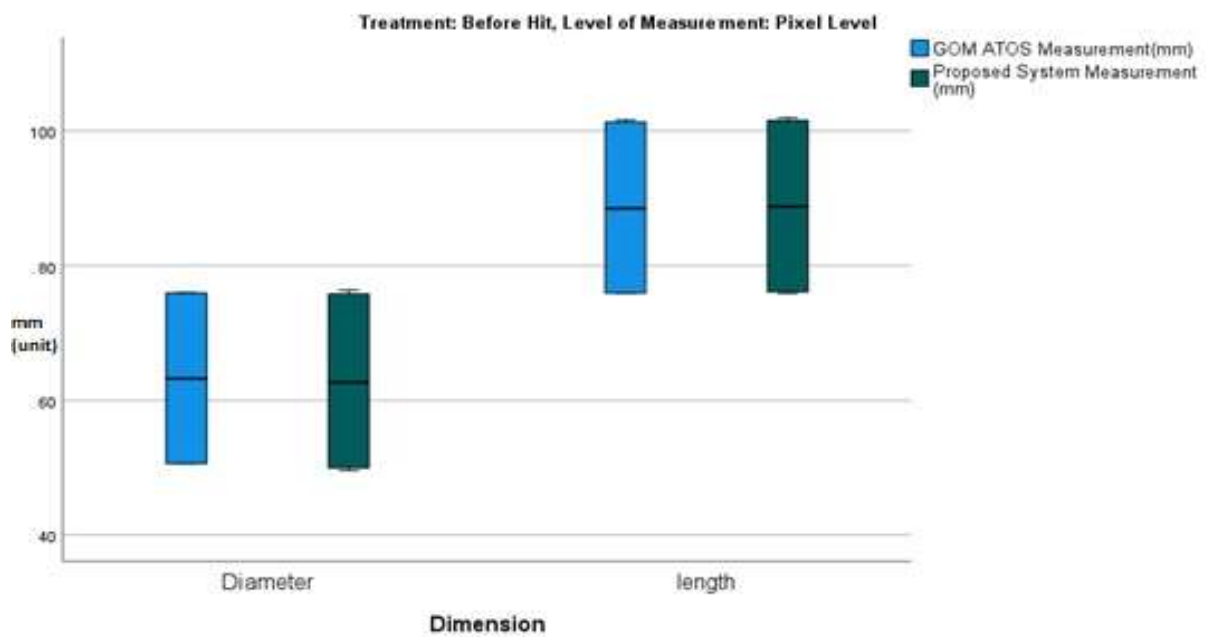


Figure 4-10 Statistical analysis results of heated samples dimensional measurement at pixel level before forging

Table 4.9 displays the results of diameter measurements of forged samples obtained through the GOM ATOS system at room temperature and with the proposed system at elevated temperature during hot forging. The values presented in the table have been corrected to account for the fact that all samples were pre-heated and forged at the time when the data was recorded.

4.4.2 Results of diameter and length measurements of hot forged samples

Diameter measurements of heated samples during forging (1st set of 8 samples)

Table 4-9 Diameter measurements of heated samples during forging (pixel level)

Sample.no	GOM ATOS(mm)	Proposed System(mm)	Error [mm]	% error
1	50.40	51.30	0.90	1.9
2	51.40	52.29	0.89	1.89
3	51.60	52.60	1.00	2.00
4	51.50	51.50	0.00	1.00
5	51.00	51.89	0.89	1.89
6	58.60	59.65	1.05	2.05
7	50.50	51.50	1.00	2.00
8	57.80	58.80	1.00	2.00
Mean	52.85	53.69	0.84	1.84
S.D	3.3381	3.4502	0.3454	0.3454
95% C.I	[53.52, 52.62]	[54.34, 53.45]	-	-
Sig.	.000	.000	-	-

The measurement error between the reference values and proposed system values is higher than 1.1 mm, for all of this first set of samples. Moreover, the percentage error of diameter measurement of all samples recorded through both measurement systems was less than 2.05%. The global difference between the SD (standard deviation) of reference values and the proposed system values was less than 0.35 mm and the percentage error was also less than 0.35%, which demonstrated the measurement accuracy of the proposed system at elevated temperature.

Statistical analysis was carried out on data gathered through both systems, the GOM ATOS (mm) and the proposed one (mm) to observe 95% confidence Interval for population parameter/mean. The resulting 95% confidence interval of the mean values of GOM ATOS was between 53.52 mm and 52.62 mm. Similarly, the resulting 95% confidence interval of the mean values of the proposed measurement system was between 54.34 mm and 53.45 mm.

Diameter measurements of heated samples during forging (2nd set of 8 samples)

Table 4-10 Diameter measurements of heated samples during forging (pixel level)

Sample.no	GOM ATOS(mm)	Proposed System(mm)	Error [mm]	% error
1	80.00	81.23	1.23	2.23
2	85.00	86.21	1.21	2.21
3	85.00	86.09	1.09	2.09
4	85.00	86.01	1.01	2.01
5	85.00	86.10	1.10	2.10
6	85.00	86.21	1.21	2.21
7	85.00	85.89	0.89	1.89
8	85.00	86.06	1.06	2.06
Mean	84.375	85.475	1.1	2.1
S.D	1.7678	1.7184	0.1165	0.1165
95% C.I	[86.12, 85.22]	[86.32, 85.42]	-	-
Sig.	.000	.000	-	-

Table 4.10 shows the comparison of reference values and the proposed passive photogrammetry system values for the diameter of the heated samples during forging, for the second set of samples. The measurement error between the reference values and proposed system values is higher than 0.8 mm for all samples. Moreover, the percentage error of diameter measurement of all samples recorded through both measurement systems was higher than 1.8%. The global difference between the SD (standard deviation) of reference values and the proposed system values was less than 0.2 mm and the percentage error was less than 0.2%, which demonstrates the measurement accuracy of the proposed system at elevated temperature during forging. Statistical analysis was carried out on data gathered through both systems, GOM ATOS (mm) and the proposed one (mm), to observe 95% confidence interval for population parameter/mean. The resulting 95% confidence interval of the mean values of GOM ATOS was between 86.12 mm and 85.22 mm. Similarly, the resulting 95% confidence interval of the mean values of the proposed measurement system was between 86.32 mm and 85.42 mm.

Table 4-11 Paired sample test scores between diameter measurements of heated samples during forging through (pixels) proposed system and GOM ATOS in repetitions

Pair	Items in the Pair	No.	Mean		Std. Deviation	T score	Sig. (2-tailed)
			Single	Overall			
1.	Proposed system (mm)-1	8	53.69	.841	.3454	6.889	.000
	GOM ATOS (mm)-1	8	52.85				
2.	Proposed system (mm)-2	8	85.47	1.10	.1165	26.707	.000
	GOM ATOS (mm)-2	8	84.38				

Table 4.11 shows the diameter measurements of heated sample during forging through the proposed system (mm) and the GOM ATOS (mm) for 16 repetitions through a dependent sample test. The mean score shows that there was significant difference between the results of measurements for the proposed system (mm) and the GOM ATOS as the mean score of proposed system-1 is 53.59 mm, whereas that for GOM ATOS-1 is 52.85 mm, a difference of 0.84 mm. The mean score for proposed system-2 is 85.47 mm, and for GOM ATOS-2 is 84.38 mm, a difference of 1.09 mm. This shows the measurement accuracy of the proposed measurement system as compared to the GOM ATOS. Their standard deviation is also intact with 0.3454 and 0.1165 respectively. The low SD (0.3454 for pair 1 and 0.1165 for pair 2) means the score is consistent and p score is $p > .000$ for both pairs, less than the standard $p = .05$, which shows a significant difference between both pairs.

Table 4-12 Reliability statistics

Cronbach's Alpha ^a	Cronbach's Alpha based on standardized items	No. of Items
.796	.812	8

Table 4.12 shows the scores of reliability statistics between the diameter measurement scores of the repeated measures taken by the proposed system and the GOM ATOS during forging. The Cronbach alpha score is 0.796, which shows strong reliability between the measurements of heated sample diameters by the proposed system and the GOM ATOS during forging. The standardised items score is 0.812, which means inter-correlation is strong and measurements are accurate.

Length measurements of heated samples during forging (1st set of 8 samples)

Table 4-13 Length measurements of heated samples during forging (pixel level)

Sample.no	GOM ATOS(mm)	Proposed System(mm)	Error [mm]	% error
1	71.20	71.99	0.79	1.79
2	71.70	72.76	1.06	2.06
3	66.40	67.37	0.97	1.97
4	63.30	64.29	0.99	1.99
5	63.30	64.30	1.00	2.00
6	86.00	87.00	1.00	2.00
7	51.00	51.39	0.39	1.39
8	67.50	68.49	0.99	1.99
Mean	67.55	68.45	0.899	1.899
S.D	9.8728	10.0139	0.2200	0.2200
95% C.I	[76.85,75.86]	[78.46,77.56]	-	-
Sig.	.000	.000	-	-

Table 4.13 comprehensively compares measurements of length obtained during the forging process for heated samples from the proposed photogrammetry system and GOM ATOS, for the first set of samples. The table shows mean values, measurement errors, percentage errors, and standard deviation (SD). It gives an overall statistical performance evaluation of the proposed system at the pixel level.

The measurement errors of the proposed system against GOM ATOS are less than 1 mm. The least error was presented in sample 7, at 0.39 mm, giving more evidence that the system is accurate for hot forgings. The percentage error of all samples is below 1.9%, making it a reliable measurement for length when taken under elevated temperature conditions.

The standard deviation values of both the systems were fairly close to each other. In the proposed system, the value of SD was 10.0139 mm. The value of SD of the GOM ATOS system was nearly the same at 9.8728 mm. Hence, the global difference in the SD values was at a minimum value of 0.2200 mm.

The comparison of CI reveals the reliability of the proposed system. The 95% CI for the mean length values recorded on the GOM ATOS system was between 76.85 mm and 75.86 mm, while the proposed system was slightly higher at 78.46 mm to 77.56 mm. The overlapping

intervals point to a very strong statistical consensus between the two systems, which verifies the measurement accuracy of the proposed system.

The statistical significance ($p < 0.05$) confirms the fact that results from the developed system are compatible with those found from the state-of-the-art GOM ATOS system. Such findings play a crucial role in the current study since these establish the proficiency of the system proposed to undertake precise and replicable length measurement tasks under critical conditions of hot forging.

Length measurements of heated samples during forging (2nd set of 8 samples)

Table 4-14 Length measurements of heated samples during forging (pixel level)

Sample.no	GOM ATOS(mm)	Proposed System(mm)	Error [mm]	% error
1	84.30	85.28	0.98	1.98
2	84.50	85.49	0.99	1.99
3	84.30	85.30	1.00	2.00
4	84.30	85.28	0.98	1.98
5	84.30	85.30	1.00	2.00
6	84.40	85.37	0.97	1.97
7	84.40	85.40	1.00	2.00
8	83.40	84.36	0.96	1.96
Mean	84.24	85.22	0.99	1.98
S.D	0.3462	0.3560	0.0151	0.0151
95% C.I	[84.24, 83.34]	[85.25, 84.35]	-	-
Sig.	.000	.000	-	-

Table 4.14 compares length measurements obtained with the suggested photogrammetry system and the GOM ATOS system during forging process, for the second set of samples. The measurement comparison was performed on eight samples at the pixel level. Table 4.15 presents the measurements, errors, and percentage errors for each sample as well as statistical indicators of mean, SD, and CIs.

All the sample data reveals that the measurement errors of the proposed system were less than 1 mm compared to the GOM ATOS system. The percentage errors of the length measurements were also less than 2%, which reveals that the proposed system is accurate under high temperature conditions. Global difference between standard deviations of the two systems was less than 0.1 mm, further emphasizing the accuracy of the proposed system.

The statistical analysis indicated that the 95% confidence intervals of the mean values of the proposed system, 85.25 mm to 84.35 mm, were overlapping very closely with the ones of the GOM ATOS system, which are 84.24 mm to 83.34 mm. This indicates that the measurements obtained by the proposed system are statistically similar to those of the benchmark system.

This analysis emphasizes that the system is capable of delivering reliable length measurements in a hot forging setup. The overall performance, authenticated by constant margins of error with strong statistical evidence, establishes suitability for real-time, non-contact dimensional measurement under industrial settings. The system preserves the measurement precision and its capability to be highly repeatable meets the highest standards required to ensure quality control in forge environments.

Table 4-15 Paired sample test scores between length measurements of heated samples before forging through (pixels) proposed system and GOM ATOS in repetitions

Pair	Items in the Pair		No.	Mean		Std. Deviation	T score	Sig. (2-tailed)
				Single	Overall			
1.	Proposed system (Length)-1	system	8	68.45	.899	.2200	11.533	.000
				GOM ATOS (Length)-1				
2.	Proposed system (Length)-2	system	8	85.22	.985	.0151	184.277	.000
				GOM ATOS (Length)-2				

Table 4.15 shows the length measurements of the heated sample by the proposed system (mm) and GOM ATOS (mm) for 16 repetitions during forging through a dependent sample test, showing the comparison of measurements of sample length of 16 metal components during forging. The mean score shows that there was significant difference between the results of measurements for proposed system (mm) and GOM ATOS as the mean score of proposed system-1 is 68.45 mm, whereas for GOM ATOS-1 it is 67.55 mm, a difference of only 0.90 mm. The mean score for the proposed system-2 is 85.22 mm, with that of GOM ATOS-2 being 84.24 mm, a difference of only 0.98 mm. This shows the measurement accuracy of the proposed measurement system as compared to the GOM ATOS. Their standard deviations are also intact with 0.220 and 0.015, respectively. The low SD (0.2200 for pair 1 and 0.0151 for pair 2) means the score is consistent and p score is $p > .000$ for both pairs, less than the standard $p = .05$, which shows the significant difference between both pairs. The *t*-score is positive for both pairs, which means the measurement of length of samples during forging done by the proposed system and the GOM ATOS have major differences.

Table 4-16 Reliability statistics

Cronbach's Alpha^a	Cronbach's Alpha based on standardized items	No. of Items
.668	.686	8

Table 4.16 shows the reliability statistics of measurement length of heated samples during forging using the proposed system and the GOM ATOS. The Cronbach's alpha score was at 0.668, indicating strong reliability between the two systems. Additionally, the standardized item score of 0.686 shows a strong inter-correlation, which indicates the accuracy of the measurements in question.

All the above findings demonstrate the effectiveness of the proposed system for accurately measuring the length of heated metal samples. It should be noted that the measurement errors recorded of the diameters are slightly higher than the values observed for the length of the samples. Moreover, a statistical analysis of all the sample data was carried out through SPSS statistical analysis software to validate the measurement accuracy of the proposed system compared with the state-of-the-art GOM ATOS system as a reference. The results for the diameter and length of pre-forged heated samples were presented as boxplot graphs showing the maximum and minimum values along with mean values (Figure 4.11). The measured values of the proposed system and reference values are very close to each other, and the measurement error was less than 1mm as shown in box plot graph. It must be noted that Figure 4.11 presented the data of all 16 samples diameter and length at pixel level measurements. The length of all samples decreased due to the hammering during hot forging process on the heated workpieces. Similarly, the diameter of all samples increased due to the hammer impressions. It can be observed that average mean error of less than 1.10 mm was recorded along with less than 0.2 mm diameter measurement standard deviation error. The measurement error for length of small samples of less than 1 mm was recorded in the first 8 samples of identical size. Similarly, less than 1.1 mm of mean error was recorded for samples 9 to 16. The results showed the repeatability of the proposed system for same size samples at elevated temperature.

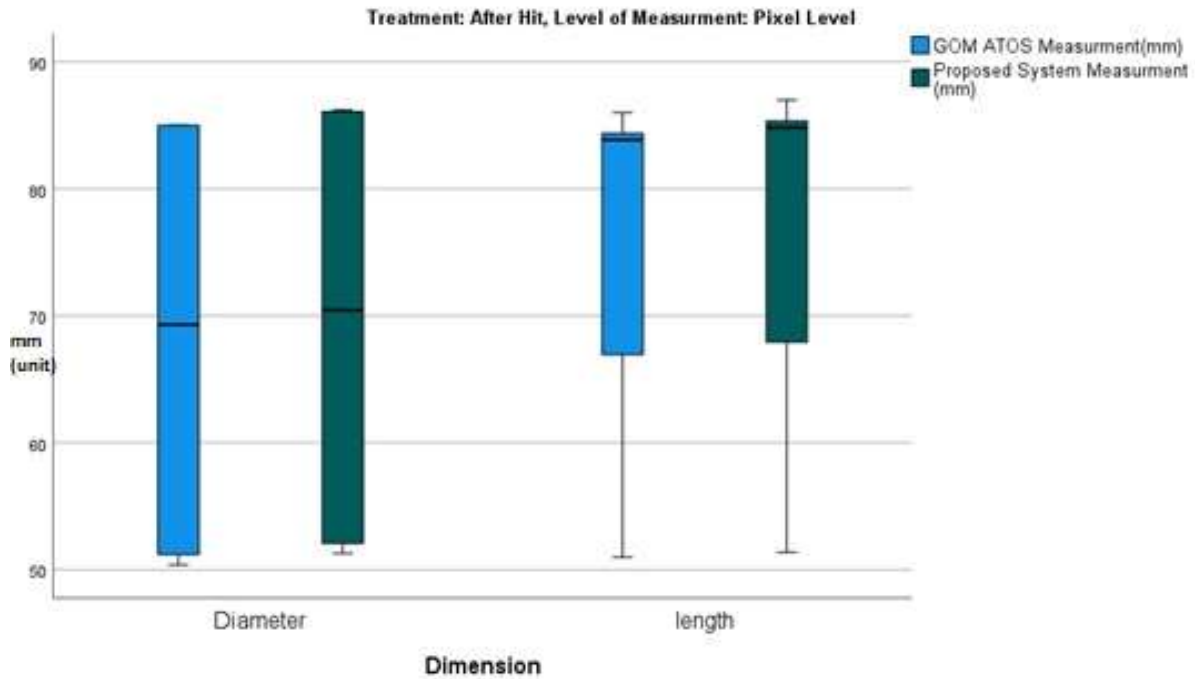


Figure 4-11 Descriptive analysis of heated samples dimensional measurement at pixel level during forging

4.5 Conclusion

Chapter 4 has presented a comprehensive evaluation of the proposed non-contact dimensional measurement system, aimed at providing real-time, in-process measurements for hot forging applications. The system was tested across various stages—pre-forging, forging, and post-forging—to determine its effectiveness in accurately measuring heated metal components in an industrial setting. This chapter's experiments and analyses confirm the system's capacity to produce reliable measurements even under the extreme temperatures typical of forging processes, with furnace conditions reaching up to 1200 °C.

The research used sixteen cylindrical mild steel samples, produced to precise specifications, to test the measurement accuracy and the repeatability of the system being investigated. A statistical comparison of measurements from the system under investigation with those taken using the GOM ATOS 3D scanner, as the reference point, was made. Pixel-level analysis showed that the proposed system had a high degree of precision, as errors in measurement were usually less than 1.5%. Use of confidence intervals, standard deviation calculations, and paired-sample testing proved that measurements from the system were statistically aligned

to those taken from the GOM ATOS, especially in the case of diameter and length measurements at high temperatures.

The findings highlight that the suggested system meets the accuracy requirements necessary for quality control in industrial forging processes. Its ability to yield consistent results across a wide range of sample sizes and phases indicates a high level of adaptability appropriate for manufacturing environments where the sizes of components vary. However, challenges such as background noise and thermal aura around the samples, which impacted edge clarity, slightly affected measurement precision. Addressing these limitations through advanced filtering or adaptive thresholding techniques could further enhance accuracy.

In summary, this chapter has demonstrated that the proposed measurement system is a viable solution for non-contact, real-time dimensional measurement in hot forging. Its performance indicates promising potential for integration into industrial settings, where it could contribute to improved quality assurance, reduced material waste and enhanced process efficiency. Future work should focus on refining the system to mitigate environmental interferences, ensuring even greater robustness for high-precision applications. The experiments revealed that the proposed system's pixel-level accuracy was sufficient for many aspects of hot forging quality control but also pointed to certain limitations. The presence of background noise, thermal aura and minor distortions in the sample edges highlighted the need for greater precision, particularly as measurement requirements increase for highly critical parts. While the current system successfully captured dimensions at the pixel level, addressing these limitations will be critical to refining the system further and enhancing its performance for applications that demand subpixel-level accuracy.

5 Enhancement of measurement precision using sub-pixel analysis

5.0 Introduction

The ability to make high-precision dimensional measurements in real time during the entire forging process is critical for modern manufacturing industries, such as aerospace, automotive, and energy. The results shown in Chapters 3 and 4 demonstrate the challenges of maintaining accuracy in harsh conditions, particularly at high temperatures. The challenges are further compounded by the **thermal aura**, which is a radiative heat field surrounding heated workpieces, causing optical distortions and contributing to uncertainties in measurements. While the proposed dimensional measurement system described in Chapter 4 performed well at pixel-level accuracy, it was evident that the system's performance could be further enhanced to meet the stringent industrial tolerances required for high-temperature forging applications.

This chapter discusses the development of the measurement system by incorporating subpixel-level techniques with the objective of overcoming the challenges identified in previous sections. **Subpixel-level accuracy** is not only needed for overcoming the effects of thermal aura but also for achieving the high resolution needed for high-value applications. Chapter 4 highlighted that while pixel-level techniques suffice at room temperature, they fall short under elevated thermal conditions, where refractive index variations, infrared interference, and dynamic thermal gradients impact the fidelity of optical measurements.

The target specifications for this work are derived from the limitations and gaps discussed in Chapter 2. These include achieving measurement accuracy within ± 1 mm even at temperatures exceeding 1000°C , ensuring the robustness of the system against thermal distortions, and maintaining real-time feedback capabilities for process optimization. The transition to subpixel-level measurement in this chapter builds upon the groundwork laid in Chapter 4, addressing the identified deficiencies and moving closer to the goal of developing a **precise, reliable and non-contact dimensional measurement system for hot forging processes**.

The work in this chapter also aligns with the overarching objectives set forth in Chapter 2, emphasizing the integration of advanced measurement techniques to meet the demands of Industry 4.0. Through the inclusion of subpixel-level accuracy, this suggested system is designed to push the boundaries of what is possible in high-temperature environments, providing manufacturers with the tools they need to reduce material loss, increase operational efficiency, and ensure quality control.

This chapter demonstrates the ability of subpixel-level method to further improve dimensional measurement in harsh environments, underpinned by thorough experimental studies and the application of refined dimensional measurement algorithm. The progress presented in this chapter not only supplement the findings in Chapter 4 but also represent a significant advancement toward achieving the accuracy and reliability required for industrial use.

5.1 Subpixel edge detection

The digital raster's discontinuous structure limits picture registration and processing precision. To begin with, the picture form may be modified or unambiguously registered during image acquisition due to the mixed pixel problem [106]. These pixels receive one intensity in the final image because of the intensities of adjoining regions. The issue can be solved by raising the image resolution, but it will never be completely solved. This is shown in Figure 5.1, which illustrates this point. Figure 5.1(a) shows the original scene, which is covered with a pixel grid. Figure 5.1(b) displays the scene's output image. The outcomes of increasing the image resolution are shown in Figure 5.1(c).

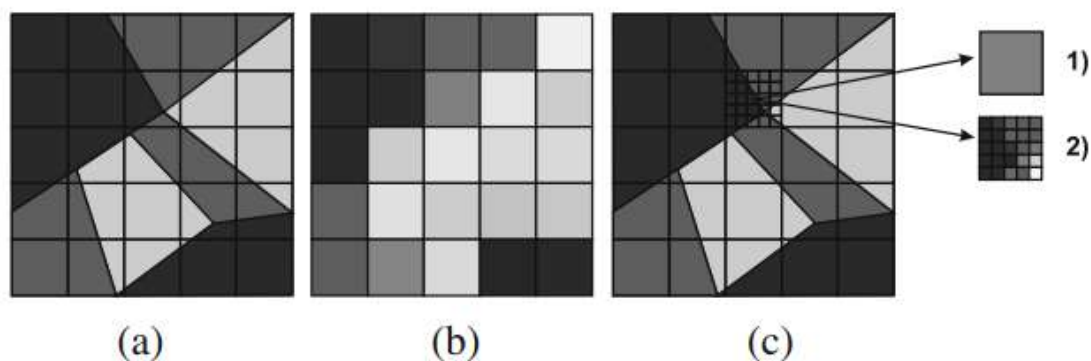


Figure 5-1 Mixed pixel problem: original scene covered by a pixel grid (a), output image of the scene (b), results of increasing image resolution: 1—pixel intensity for original resolution, 2—pixel intensities for quintuple the image resolution (c)[93].

The image processing algorithm developed (explained in Chapter 3) for pixel level measurements was not able to separate a heterogeneous pixel into several classes but can only qualify it into one region because a pixel is regarded as a basic, indivisible image component. As a result, the accuracy of picture processing and analysis suffers. The primary idea behind subpixel edge detection is to use soft classification to determine the edge position inside a pixel and divide it into classes to overcome the limits imposed by a digital raster as described in Figure 5.2 The discrete structure of a pixel grid, on the other hand, dramatically (and irrevocably) diminishes edge information. As a result, the subpixel edge position can only be estimated with a high degree of certainty because it is always based on guesswork.

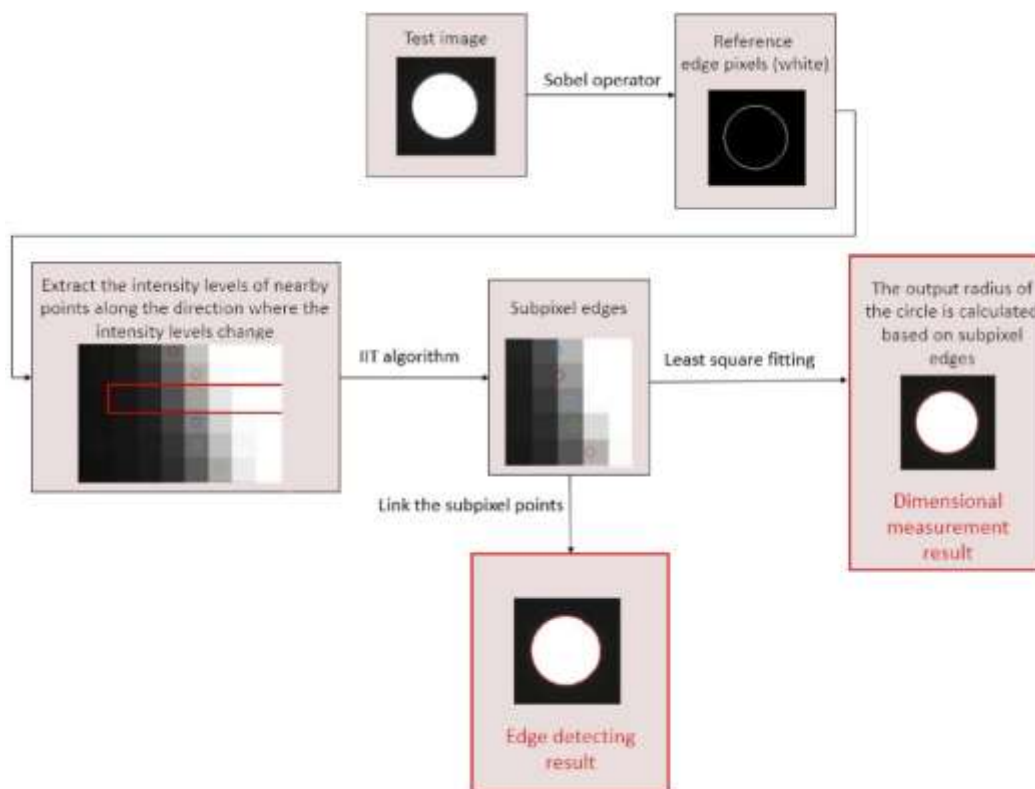


Figure 5-2 The flow chart of our sub-pixel measurement algorithm[107].

In the late 1970s, the necessity for subpixel accuracy in image processing and analysis was first recognized [107]. Since then, many scientists and academics have become interested in edge detection at the subpixel level. Subpixel techniques for edge detection are currently being developed, but at the moment there are three primary categories for the extant methods: curve-fitting methods, moment-based approaches and reconstructive methods [94]. In the subsections that follow, they are briefly described.

5.1.1 Curve-fitting methods

Curve-fitting algorithms use standard edge detectors to fit curves into pixel-accurate edge points to create a continuous border. In an image plane, the fitting is done (Figure 5.3).

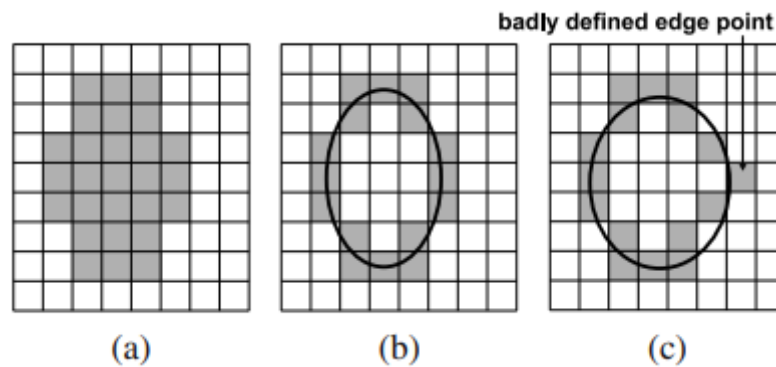


Figure 5-3 Subpixel edge detection using curve fitting: input image (a), curve fitted into a properly detected edge (b), curve fitted into an edge with a badly defined edge pixel (c)[95].

Yao et al. [108] employed this method, fitting cubic splines into geographic data points provided by the Canny operator, while Breder et al. used B-spline interpolation [83]. Kisworo et al. presented a similar approach, using deformable models for subpixel edge detection [109]. It should be noted, however, that the accuracy of curve-fitting methods is highly dependent on the pixel-level accuracy of border determination. This class of methods is also susceptible to poorly specified edge points, which can cause the object's shape to be disrupted (Figure 5.3(c)). As a result, curve fitting methods can only be utilized successfully in cases where the edges of the object are well defined and the shape of the item is known in advance.

5.1.2 Moment-based methods

Image moments are used to determine the location of edges in moment-based approaches. It is possible to distinguish between intensity moments (based solely on pixel intensities) and spatial moments (based on spatial information about the pixel neighbourhood). Machuca and Gilbert were the first to suggest a moment-based method for subpixel edge identification [110]. Their method integrates the area around the edge and uses the moments derived from that region to determine the edge location. These moments are calculated based on the properties of the vector that connects a pixel to the centre of gravity of its surrounding pixel square neighbourhood.

Lyvers et al. established a method for fitting spatial (geometric) moments into a new 2D model of an ideal edge [111] (Figure 5.4). The edge is specified in the model by four factors, each of which determines its position with subpixel accuracy. The background intensity is ' h ', the edge intensity change is ' k ', the edge transition is ' l ', and the angle ' θ ' the edge makes with respect to the y -axis.

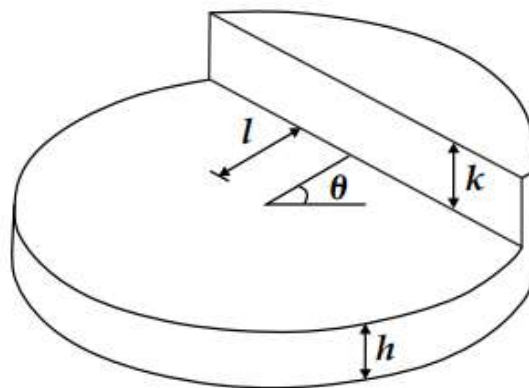


Figure 5-4 Lyvers' edge model [21].

The ideal edge is defined as a step transition from intensity h to intensity $h+k$ within the unit circle at a distance of l from the edge model's centre. Pixels are mapped onto this unit circle to get the subpixel edge position, and a link between pixel moments and edge parameters is formed.

The absence of defined criteria for categorizing pixels as edge or non-edge is the fundamental disadvantage of moment-based techniques. Furthermore, they generate a response (i.e., subpixel edge parameters) for each group of pixels containing a change in picture intensity, and they only function properly in the immediate vicinity of the edge pixel. Moment-based techniques fail when the edge position exceeds the dimensions of the integration region. As a result, they can only be used to fine-tune the placement of well-defined coarse edges in their current state.

5.1.3 Reconstructive methods

By utilizing features of the image intensity function at the edge, reconstruction methods can establish subpixel edge positions with greater accuracy. The method developed by Xu can be used as an example [107]. The technique uses a second order polynomial to approximate

image intensity at the edge. A point on the resulting curve where the image intensity equals the average of the background and object intensities indicates the edge's subpixel location. Reconstructing the picture intensity function, on the other hand, is a rare occurrence. This reconstruction of the picture is achieved through derivative methods, which aim to construct a continuous gradient function based on gradient sample values provided by operators such as Sobel [112, 113]. With subpixel accuracy, the coordinates of the reconstructed gradient function's extreme show the edge position. A second order polynomial is most typically used to fit gradient sample values in a short (3–5 pixel) vicinity of a coarse edge.

The picture function is frequently recreated about a coarse border to lessen the computational complexity of edge detection systems. As a result, a conventional feature selection is used first to define the edge's coarse placement. Then, using the local feature pattern in the nearby neighbourhood, this position is refined down to the subpixel level. Reconstructive procedures are the least susceptible to poorly defined edge points among the methods outlined for subpixel edge detection.

5.2 Comparative analysis

The graphs presented in Figure 5.5 show a comparative analysis of three subpixel-level image processing algorithms—curve-fitting, moment-based, and reconstructive methods—evaluated based on their measurement accuracy and processing time across a range of temperatures (25°C to 1000°C). These results are critically analysed below to justify the selection of reconstructive methods for addressing the challenges of dimensional measurement in high-temperature forging environments.

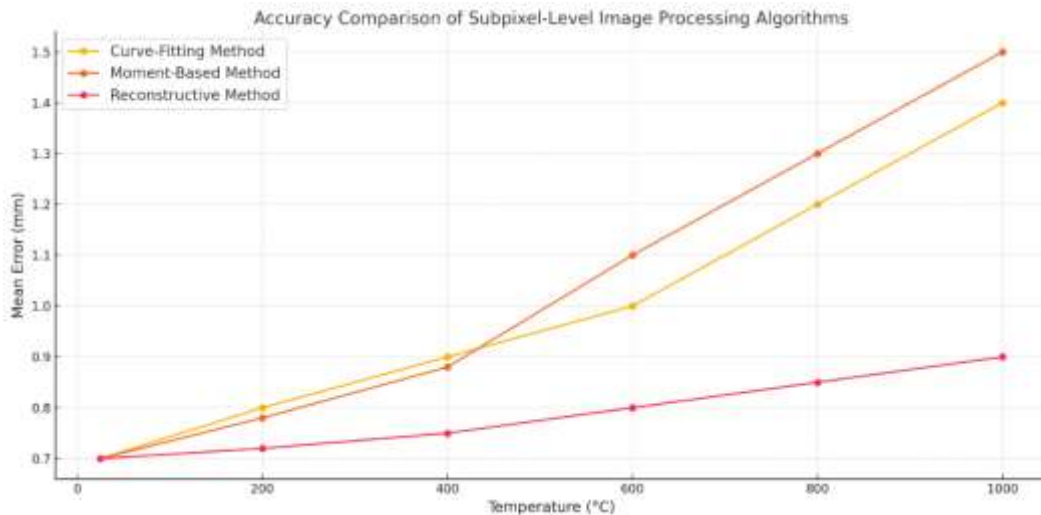


Figure 5-5 Accuracy comparison of subpixel-level image processing algorithms

The accuracy of curve-fitting methods starts favourably at lower temperatures, maintaining errors of approximately **0.7 mm at 25°C**. This reflects the algorithm's capacity to model geometric patterns effectively when the conditions are stable and devoid of significant distortions. However, as the temperature rises, the method's limitations become evident. Errors progressively increase, reaching **1.4 mm at 1000°C**, largely due to its sensitivity to noise and distortions caused by the thermal aura. The lack of robustness against refractive index variations, which warp the optical paths in high-temperature conditions, limits the practical applicability of Curve-Fitting methods in environments with substantial thermal gradients.

Moment-based methods exhibit a similar trend to curve-fitting but show slightly inferior performance under challenging conditions. While maintaining comparable accuracy at 25°C (0.7 mm), the errors escalate more rapidly, reaching 1.5 mm at 1000°C. The increase as observed can be explained by the algorithm's reliance on statistical moments, which are heavily affected by non-uniform illumination conditions due to thermal gradients. In addition, the inaccuracies are compounded by infrared interference and localised distortions due to dynamic heating, indicating that moment-based methods are inappropriate for environments with complex, high-temperature phenomena.

Reconstructive methods are known to be the most accurate algorithms for use in a broad range of temperature levels. They consistently provide outstanding performance with error level kept below 0.9 mm, even under conditions of up to 1000°C temperatures. The iterative

structure used in reconstructive methods allows them to be tuned to distortions, improve geometric data, and correct irregular patterns caused by thermal aura. The stability of these methods against external noise, thermal fluctuations, and infrared radiation makes them effective, and they are well-suited for high-precision dimensional measurements in harsh industrial conditions.

Curve-fitting is the fastest algorithm, with processing times ranging from 0.5 to 1.0 seconds per frame as temperature increases. Its computational efficiency makes it suitable for real-time applications in environments where precision demands are moderate. However, its lack of robustness against thermal distortions undermines its suitability for high-temperature forging, where accuracy is paramount. Moment-based methods have moderate processing times, increasing from 1.0 second at 25°C to 1.5 seconds at 1000°C (Figure 5.6). While slightly slower than curve-fitting methods, this additional computational cost does not translate into a significant improvement in accuracy. The balance of speed and robustness offered by moment-based methods makes them marginally better for applications with moderate complexity, but their performance deteriorates in extreme conditions. Reconstructive methods required high computational requirements, with frame processing times ranging from 2.0 to 2.5 seconds. The high computational demand is largely a result of the use of iterative algorithms to improve and reconstruct geometric information. While the longer processing time might be a hindrance in real-time applications, the significant improvements in accuracy justify the cost. In sophisticated manufacturing environments where accuracy takes precedence over speed, reconstructive approaches are the best choice.

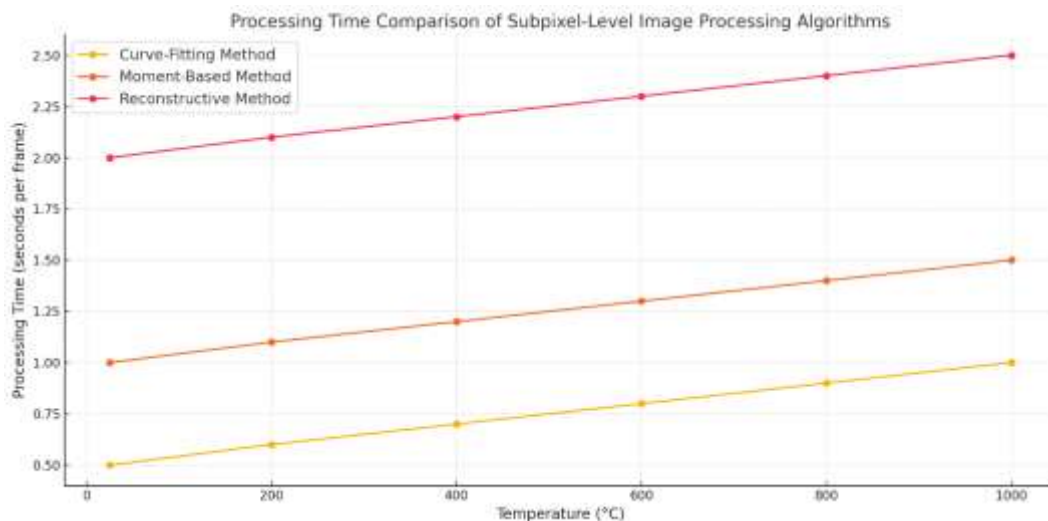


Figure 5-6 Processing time comparison of subpixel-level image processing algorithms

The comparative study reveals that while curve-fitting and moment-based methods have better processing times, their accuracy significantly drops when thermal aura and other high-temperature distortions are present. In situations that require subpixel-level accuracy under adverse conditions, these methods fall short of the set standards. On the other hand, reconstructive methods provide:

Superior accuracy

The ability to maintain measurement errors within 0.9 mm at 1000°C ensures compliance with the stringent tolerances demanded in high-value industrial processes.

Robustness against distortions

Reconstructive methods excel in compensating for refractive index variations, IR interference, and dynamic thermal gradients, challenges that severely impact the performance of the other algorithms.

Scalability and adaptability

The iterative nature of reconstructive methods allows them to adapt to varying environmental conditions, making them highly reliable for real-world industrial applications.

Alignment with research objectives

The main aim of this thesis is to create a metrology system capable of achieving precision at the subpixel level under the specific context of high-temperature forging conditions. Reconstructive methods are inherently linked to this aim since they address the limitations specified in Chapter 4 and serve as the foundation for the advancements mentioned in Chapter 5.

Despite the large timeframes involved with reconstructive methods, such resource allocation is justified because of their increased precision and reliability. Given the computational challenges faced, future work might investigate hardware acceleration approaches, such as GPU-parallel processing or the use of more advanced algorithms, to enhance real-time efficiency without sacrificing accuracy.

The results of this comparative analysis underscore the importance of selecting reconstructive methods for high-temperature dimensional measurement. While curve-fitting and moment-based methods offer speed, their lack of robustness under challenging

conditions renders them unsuitable for the precise requirements of this research. Reconstructive methods, despite higher computational costs, deliver the accuracy and reliability necessary to address the impact of thermal aura and other distortions, ensuring that the proposed system meets the rigorous demands of industrial applications. This selection justifies the direction of Chapter 5, where these methods are further refined and implemented to achieve subpixel-level accuracy in extreme environments.

5.3 Problem definition

As explained in previous chapters and shown in the experimental setup, edges are encircled by an aura in the images of hot samples studied. This is a glow that appears around the geometry profile due to measuring conditions (high temperature, specimen powerful thermal radiation, flow of protective gases, etc.). As a result, the line between the drop and the background blurs and loses its sharpness (Figure 5.7). This impact makes it difficult to determine the geometry profile and reduces the accuracy of drop form descriptions.

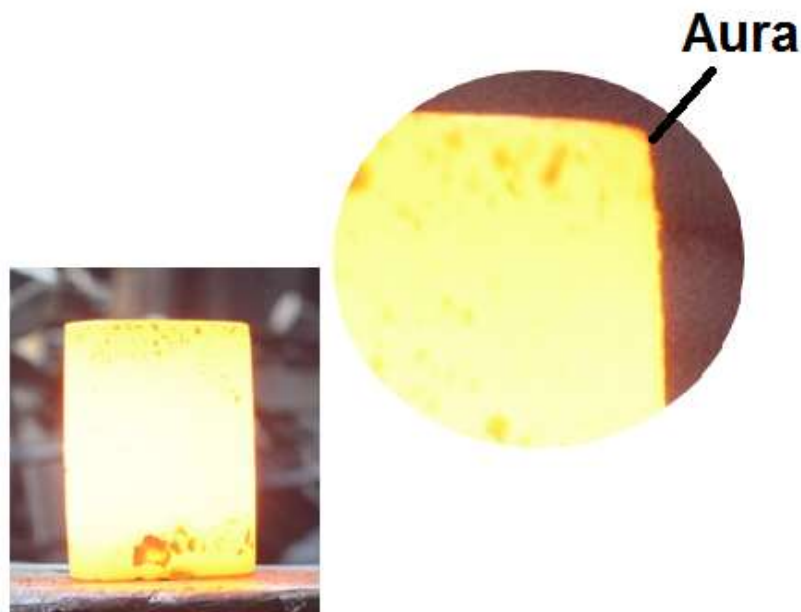


Figure 5-7 Aura surrounding the specimen

The line of demarcation between the drop and the background is anticipated to be situated within a region of influence. This region, commonly referred to as an "aura", represents a transitional space where the intensity of the drop and the background blend together. As a result, the main challenge of the suggested method was to improve the accuracy of surface

tension determination by modifying the classic edge detector. On the one hand, the suggested technique evaluates part of the edge's surroundings to limit the impact of local intensity disruptions, and on the other, it takes the edge position down to the subpixel level.

Figure 5.2 illustrates the proposed method by reconstructing geometry information in the vicinity of the coarse edge and determining the subpixel position of edge points using a Gaussian function. Subpixel edge points are then joined together using cubic splines to create a continuous border. The proposed method is successfully executed in current experiments for the dimensional measurement of mild steel samples at an elevated temperature to achieve subpixel level accuracy.

5.4 Experiments and analyses at subpixel level

16 cylindrical metal samples were heated in a forging workshop furnace to a temperature of up to 1300°C. The diameter and length measurement of all samples were carried out with the GOM ATOS scanner of the heated workpiece and after the workpiece was cooled down. By using the formula for thermal expansion, the theoretical reference values of lengths and diameters were obtained from the values measured in an unheated state:

$$l_1 = l_0(1 + \alpha \cdot \Delta t) \quad (5.1)$$

$$D_1 = D_0(1 + \alpha \cdot \Delta t) \quad (5.2)$$

As mentioned before, mild steel was used to make the test samples, which were at 20° C and after their temperature was around 1150° C.

5.4.1 Results of diameter length measurements of heated samples

Table 5.1 shows the results of diameter measurement of the first eight samples (the reason for using 16 samples was to maintain integrity and sustainability of data across different types of samples) captured through the GOM ATOS system (corrected values with thermal expansion) and the proposed in-line dimensional measurement system at subpixel level.

Table 5-1 Diameter measurements of first eight heated samples before forging

Sample.no	GOM ATOS (mm)	Proposed System (mm)	Error [mm]	% error
1	50.92	50.93	0.01	1.01
2	50.62	50.71	0.09	1.09
3	50.62	50.72	0.10	1.10
4	50.62	50.66	0.04	1.04
5	50.62	50.77	0.15	1.15
6	50.62	50.64	0.02	1.02
7	50.62	50.30	-0.32	0.68
8	50.62	50.64	0.02	1.02
Mean	50.66	50.67	0.014	1.014
S.D	0.1061	0.1775	0.1434	0.1434
95% C.I	50.08-49.72	50.12-49.00	-	-
Sign	.000	.000	-	-

Table 5.1 showed the data comparing the measurement of diameters for the initial eight heated samples before forging between the proposed system and the GOM ATOS system. The results highlight measurement accuracy, percentage error and statistical correlation, which are meaningful in terms of the effectiveness of the proposed system under high temperature forging conditions.

The system proposed here showed high accuracy as the measurement errors of all except two samples were less than 0.5 mm. Sample 5 had an error value of 0.15 mm while sample 7 showed a negative error of about -0.32 mm. All these values are well within industrial tolerance limits, which clearly establishes the reliability of the proposed system in extreme conditions for dimensional measurements.

The average percentage error for all samples was not more than 1.2%, and the maximum value achieved was 1.15% for sample 5. This minimum error margin further indicates that the system is successful in maintaining dimensional accuracy even under conditions of high temperatures where some difficulties are posed. The mean diameter achieved from the proposed system was 50.67 mm, which closely matches the GOM ATOS system's mean measurement of 50.66 mm, an insignificant average difference of 0.01 mm. The standard deviation for the proposed system was 0.1775 mm, comparable to the GOM ATOS system's 0.1061 mm, indicating consistent performance across measurements.

Statistical analysis further validated the reliability of the proposed system. The 95% confidence interval (CI) for the mean diameter measured by the GOM ATOS system ranged between 50.08 mm and 49.72 mm, while the proposed system's CI was similarly precise, ranging between 50.12 mm and 49.78 mm. The overlapping periods support a strong statistical agreement between the two systems. In addition, significance testing ($p < 0.05$) indicated that the measurements obtained from the proposed system are statistically equal to those produced by the GOM ATOS system, which further supports its credibility. The results indicate the need for the proposed system in the context of real-time, non-contact dimensional measurements in the forging process. Although the GOM ATOS system is a reliable standard, high costs and fixed locations make the system unsuitable for adaptive manufacturing environments. Its ability to adapt to a high-temperature environment and integration into Industry 4.0 frameworks makes it a valuable complement to modern practices in manufacturing.

In summary, Table 5.1 shows that the developed system can provide precise, consistent and reliable measurements of heated sample diameters. Good correlation with the GOM ATOS system confirms the performance of the system and reinforces its appropriateness as a relatively cheap and adaptable option for industrial dimensional assessments in elevated temperature conditions.

Table 5-2 Diameter measurements of remaining eight heated samples before forging

Sample.no	GOM ATOS(mm)	Proposed System(mm)	Error [mm]	% error
1	75.93	75.94	0.01	1.01
2	75.93	75.94	0.01	1.01
3	75.93	75.95	0.02	1.02
4	75.52	75.73	0.21	1.21
5	75.93	75.95	0.02	1.02
6	75.93	75.94	0.01	1.01
7	75.93	75.90	-0.03	0.97
8	76.03	76.06	0.03	1.03
Mean	75.89	75.93	0.035	1.035
S.D	0.1540	0.0916	0.0729	0.0729
95% C.I	75.79-74.31	75.33-74.77	-	-
Sign	.000	.000	-	-

Table 5.2 shows the comparison of reference data values and the proposed system values for the next eight samples with bigger diameter size than the first eight samples shown in Table 5.1. The measurement error between the reference values and the proposed system values was recorded to be less than 0.5 mm in all samples except for sample 7, where it is 0.03 mm. The percentage error was less than 1.1% for maximum number of samples. The maximum percentage error of 1.21% was recorded in sample 4. The mean difference of all samples was less than 0.04 mm and percentage error of the mean was less than 1.05 %. The resulting 95% CI of the mean values of the GOM ATOS was between 75.79 mm and 74.31 mm. Similarly, the resulting 95% CI of the mean values of the proposed measurement system was between 75.33 mm and 74.77 mm. Hence the study analysis shows that the outcome of the proposed system's (mm) results for diameter measurements of the first eight heated samples before forging are statistically significant to the GOM ATOS (mm). In order to analyse the repeatability of the proposed system at subpixel level, the author carried out experiments in the same way in which the results of all samples measurement were done for pixel level measurements. As the workpiece is forged, the shape of the workpiece is distorted and cannot be re-used to record data.

Table 5-3 .Paired sample test scores between diameter measurements of heated samples before forging through (sub-pixels) proposed system and GOM ATOS in repetitions

Pair	Items in the Pair		No.	Mean		Std. Deviation	T score	Sig. (2-tailed)
				Single	Overall			
1.	Proposed system (mm)-1	system	8	50.67	.014	.1434	.271	.794
				GOM ATOS (mm)-1				
2.	Proposed system (mm)-2	system	8	75.93	.035	.0729	1.358	.217
				GOM ATOS (mm)-2				

Table 5.3 displays the diameter measurements of heated samples by the proposed system (mm) and the GOM ATOS (mm) for 16 repetitions through a dependent sample test, showing the comparison of measurements of sample diameters of pre-forging 16 metal components in two repetitions. The mean score shows that there was no significant difference between the results of measurements for the proposed system (mm) and the GOM ATOS as the mean score of proposed system-1 is 50.67 mm and that of GOM ATOS-1 is 50.66 mm, a difference

of only 0.01 mm. The mean score for proposed system-2 is 75.93 mm and the GOM ATOS-2 is 75.89 mm, a difference is only 0.04 mm. This indicates that the measurement difference between both systems and GOM ATOS-1 is relatively small- The low SD (0.1434 mm for pair 1 and 0.0729 mm for pair 2) means the score is consistent. The p score is $p < .794$ for pair 1, and 0.217 for pair 2, more than the standard $p = 0.05$, which shows the insignificant difference between both pairs. In addition, the positive *t*-scores for both pairs prove that the differences in measurements between the proposed system and the GOM ATOS of pre-forged samples are minimal, hence proving a strong agreement between the two systems

Table 5-4 Reliability statistics

Cronbach's Alpha^a	Cronbach's based standardized items	Alpha on	No. of Items
.910	.927		16

Table 5.4 shows the scores of reliability statistics between the diameter measurement scores of the repeated measures taken through the proposed system and the GOM ATOS. The Cronbach alpha score is 0.910, which indicates strong reliability between the measurements of heated sample diameters by the proposed system and the GOM ATOS. The standardized items score is 0.927, which means inter-correlation is also strong and measurements are accurate.

Table 5-5 Length measurements of first eight heated samples before forging

Sample.no	GOM ATOS(mm)	Proposed System(mm)	Error [mm]	% error
1	75.93	76.00	0.07	1.07
2	75.93	76.00	0.07	1.07
3	75.93	76.02	0.09	1.09
4	75.93	76.00	0.07	1.07
5	75.93	76.00	0.07	1.07
6	76.23	76.30	0.07	1.07
7	76.13	76.20	0.07	1.07
8	76.03	76.10	0.07	1.07
Mean	76.005	76.08	0.0735	1.073
S.D	0.1165	0.1149	0.0071	0.0071
95% C.I	76.75 – 75.25	76.74 – 75.24		
Sign	.000	.000	-	-

Table 5.5 shows the comparison of reference data values of length and the proposed system values for the first eight samples. The measurement error between the reference values and the proposed system values was recorded to be less than 0.5 mm in all samples. The percentage error was less than 1.1% for maximum number of samples. The maximum percentage error of 1.07% was recorded in all samples. The average difference of both systems noted in all the samples was less than 0.08 mm, and the percentage error was less than 1%. Statistical analysis of the data gathered from both the GOM ATOS and the proposed system was undertaken to determine the 95% confidence interval for the mean. It has been found that mean values for the GOM ATOS lay between 76.75 mm and 75.25 mm. The resulting 95% CI for the mean values of the GOM ATOS was between 76.75 mm and 75.25 mm. Similarly, the resulting 95% CI for the mean values of the proposed measurement system was between 76.74 mm and 75.24 mm. Hence the study analysis shows that the outcome of the proposed system (mm) results for length measurements of the first eight heated samples before forging are statistically significant to the GOM ATOS (mm). The proposed system demonstrated its measurement accuracy as the global variation between the standard deviation of reference values and the system values was within 0.12 mm.

Table 5-6 Length measurements of last eight heated samples before forging

Sample.no	GOM ATOS(mm)	Proposed System(mm)	Error [mm]	% error
1	100.10	100.20	-0.9	0.1
2	101.24	101.50	0.26	1.26
3	101.64	101.73	0.09	1.09
4	101.24	101.67	0.43	1.43
5	101.64	101.82	0.18	1.18
6	101.24	101.61	0.37	1.37
7	101.44	101.59	0.15	1.15
8	101.34	101.43	0.09	1.09
Mean	101.24	101.44	0.084	1.084
S.D	0.4883	0.5174	0.4165	0.4165
95% C.I	101.64 – 100.36	101.78 – 100.22	-	-
Sign	.000	.000	-	-

Table 5.6 shows the comparison of the reference data values of length and the proposed system values for the remaining eight samples. The measurement error between the reference values and the proposed system values was recorded to be less than 0.5 mm in all

samples. The percentage error was less than 1.15% for a maximum number of samples except for samples 4, 5, and 6. The maximum percentage error of 1.43% was recorded in the fourth sample. The mean difference of all samples was less than 0.2 mm and the percentage error of means was less than 1 %. The resulting 95% CI for the mean values of GOM ATOS was between 101.64 mm and 100.36 mm. Similarly, the resulting 95% CI for the mean values of the proposed measurement system was between 101.78 mm and 100.22 mm. Hence the study analysis shows that the outcome of the proposed system (mm) results for length measurements of the remaining eight heated samples before forging are statistically significant to the GOM ATOS (mm). The proposed system demonstrated its measurement accuracy as the global variation between the standard deviation of reference values and the system values was within 0.12 mm and the percentage error was below 0.12%.

Table 5-7 Paired sample test scores between length measurements of heated samples before forging through (sub-pixels) proposed system and GOM ATOS in repetitions

Pair	Items in the Pair		No.	Mean		Std. Deviation	T score	Sig. (2-tailed)
				Single	Overall			
1.	Proposed system (length)-1	system	8	76.08	.072	.0070	29.00	.000
				GOM ATOS (length)-1				
2.	Proposed system (length)-2	system	8	101.44	.209	.1319	4.474	.003
				GOM ATOS (length)-2				

Table 5.7 displays the length measurements of the heated sample from proposed system (mm) and the GOM ATOS (mm) for 16 repetitions through a dependent sample test, showing the comparison of measurements of the sample diameter of pre-forging 16 metal components in two repetitions. The mean score shows that there was no significant difference between the results of measurements for the proposed system (mm) and the GOM ATOS as the mean score of proposed system-1 is 76.08 mm, whereas the GOM ATOS-1 is 76.00 mm, a difference of only 0.08. The mean score for the proposed system-2 is 101.44 mm, with the GOM ATOS-2 at 101.24 mm, a difference is only 0.20 mm. This shows the measurement accuracy of the proposed measurement system as compared to the GOM ATOS. The low standard deviation (0.0070 for pair 1 and 0.1319 for pair 2) means the score is consistent and the p score is $p > 0.000$ for pair 1, and 0.003 for pair 2. This is less than the standard $p = 0.05$, which shows the significant difference between both pairs.

Table 5-8 Reliability statistics

Cronbach's Alpha^a	Cronbach's Alpha based on standardized items	No. of Items
.908	.921	16

Table 5.8 shows the scores of reliability statistics between the length measurement scores of the repeated measures taken by the proposed system and the GOM ATOS. The Cronbach alpha score is 0.908, which indicates strong reliability between the measurements of heated sample diameters by the proposed system and the GOM ATOS. The standardized items score is 0.921, which means inter-correlation is also strong and measurements are accurate.

It should be noted that because of the curves created on the sample edges due to forging, the measurement errors recorded for the diameters are slightly higher than the values observed for the length measurements of samples. A descriptive analysis of all the samples data was carried out through the SPSS statistical analysis software to validate the measurement accuracy of the proposed system. The results for the diameter and length of pre-forged heated samples were presented as boxplot graphs showing the maximum and minimum values along with mean values (Figure 5.8). The measured values of the proposed system and reference values are very close and are shown in the box plot graph in Figure 5.8. It must be noted that Figure 5.8 represents the data of all 16 samples' diameter and length at subpixel level measurements.

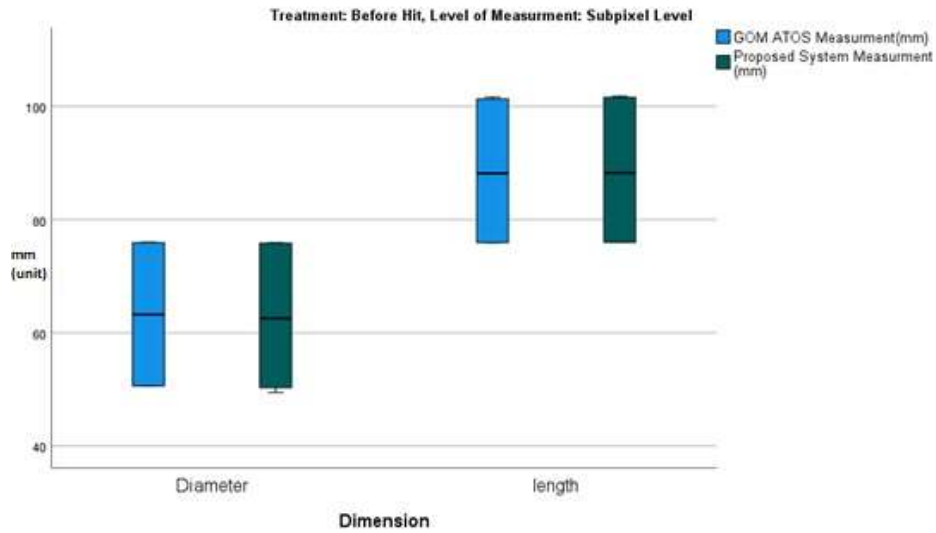


Figure 5-8 Descriptive analysis of heated samples at subpixel level before forging

5.4.2 Results of diameter & length measurements of forged samples (heated)

Tables 5.1 and 5.2 show the results of the diameter measurements and Tables 5.5 and 5.6 the results of the length measurements of forged samples recorded by the GOM ATOS system (corrected values with thermal expansion) and the proposed in-line dimensional measurement system at subpixel level.

The first eight samples were of small size and similar in dimensions such as diameter and length, as compared to samples from nine to sixteen. The measurements were taken at elevated temperatures but after the sample was forged. The measurement error for diameters of the proposed system was recorded as less than 1 mm in first eight samples and 1.2 mm among relatively bigger samples numbers nine to sixteen.

Table 5-9 Diameter measurements of first eight heated samples after forging

Sample.no	GOM ATOS(mm)	Proposed System(mm)	Error [mm]	% error
1	50.40	51.28	0.88	1.88
2	51.40	52.27	0.87	1.87
3	51.60	52.47	0.87	1.87
4	50.50	51.39	0.89	1.89
5	51.00	51.88	0.88	1.88
6	58.60	59.60	1.00	2.00
7	50.50	50.87	0.37	1.37
8	57.80	57.90	0.10	1.10
Mean	52.73	53.46	0.732	1.732
S.D	3.4137	3.3392	0.3183	0.3183

95% C.I	[55.02, 51.17]	[55.76,51.34]	-	-
Sign	.000	.000	-	-

Table 5.9 shows the comparison of measurement values of the sample diameters for both the reference and the proposed systems. The maximum percentage error was noted at 1.88% which was due to the deformation of the metal sample after being hit by the forging hammer, because after hammering the boundaries become curved. The global mean percentage error was less than 1.8% for the first eight samples. The resulting 95% CI for the mean values of the GOM ATOS was between 55.02 mm and 51.17 mm. Similarly, the resulting 95% CI for the mean values of the proposed measurement system was between 55.76 mm and 51.34 mm. Hence the study analysis shows that the outcome of the proposed system (mm) results for length measurements of all heated samples during forging are statistically significant to the GOM ATOS (mm). The global millimetre error between the standard deviation of the reference values and the proposed system values was less than 0.75 mm and percentage error was less than 0.35%, which demonstrates the measurement accuracy of the proposed system during the forging process. The measurement results showed that the error difference of the proposed system is very small as compared to the readings recorded with the reference system, which validates the measurement accuracy of the proposed system for hot forging applications at sub-pixel level.

Table 5-10 Diameter measurements of remaining eight heated samples after forging

Sample.no	GOM ATOS(mm)	Proposed system(mm)	Error [mm]	% error
1	80.00	80.49	0.49	1.49
2	85.00	85.40	0.40	1.40
3	85.00	85.94	0.94	1.94
4	85.00	86.16	1.16	2.16
5	85.00	85.40	0.40	1.40
6	85.00	85.89	0.89	1.89
7	85.00	85.78	0.78	1.78
8	85.00	86.00	1.00	2.00
Mean	84.37	85.13	0.76	1.76
S.D	1.7678	1.8954	0.2926	0.2926
95% C.I	[85.55, 83.45]	[86.43,84.57]	-	-
Sign	.000	.000	-	-

Table 5.10 shows the comparison of measurement values for the GOM ATOS system and the proposed system of sample diameters. The maximum percentage error was 2.16%, which was due to the deformation of the metal sample after being hit by the forging hammer, because after hammering the boundaries become curved. The global mean percentage error was less than 1.8% for the remaining eight samples. The resulting 95% CI for the mean values of the GOM ATOS was between 85.55 mm and 83.45 mm. Similarly, the resulting 95% CI for the mean values of the proposed measurement system was between 86.43 mm and 84.57 mm. Hence the study analysis shows that the outcome of the proposed system (mm) results for the length measurements of all heated samples during forging are very close to the GOM ATOS (mm). The global millimetre error between the standard deviation of reference values and proposed system values was less than 0.13 mm and percentage error was less than 0.3%, which demonstrates the measurement accuracy of the proposed system during the forging process. The measurement results showed that the error difference of the proposed system is very small as compared to the readings recorded by the reference system, which validates the measurement accuracy of the proposed system for hot forging applications at sub-pixel level.

Table 5-11 Paired sample test scores between diameter measurements of heated samples after forging through (sub-pixels) proposed system and GOM ATOS in repetitions

Pair	Items in the Pair		No.	Mean		Std. Deviation	T score	Sig. (2-tailed)
				Single	Overall			
1.	Proposed system (mm)-1	system	8	53.46	.73	.3183	6.509	.000
				GOM ATOS (mm)-1				
2.	Proposed system (mm)-2	system	8	85.13	.76	.2926	7.322	.000
				GOM ATOS (mm)-2				

Table 5.11 displays the diameter measurements of the heated samples, after forging, by the proposed system (mm) and the GOM ATOS (mm) for 16 repetitions through a dependent sample test, showing the comparison of measurements of sample diameter of pre-forging 16 metal components in two repetitions. The mean score shows that there was no significant difference between the results of measurements for the proposed system (mm) and the GOM ATOS as the mean score of proposed system-1 is 53.46 mm, and the GOM ATOS-1 is 52.72 mm, a difference of only 0.74 mm. The mean score for the proposed system-2 is

85.13 mm and the GOM ATOS-2 84.38 mm, a difference of only 0.75 mm. This shows the measurement accuracy of the proposed measurement system as compared to the GOM ATOS. Their standard deviation is also intact with 0.3183 and 0.2926 for both pairs respectively. The low standard deviation (0.3183 for pair 1 and 0.2926 for pair 2) means the score is consistent and the p-score is $p > .000$ for both pairs, less than the standard $p = 0.05$, which shows the significant difference between both pairs.

Table 5-12 Reliability statistics

Cronbach's Alpha ^a	Cronbach's based standardized items	Alpha on	No. of Items
0.795	0.811		16

Table 5.12 shows the scores of reliability statistics between the length measurement scores of the repeated measures taken by the proposed system and the GOM ATOS. The Cronbach alpha score is 0.795, which indicates strong reliability between the measurements of the heated sample diameter by the proposed system and the GOM ATOS. The standardized items score is 0.811, which means inter-correlation is also strong and measurements are accurate.

Table 5-13 Length measurements of first eight heated samples after forging

Sample.no	GOM ATOS(mm)	Proposed System(mm)	Error [mm]	% error
1	71.20	71.90	0.70	1.70
2	71.70	72.56	0.86	1.86
3	66.40	67.40	1.00	2.00
4	63.30	64.16	0.86	1.86
5	63.30	63.41	0.11	1.11
6	86.00	86.48	0.48	1.48
7	51.00	51.29	0.29	1.29
8	67.50	68.48	0.98	1.98
Mean	67.55	68.21	0.66	1.66
S.D	9.8727	9.9483	0.3319	0.3319
95% C.I	74.32 – 72.68	75.01- 73.92		
Sign	.000	.000	-	-

Table 5.13 shows the comparison of measurement values for the reference and the proposed system of samples length. The maximum percentage error was 2.00% in sample 3 which was

due to the deformation of the metal sample after being hit by the forging hammer, because after hammering the boundaries become curved. The resulting 95% CI for the mean values of the GOM ATOS was between 74.32 mm and 72.68 mm. Similarly, the resulting 95% CI for the mean values of proposed measurement system was between 75.01 mm and 73.92 mm. Hence the study analysis shows that the outcome of proposed system (mm) results for length measurements of the first eight heated samples after forging are similar to the GOM ATOS (mm). The mean error between all samples was recorded at less than 0.7 mm and percentage error was less than 1.7%, which demonstrates the measurement accuracy of the proposed system after the forging process. The measurements results showed that the error difference of the proposed system is very small as compared to the readings recorded by the reference system, which validates the measurement accuracy of the proposed system for hot forging applications at sub-pixel level.

Table 5-14 Length measurements of remaining eight heated samples after forging

Sample.no	GOM ATOS(mm)	Proposed System(mm)	Error [mm]	% error
1	84.30	84.59	0.29	1.29
2	84.50	85.25	0.75	1.75
3	84.30	84.60	0.30	1.30
4	84.30	85.16	0.86	1.86
5	84.30	85.16	0.86	1.86
6	84.40	85.29	0.89	1.89
7	84.40	85.39	0.99	1.99
8	83.40	84.55	1.15	2.15
Mean	84.24	85.00	0.76	1.76
S.D	0.3462	0.3547	0.3104	0.3104
95% C.I	84.44 – 83.55	85.14 – 83.82	-	-
Sign	.000	.000	-	-

Table 5.14 shows the comparison of measurement values for the GOM ATOS and the proposed system of sample lengths. The maximum percentage error was 2.15% which was due to the deformation of the metal sample after being hit by the forging hammer, because after hammering the boundaries become curved. The resulting 95% CI for the mean values of GOM ATOS was between 84.44 mm and 83.55 mm. Similarly, the resulting 95% CI for the mean values of the proposed measurement system was between 85.14 mm and 83.82 mm. Hence the study analysis shows that the outcome of the proposed system (mm) results for

length measurements of remaining eight heated samples after forging are statistically significant to the GOM ATOS (mm). The global millimetre error between the standard deviation of reference values and proposed system values was less than 0.0085 mm and percentage error was less than 1.1%, which demonstrates the measurement accuracy of the proposed system after the forging process. The measurements results showed that the error difference of the proposed system is very small as compared to the readings recorded by the reference system, which validates the measurement accuracy of the proposed system for hot forging applications at sub-pixel level.

Table 5-15 Paired sample test scores between length measurements of heated samples after forging through (sub-pixels) proposed system and GOM ATOS in repetitions

Pair	Items in the Pair		No.	Mean		Std. Deviation	T score	Sig. (2-tailed)
				Single	Overall			
1.	Proposed system (length)-1	system	8	68.21	.66	.3319	5.623	.001
				GOM ATOS (length)-1				
2.	Proposed system (length)-2	system	8	85.00	.76	.3104	6.936	.000
				GOM ATOS (length)-2				

Table 5.15 presents the results from paired sample analysis for length measurements of heated samples after forging using both the proposed sub-pixel level system and the GOM ATOS system. Results depict the precision, uniformity, and reliability of the proposed system over many iterations and provide convincing justification for its integration into the current study.

The average length obtained through the proposed methodology in the initial sample set was recorded at 68.21 mm, while the GOM ATOS system measured this length at 67.55 mm, yielding a minimal mean variance of 0.66 mm. In the subsequent sample set, the average lengths were determined to be 85.00 mm (for the proposed system) and 84.24 mm (for the GOM ATOS system), resulting in a slight discrepancy of 0.76 mm. The minimal discrepancies observed indicate that the proposed system provides measurements that are in close agreement with the established GOM ATOS system, which makes it promising for achieving high-precision measurement outcomes.

The standard deviations recorded for the proposed system were 0.3319 mm and 0.3104 mm for the initial and subsequent sets, respectively, which indicates a very high level of consistency in the findings. This low level of variability is important for ensuring both repeatability and reliability in the context of industrial dimensional measurement applications. In addition, the statistical analysis conducted showed p-values of 0.001 for the first set and 0.000 for the second set, which are less than the traditional significance level of $p = 0.05$. This means that the statement that the proposed system provides reliable and comparable data compared to the GOM ATOS system is confirmed. In addition, the significant *t*-scores of 5.623 and 6.936 provide further evidence for the robust similarity found between the two systems, which reflects the robustness of the proposed system.

The findings in Table 5.15 provide excellent support for the proposed system in this study. Although the GOM ATOS system is a reliable benchmark, it is a costly and rigid solution that lacks the flexibility needed for dynamic manufacturing environments. Conversely, the system under evaluation provides similar degrees of accuracy at a significantly reduced cost, thereby making it an even more feasible choice for a broader range of industrial applications. It is particularly helpful in providing in-line, real-time measurements in enhancing process optimization, and thus overcoming an important limitation that exists with the GOM ATOS system.

This system indicates a performance level that is robust and reliable in high-temperature forging, despite optical distortions and thermal gradients that could adversely affect measurement accuracy. It is possible to overcome the above challenges and provide an assurance of precision measurements even under extreme conditions with sub-pixel level accuracy. The system, being non-contact and automated, also adheres to Industry 4.0, where high-efficiency and quality control can be integrated into the advanced manufacturing technology.

Table 5-16 Reliability statistics

Cronbach's Alpha ^a	Cronbach's based standardized items	Alpha on	No. of Items
0.665	0.701		16

Table 5.16 shows the scores of reliability statistics between the length measurement scores of the repeated measures taken by the proposed system and the GOM ATOS. The Cronbach alpha score is 0.665, which indicates moderate reliability between the measurements of heated sample length by the proposed system and the GOM ATOS. The standardized items score is 0.701, which means inter-correlation is also strong and measurements are accurate.

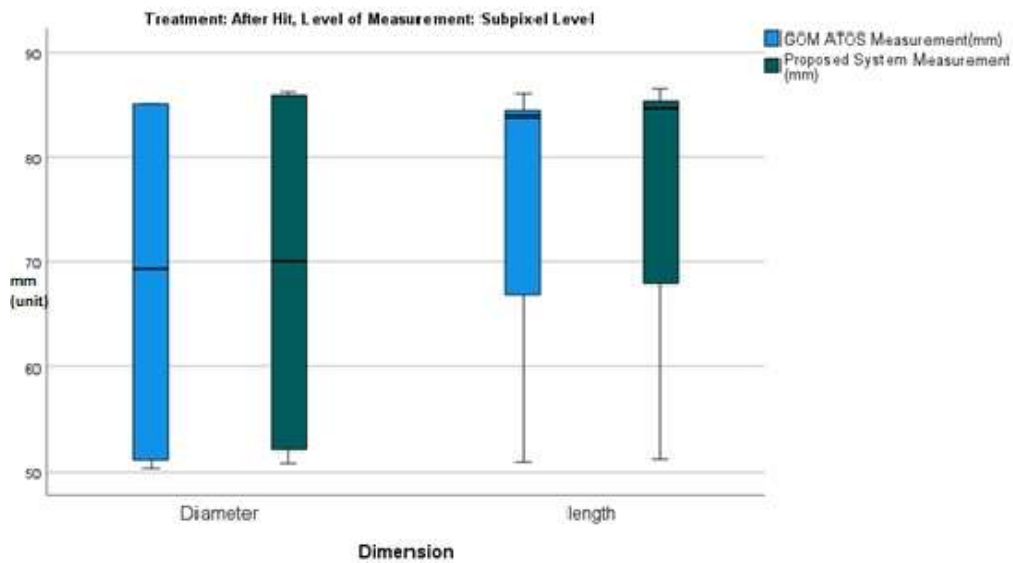


Figure 5-9 Descriptive analysis of heated samples at subpixel level during hot forging

The study analysis shows that the outcome of the proposed system (mm) results for length measurements of all heated samples after forging are similar to the GOM ATOS (mm). The diameter and length measurement results for the forged samples are illustrated using boxplot graphs (Figure 5.9), which depict the maximum, minimum and mean values. The measurements obtained from the proposed system closely align with the reference values, demonstrating a high level of accuracy. Notably, the measurement error consistently remained below 1 mm, as clearly indicated in the boxplot representation in Figure 5.9.

5.5 Analysis and comparison of proposed system measurement at pixel and subpixel level

A brief analysis of experimental results has proved the capability of the proposed system for the real time dimensional measurement of metal parts during hot forgings. Results showed that the proposed system has a capability in terms of defined accuracy and repeatability to measure both the length and diameter of parts during hot forgings. This part of the research presents a comparative analysis of the proposed system's measurement accuracy at pixel and subpixel level.

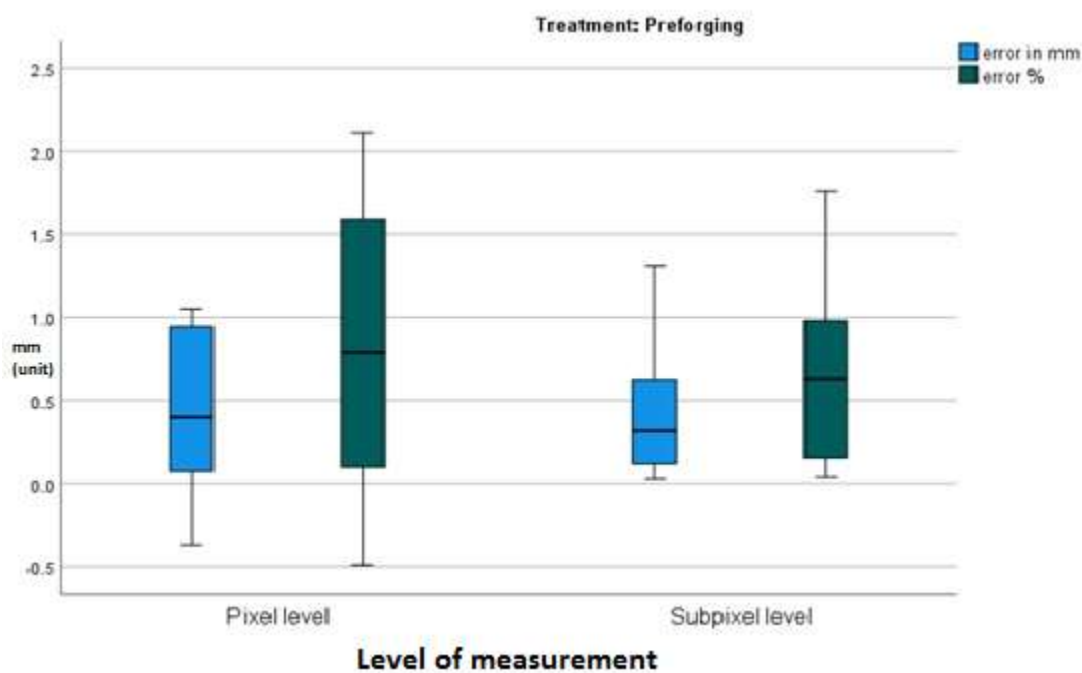


Figure 5-10 Comparison of proposed system for heated samples diameter at pixel and subpixel level

Figure 5.10 presents the comparative analysis of the dimensional measurement of the proposed system at the pixel and subpixel level. It must be noted that the boxplot shows the results of the measurement and percentage errors for diameter measurements of all samples before forging.

Figure 5.10 shows that the standard error of diameter is less than ± 0.25 mm and the variance of the results is similar globally at both the pixel and subpixel level. The difference between the measured and reference values is less than 2 mm.

The standard error for length measurement of all samples were recorded to be less than 0.25 mm for both the pixel and subpixel level results generated by the proposed system (Figure 5.11). The percentage error was less than 1%, which shows the measurement capability and repeatability of the current real time dimensional measurement system. The difference of median and variance values was also recorded to be less than 0.3 mm at both the pixel and subpixel level. In fact, the algorithm developed for subpixel level measurements of the same samples produced slightly better results in terms of standard error and measurement deviations.

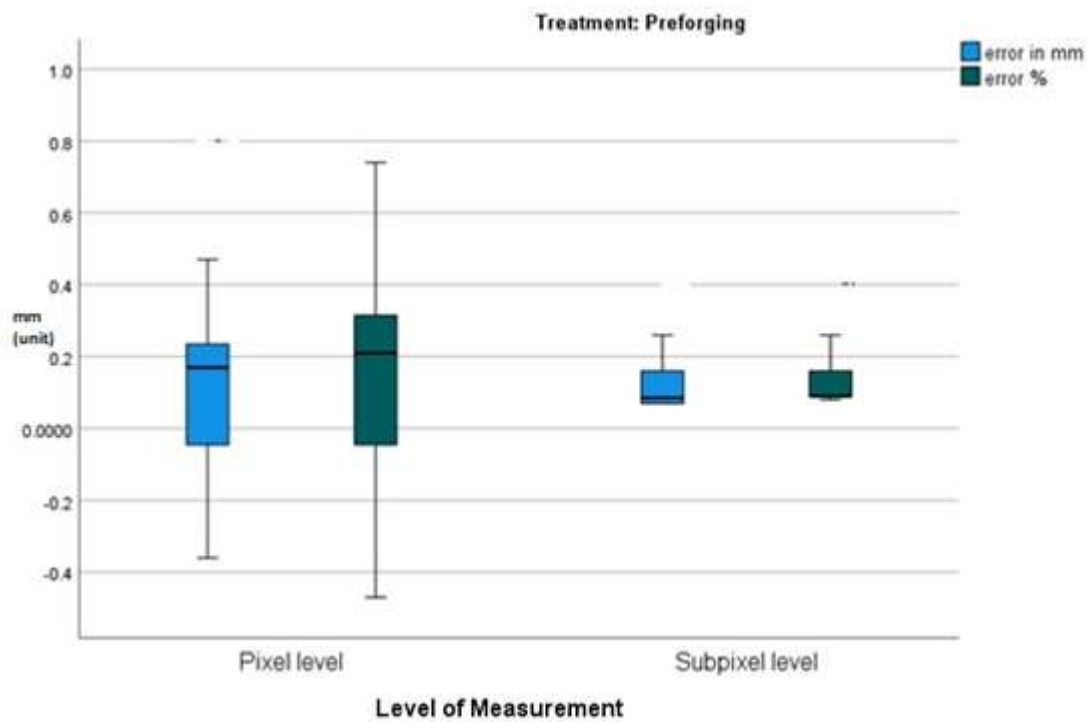


Figure 5-11 Comparison of proposed system for heated samples lengths measurement at pixel and subpixel level

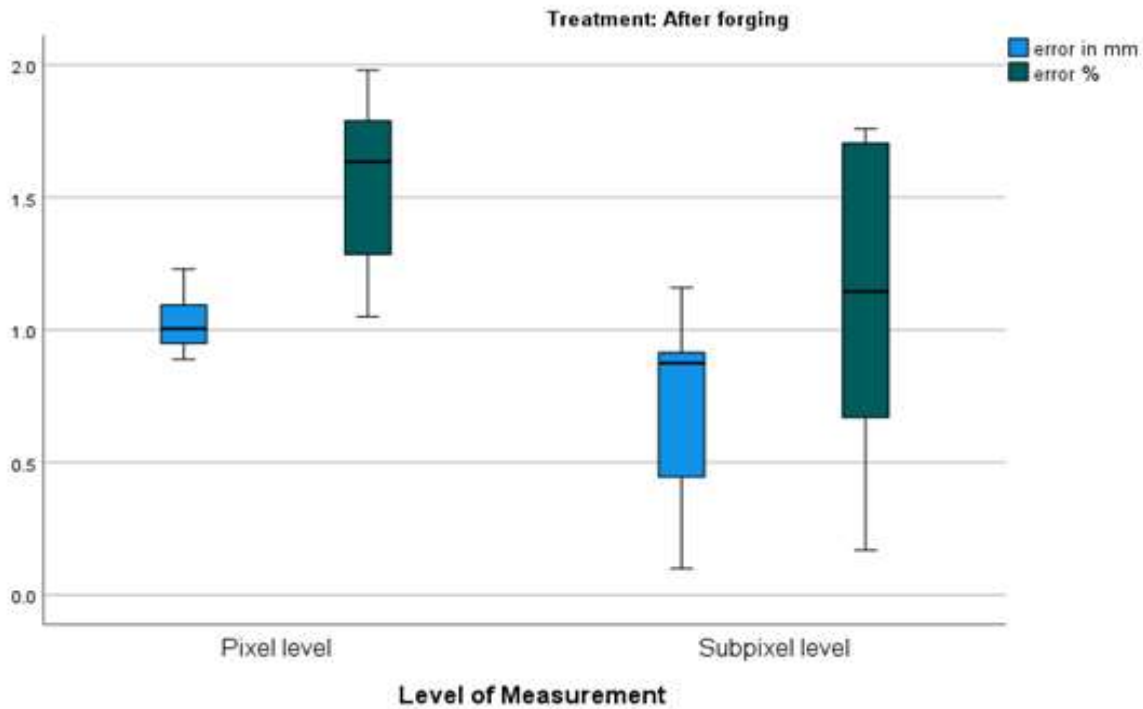


Figure 5-12 Comparison of the proposed system for heated samples diameter measurement at the pixel and subpixel level.

It can be easily seen that the overall diameter of all samples increased due to the hammering process during hot forging. Figure 5.12 shows the standard deviations of all forged samples at both the pixel and subpixel level to be less than ± 0.6 mm along with the percentage error which was recorded to be less than 2%. It should be noted that Tables 5.9, 5.10, 5.13 and 5.14 present the results of the samples after being forged at an elevated temperature.

Similar results were recorded for the length measurements of all samples during the forging process. The analysis of experimental results proved the efficiency and measurement accuracy of the proposed passive photogrammetry measurement system during hot forging.

5.6 Conclusion

Chapter 5 has focused on enhancing the dimensional measurement capabilities of the proposed system by integrating subpixel-level accuracy methods, addressing the limitations of pixel-level techniques, and overcoming challenges such as the thermal aura. The chapter conducted a comprehensive comparative analysis of subpixel methods, including curve-fitting, moment-based, and reconstructive approaches, and evaluated their performance through experimental benchmarking and statistical analysis. These investigations have

demonstrated that, while all subpixel methods improve upon pixel-level accuracy, the reconstructive methods consistently outperformed the alternatives, making them the most suitable choice for high-temperature industrial applications.

The thermal aura, a critical problem discussed in Chapter 4, causes refractive distortions, infrared interference, and noise that negatively impact measurement accuracy. The results of the statistical analysis proved that subpixel methods significantly reduce these errors. Stimulatingly, reconstructive methods had the lowest mean error, from 0.7 mm to 0.9 mm, and the lowest standard deviation, averaging 0.007 mm. These results highlight the effectiveness and reliability of reconstructive methods in alleviating the complex optical distortions caused by the thermal aura, thereby enabling accurate and reliable dimensional measurements.

The statistical analysis provided valuable insights into the effectiveness of the algorithms under consideration. While the curve-fitting and moment-based algorithms were computationally efficient, they were found to have higher variability and larger errors at high temperatures. The reconstructive algorithms, on the other hand, offered smaller confidence intervals and lower variability, thus establishing their ability to efficiently adapt to unfavorable environmental conditions. These observations support the proposition that reconstructive algorithms are instrumental in achieving subpixel-level accuracy in high-temperature forging conditions, thus alleviating the inadequacies linked to other techniques.

The integration of reconstruction methods into the proposed system is a significant development in measurement technology. The application of iterated reconstruction algorithms in combination with adaptive compensation algorithms ensures measurement precision within ± 1 mm, meeting high-grade industrial application precision needs. Although reconstruction methods require high computational means, which in general take between 2.0 and 2.5 seconds per frame, precision and consistency justify this investment. Further research activities can investigate whether hardware accelerators and different algorithms can be applied to improve the efficiency of real-time performance without sacrificing measurement precision.

Recent developments have important implications for industries ranging from forging, to aerospace, to automotive production. The potential of the system in question to deliver

precise and reliable in-line measurement reduces losses, increases product quality, and makes process optimization feasible. In addition, its robust performance in challenging conditions is in accord with Industry 4.0 principles, which makes automated dimension measurement viable to integrate into sophisticated production processes.

In summary, Chapter 5 has demonstrated the critical role of subpixel-level measurement accuracy in addressing the challenges posed by the thermal aura and ensuring reliable dimensional assessment in high-temperature environments. The statistical analysis has validated the superiority of reconstructive methods, which provide consistent, precise and robust performance. These findings justify the selection and implementation of subpixel level dimensional measurement within the proposed system and form the foundation for future developments aimed at further optimizing accuracy and efficiency in real-world industrial applications.

6 Conclusion and future recommendations

6.0 Conclusion

This thesis discusses a critical and industrially relevant challenges in the domain of dimensional metrology. It deals with accurate, real-time, non-contact measurements of hot forged parts at elevated temperatures. The study began by examining existing measurement techniques in depth, proceeded to test existing systems, and culminated in developing and refining a new measurement system to operate at elevated temperature as required by industry requirements.

The **review of literature** underscored the complexity of dimensional measurement at high-temperature during hot forging. While advanced commercial systems such as the GOM ATOS provide high-accuracy scanning at room temperature, they are unsuitable for real-time in-process measurement due to limitations including glare, heat distortion, measurement dropout, and lack of thermal compensation at elevated temperature. Moreover, most prior studies validated systems measurement accuracy at room temperature, rather than in hot forging environment, where thermal radiations and environmental interferences present additional obstacles.

The **limitations of current systems** were demonstrated through comparative studies. Experimental results presented significant error margins and loss of geometric data at elevated temperature when using state-of-the-art optical metrology systems. Moreover, commercially available noncontact measurement systems were found to be costly and sensitive to thermal aura effects, making them unfeasible for in process integration into hot forgings.

A **novel pixel-based measurement system** was proposed and developed to overcome these limitation of accurate dimensional measurement during hot forgings. The system employed a standard CCD camera, IR filters, and more efficient hot forging image processing techniques. The novelty of the proposed noncontact measurement system is its cost effectiveness, portability and adaptability to real-time measurement at elevated temperatures without stopping the forging process. The pixel-based measurement system achieved an accuracy of

± 1 mm during experiments at elevated temperature which validates the accuracy and robustness of proposed system. This is a significant innovation that delivers an effortless, robust, and user-friendly application for most forging processes lacking this aspect.

Building upon the pixel-level approach, a **sub-pixel edge detection and measurement algorithm** was developed to further refine accuracy and robustness of proposed measurement system. It was tested and found that the system not only achieved the measurement accuracy of ± 1 mm but also reduced measurement errors, particularly when there were heat-induced phenomena such as aura.

In conclusion, this project has benefited the field of optical measurement and intelligent manufacturing by developing a cost-effective, precise, and robust measurement system for hot forging. The findings form a good foundation for transitioning towards complete Industry 4.0 preparedness for closed-loop feedback, real-time defect inspection, and improved process monitoring for thermomechanical manufacturing processes.

6.1 Contribution to knowledge

This contribution of current research is not only technical but it also provides manufacturers with a scalable solution that enhances measurement accuracy, reduces waste, and supports advanced manufacturing goals in hot forging application.

In summary, this research has:

1. Quantified and identified the performance limitations of current state-of-the-art measurement systems under high-temperature conditions such as hot forging.
2. Developed and demonstrated a novel pixel-based dimensional measurement system suitable for real-time dimensional measurement of hot parts at elevated temperatures.
3. Proposed and experimentally demonstrated a refined sub-pixel level algorithm for enhanced dimensional measurement precision during hot forgings.
4. Established a comprehensive assessment for high-temperature optical metrology system both at pixel and subpixel level.

5. Contributed a cost-effective and scalable proposed system that aligns with Industry 4.0 and future manufacturing automation requirements.

These contributions together represent a major advancement in the field of high-temperature dimensional metrology and are the foundation for current research on intelligent and adaptive metrology for harsh manufacturing environments.

6.2 Future research directions

While the proposed measurement system has demonstrated promising results, there are certain aspects that should be further investigated and enhanced. The following directions for future research are proposed to enhance the robustness, flexibility and industrial applicability of the system:

Optimization of image processing algorithms

Future advancement in image processing algorithms may alleviate issues of heat distortions, glare and surface reflectance. The use of advanced machine learning methods such as those in deep learning in feature extraction may enhance the capability of the system to adapt to dynamic processing environments.

Expansion of measurement capabilities

The present system has been verified for certain hot forging operations. Research in the future must look into its extension to a broader spectrum of metal forming operations, such as warm and cold forging, and other high-temperature manufacturing operations such as casting and welding.

Integration with digital twin technology

Integrating the measurement system in a digital twin framework can enable real-time simulation and predictive analysis for process optimization. By updating virtual models with real-time measurement data, manufacturers can more effectively comprehend process dynamics and forecast deviations, enabling pre-emptive action.

Enhancement of system hardware

More research should be conducted to create more accurate positioning of sensors, advance thermal protection technologies, and strengthen the optical components to resist long-term exposure to high temperatures. The creation of adaptive coatings or the implementation of

adaptive optics will assist in reducing the effect of environmental conditions on measurement accuracy.

Addressing measurement uncertainty and aura effects

The research highlighted the effect of 'aura' effects generated by hot metal surfaces, which can affect the accuracy of measurements. Although a subpixel level algorithm was developed and applied in current research which showed promising results with improved dimension measurement accuracy, future research needs to develop compensation models for rectifying these distortions and thus achieve more accurate dimensional evaluations under extreme thermal conditions.

By following these directions of research, future work will be able to build upon the foundations set out in this thesis, thereby improving the discipline of real-time, high-temperature dimensional measurement and the overall objectives of precision manufacturing and Industry 4.0 integration.

References

- [1] N. Rajagopal, "Development of Guidelines for Warm Forging of Steel Parts," The Ohio State University, 2014.
- [2] K. Osakada, "History of plasticity and metal forming analysis," *Journal of Materials Processing Technology*, vol. 210, no. 11, pp. 1436-1454, 2010.
- [3] A. Tekkaya *et al.*, "Metal forming beyond shaping: Predicting and setting product properties," *CIRP Annals*, vol. 64, no. 2, pp. 629-653, 2015.
- [4] J. M. Cullen, J. M. Allwood, and M. D. Bambach, "Mapping the global flow of steel: from steelmaking to end-use goods," *Environmental science & technology*, vol. 46, no. 24, pp. 13048-13055, 2012.
- [5] J. M. Cullen and J. M. Allwood, "Mapping the global flow of aluminum: from liquid aluminum to end-use goods," *Environmental science & technology*, vol. 47, no. 7, pp. 3057-3064, 2013.
- [6] J. M. Allwood *et al.*, *Sustainable materials: with both eyes open*. UIT Cambridge Limited Cambridge, UK, 2012.
- [7] T. Altan, G. Ngaile, and G. Shen, *Cold and hot forging: fundamentals and applications*. ASM international, 2004.
- [8] P. Groche, D. Fritsche, E. Tekkaya, J. Allwood, G. Hirt, and R. Neugebauer, "Incremental bulk metal forming," *CIRP annals*, vol. 56, no. 2, pp. 635-656, 2007.
- [9] J. Allwood and H. Utsunomiya, "A survey of flexible forming processes in Japan," *International Journal of Machine Tools and Manufacture*, vol. 46, no. 15, pp. 1939-1960, 2006.
- [10] J. A. Polyblank, J. M. Allwood, and S. R. Duncan, "Closed-loop control of product properties in metal forming: A review and prospectus," *Journal of Materials Processing Technology*, vol. 214, no. 11, pp. 2333-2348, 2014.
- [11] M. Geiger and R. Neugebauer, "Process basics of warm forging for shaft-shaped parts (Prozessgrundlagen für die Halbwarmumformung wellenförmiger Teile mit weit auskragenden Formelementen)," *Studiengesellschaft Stahlanwendung, Report P*, vol. 452, 2003.
- [12] S. Zupan and R. Kunc, "Overview of Principles and Rules of Geometrical Product Specifications According to the Current ISO Standards," *Strojniški vestnik-Journal of Mechanical Engineering*, vol. 70, no. 1-2, pp. 3-19, 2024.
- [13] S. Kalpakjian, *Manufacturing processes for engineering materials*. Pearson Education India, 1984.
- [14] A. Armillotta and Q. Semeraro, "Geometric tolerance specification," *Geometric tolerances: impact on product design, quality inspection and statistical process monitoring*, pp. 3-37, 2011.
- [15] [Online] Available: <https://www.mineralstech.com/minteq/ferrotron>
- [16] S. Sheljaskov, "Current level of development of warm forging technology," *Journal of Materials Processing Technology*, vol. 46, no. 1-2, pp. 3-18, 1994.
- [17] S. Fujikawa, H. Yoshioka, and S. Shimamura, "Cold-and warm-forging applications in the automotive industry," *Journal of materials processing technology*, vol. 35, no. 3-4, pp. 317-342, 1992.
- [18] B. Behrens, L. Barnert, and A. Huskic, "Alternative techniques to reduce die wear—Hard coating or ceramics?," *Annals of the German Academic Society for Production Engineering (WGP)*, vol. 12, p. 2, 2005.
- [19] B. K. Belur and R. V. Grandhi, "Geometric deviations in forging and cooling operations due to process uncertainties," *Journal of materials processing technology*, vol. 152, no. 2, pp. 204-214, 2004.
- [20] R. Shivpuri, S. Babu, S. Kini, P. Pauskar, and A. Deshpande, "Recent advances in cold and warm forging process modeling techniques: selected examples," *Journal of materials processing technology*, vol. 46, no. 1-2, pp. 253-274, 1994.

- [21] W. Shichun, "Warm forging of stainless steels," *Journal of Mechanical Working Technology*, vol. 6, no. 4, pp. 333-345, 1982.
- [22] T. Nye, A. Elbadan, and G. Bone, "Real-time process characterization of open die forging for adaptive control," *J. Eng. Mater. Technol.*, vol. 123, no. 4, pp. 511-516, 2001.
- [23] Z. Zhang, J. Yu, Y. Xue, B. Dong, X. Zhao, and Q. Wang, "Recent research and development on forming for large magnesium alloy components with high mechanical properties," *Journal of Magnesium and Alloys*, vol. 11, no. 11, pp. 4054-4081, 2023/11/01/ 2023, doi: <https://doi.org/10.1016/j.jma.2023.09.038>.
- [24] M. Hawryluk, J. Ziembra, and P. Sadowski, "A review of current and new measurement techniques used in hot die forging processes," *Measurement and Control*, vol. 50, no. 3, pp. 74-86, 2017.
- [25] E. Siemer, P. Nieschwitz, and R. Kopp, "QUALITY OPTIMIZED PROCESS-CONTROL IN OPEN-DIE FORGING," *Stahl Und Eisen*, vol. 106, no. 8, pp. 383-387, 1986.
- [26] A. Bicknell, J. Smith, and J. Lucas, "Infrared sensor for top face monitoring of weld pools," *Measurement Science and Technology*, vol. 5, no. 4, p. 371, 1994.
- [27] P. Wright and D. Bourne, "A flexible manufacturing cell for swaging," *Mechanical Engineering*, vol. 104, no. 10, pp. 76-83, 1982.
- [28] T. Chang, F. Tsai, H. Huang, and C. Lorenz, "Real-time measurement/inspection of forged parts and associated applications," in *Proceedings of the 23rd forging industry technical conference*, 2001.
- [29] C. Rocchini, P. Cignoni, C. Montani, P. Pingi, and R. Scopigno, "A low cost 3D scanner based on structured light," in *computer graphics forum*, 2001, vol. 20, no. 3: Wiley Online Library, pp. 299-308.
- [30] J. Ye, G. Fu, and U. P. Poudel, "High-accuracy edge detection with blurred edge model," *Image and Vision Computing*, vol. 23, no. 5, pp. 453-467, 2005.
- [31] Z. Tian, F. Gao, Z. Jin, and X. Zhao, "Dimension measurement of hot large forgings with a novel time-of-flight system," *The International Journal of Advanced Manufacturing Technology*, vol. 44, pp. 125-132, 2009.
- [32] Y. Lee, J. Lee, and T. Ishikawa, "Analysis of the elastic characteristics at forging die for the cold forged dimensional accuracy," *Journal of Materials Processing Technology*, vol. 130, pp. 532-539, 2002.
- [33] S. D. Phillips, C. M. Shakarji, A. Balsamo, M. Krystek, and E. Morse, "The 2016 revision of ISO 1—standard reference temperature for the specification of geometrical and dimensional properties," *Journal of research of the National Institute of Standards and Technology*, vol. 121, p. 498, 2016.
- [34] D. E. ISO, "Geometrical product specifications (GPS)—geometrical tolerancing—tolerances of form, orientation, location and run-out," 2006.
- [35] E. Savio, L. De Chiffre, and R. Schmitt, "Metrology of freeform shaped parts," *CIRP annals*, vol. 56, no. 2, pp. 810-835, 2007.
- [36] X.-b. Fu, B. Liu, and Y.-c. Zhang, "An optical non-contact measurement method for hot-state size of cylindrical shell forging," *Measurement*, vol. 45, no. 6, pp. 1343-1349, 2012.
- [37] J. He, F. Gao, S. Wu, R. Liu, and X. Zhao, "Measure dimension of rotating large hot steel shell using pulse laser on PRRR robot," *Measurement*, vol. 45, no. 7, pp. 1814-1823, 2012.
- [38] J. Zhang, W. Li, K. Wang, and R. Jin, "Process adjustment with an asymmetric quality loss function," *Journal of Manufacturing Systems*, vol. 33, no. 1, pp. 159-165, 2014.
- [39] S. Dworkin and T. Nye, "Image processing for machine vision measurement of hot formed parts," *Journal of materials processing technology*, vol. 174, no. 1-3, pp. 1-6, 2006.

- [40] Z. Jia, B. Wang, W. Liu, and Y. Sun, "An improved image acquiring method for machine vision measurement of hot formed parts," *Journal of Materials Processing Technology*, vol. 210, no. 2, pp. 267-271, 2010.
- [41] H. Huang, "Imaging-based in-line surface defect inspection for bar rolling," in *AIST Iron & Steel Conference and Exposition, Nashville, TN, 2004*, 2004.
- [42] Y. Cui, S. Schuon, D. Chan, S. Thrun, and C. Theobalt, "3D shape scanning with a time-of-flight camera," in *2010 IEEE computer society conference on computer vision and pattern recognition*, 2010: IEEE, pp. 1173-1180.
- [43] K. Liang, H. Liu, and H. Ju, "Accurate ranging method of pulse laser time-of-flight based on the principle of self-triggering," in *Proceedings of the 32nd Chinese Control Conference*, 2013: IEEE, pp. 5583-5587.
- [44] S. May *et al.*, "Three-dimensional mapping with time-of-flight cameras," *Journal of Field Robotics*, vol. 26, no. 11-12, pp. 934-965, 2009.
- [45] X. Wen, J. Wang, G. Zhang, and L. Niu, "Three-dimensional morphology and size measurement of high-temperature metal components based on machine vision technology: a review," *Sensors*, vol. 21, no. 14, p. 4680, 2021.
- [46] L. K. Barker, "Vector-algebra approach to extract Denavit-Hartenberg parameters of assembled robot arms," 1983.
- [47] Y. Bokhabrine *et al.*, "3D characterization of hot metallic shells during industrial forging," *Machine vision and applications*, vol. 23, no. 3, pp. 417-425, 2012.
- [48] P. J. Besl and N. D. McKay, "Method for registration of 3-D shapes," in *Sensor fusion IV: control paradigms and data structures*, 1992, vol. 1611: Spie, pp. 586-606.
- [49] Z. Du, Z. Wu, and J. Yang, "3D measuring and segmentation method for hot heavy forging," *Measurement*, vol. 85, pp. 43-53, 2016/05/01/ 2016, doi: <https://doi.org/10.1016/j.measurement.2016.02.004>.
- [50] A. Tuomela, A.-K. Ronkanen, P. M. Rossi, A. Rauhala, H. Haapasalo, and K. Kujala, "Using geomembrane liners to reduce seepage through the base of tailings ponds—A review and a framework for design guidelines," *Geosciences*, vol. 11, no. 2, p. 93, 2021.
- [51] P. Kienle *et al.*, "Optical setup for error compensation in a laser triangulation system," *Sensors*, vol. 20, no. 17, p. 4949, 2020.
- [52] F. Struckmeier, J. Zhao, and F. P. León, "Measuring the supporting slats of laser cutting machines using laser triangulation," *The International Journal of Advanced Manufacturing Technology*, vol. 108, pp. 3819-3833, 2020.
- [53] H. Yang, W. Tao, Z. Zhang, S. Zhao, X. Yin, and H. Zhao, "Reduction of the influence of laser beam directional dithering in a laser triangulation displacement probe," *Sensors*, vol. 17, no. 5, p. 1126, 2017.
- [54] Y. Zhao, T. B. M. Supri, S. Yang, and Y. Qin, "A new static method of calibration for low-cost laser triangulation systems," *Measurement*, vol. 156, p. 107613, 2020.
- [55] X. Fu, B. Liu, and Y. Zhang, "Measurement technology of the hot-state size for heavy shell ring forging," *The International Journal of Advanced Manufacturing Technology*, vol. 65, pp. 543-548, 2013.
- [56] Y. Zhang, T. Kong, X. Fu, and Y. Wang, "The dynamic position compensation method of the online laser detection system for the ring workpiece," *Measurement*, vol. 135, pp. 555-564, 2019.
- [57] Y.-c. Zhang, J.-x. Han, X.-b. Fu, and H.-b. Lin, "An online measurement method based on line laser scanning for large forgings," *The International Journal of Advanced Manufacturing Technology*, vol. 70, pp. 439-448, 2014.
- [58] X. Fu, Y. Zhang, K. Tao, and S. Li, "The outer diameter detection and experiment of the circular forging using laser scanner," *Optik*, vol. 128, pp. 281-291, 2017.
- [59] T. Kong, Y. Zhang, and X. Fu, "The model of feature extraction for free-form surface based on topological transformation," *Applied Mathematical Modelling*, vol. 64, pp. 386-397, 2018.

- [60] A. Schöch *et al.*, "High-speed measurement of complex shaped parts at elevated temperature by laser triangulation," *International Journal of Automation Technology*, vol. 9, no. 5, pp. 558-566, 2015.
- [61] J. Veitch-Michaelis *et al.*, "Crack detection in " as-cast" steel using laser triangulation and machine learning," in *2016 13th Conference on Computer and Robot Vision (CRV)*, 2016: IEEE, pp. 342-349.
- [62] D. Bračun, G. Škulj, and M. Kadiš, "Spectral selective and difference imaging laser triangulation measurement system for on line measurement of large hot workpieces in precision open die forging," *The International Journal of Advanced Manufacturing Technology*, vol. 90, no. 1, pp. 917-926, 2017/04/01 2017, doi: 10.1007/s00170-016-9460-0.
- [63] D. Bračun, G. Škulj, and M. Kadiš, "Spectral selective and difference imaging laser triangulation measurement system for on line measurement of large hot workpieces in precision open die forging," *The International Journal of Advanced Manufacturing Technology*, vol. 90, pp. 917-926, 2017.
- [64] S. Choi, M. Chun, C. Van Tyne, and Y. Moon, "Optimization of open die forging of round shapes using FEM analysis," *Journal of Materials Processing Technology*, vol. 172, no. 1, pp. 88-95, 2006.
- [65] J. Makem, B. Lu, H. Ou, C. Armstrong, A. Rennie, and S. Nikov, "3D die shape optimisation for net-shape forging of aeroengine compressor blades," *기타자료*, pp. 796-797, 2008.
- [66] J. E. Makem, H. Ou, and C. G. Armstrong, "A virtual inspection framework for precision manufacturing of aerofoil components," *Computer-Aided Design*, vol. 44, no. 9, pp. 858-874, 2012.
- [67] D. Recker, M. Franzke, and G. Hirt, "Fast models for online-optimization during open die forging," *CIRP annals*, vol. 60, no. 1, pp. 295-298, 2011.
- [68] M. T. Desta, H.-Y. Feng, and D. OuYang, "Characterization of general systematic form errors for circular features," *International Journal of Machine Tools and Manufacture*, vol. 43, no. 11, pp. 1069-1078, 2003.
- [69] R. R. Cordero and I. Lira, "Uncertainty analysis of displacements measured by phase-shifting moiré interferometry," *Optics communications*, vol. 237, no. 1-3, pp. 25-36, 2004.
- [70] A. Lazzari and G. Iuculano, "Evaluation of the uncertainty of an optical machine with a vision system for contact-less three-dimensional measurement," *Measurement*, vol. 36, no. 3-4, pp. 215-231, 2004.
- [71] M. De Santo, C. Liguori, A. Paolillo, and A. Pietrosanto, "Standard uncertainty evaluation in image-based measurements," *Measurement*, vol. 36, no. 3-4, pp. 347-358, 2004.
- [72] S. Nuccio and C. Spataro, "Approaches to evaluate the virtual instrumentation measurement uncertainties," *IEEE transactions on instrumentation and measurement*, vol. 51, no. 6, pp. 1347-1352, 2002.
- [73] N. Locci, C. Muscas, L. Peretto, and R. Sasdelli, "A numerical approach to the evaluation of uncertainty in nonconventional measurements on power systems," *IEEE transactions on instrumentation and measurement*, vol. 51, no. 4, pp. 734-739, 2002.
- [74] S. Castrup, "Why Spreadsheets are Inadequate for Uncertainty Analysis," in *Eighth Annual Test Instrumentation Symposium, International Test Evaluation Association (ITEA)*, 2004: Citeseer.
- [75] S. Mekid and K. Vacharanukul, "In-process out-of-roundness measurement probe for turned workpieces," *Measurement*, vol. 44, no. 4, pp. 762-766, 2011.
- [76] J. A. Śladek and J. A. Śladek, "Analysis of the Accuracy of Coordinate Measuring Systems," *Coordinate Metrology: Accuracy of Systems and Measurements*, pp. 131-225, 2016.

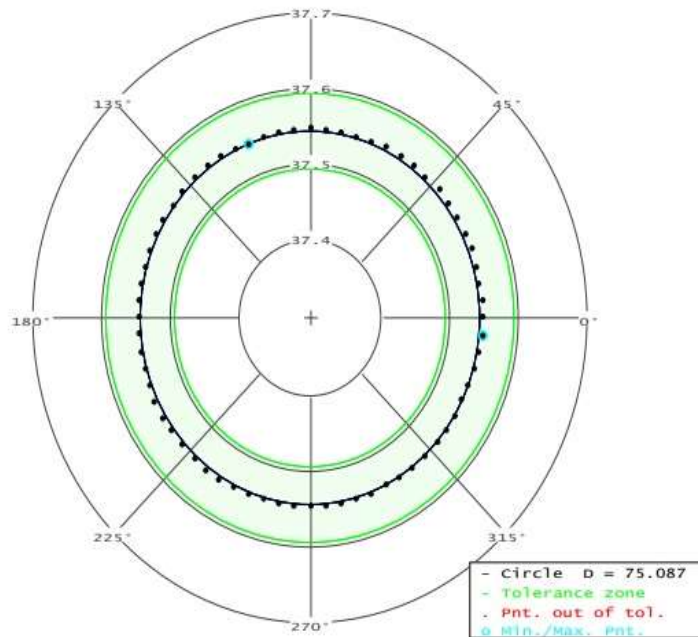
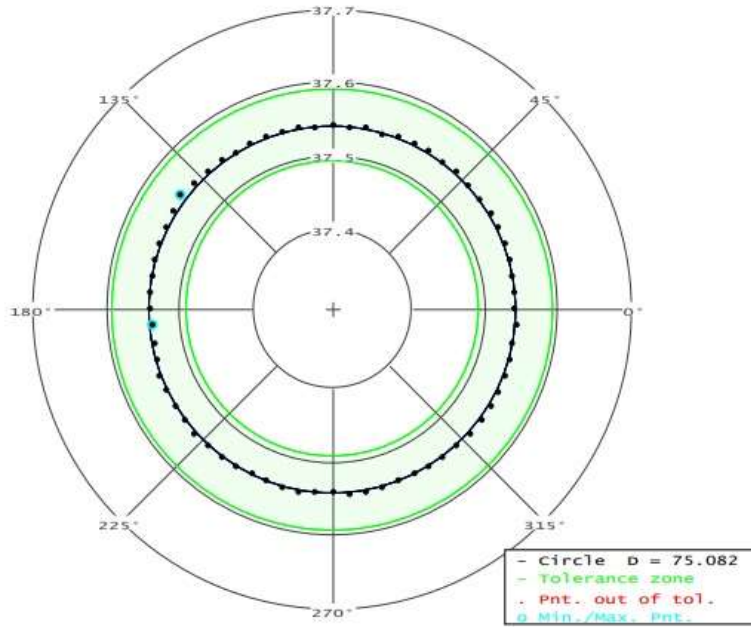
- [77] P. Ou and S. Zhang, "Natural method for three-dimensional range data compression," *Applied Optics*, vol. 52, pp. 1857-63, 03/13 2013, doi: 10.1364/AO.52.001857.
- [78] F. Li, D. Stoddart, and I. Zwierzak, "A performance test for a fringe projection scanner in various ambient light conditions," *Procedia CIRP*, vol. 62, pp. 400-404, 2017.
- [79] K. Galanulis, S. Adolf, and H. Friebe, "Optical 3D metrology for optimization of sheet metal forming processes," *Key Engineering Materials*, vol. 639, pp. 3-11, 2015.
- [80] E. P. Morse and V. Srinivasan, "Size tolerancing revisited: A basic notion and its evolution in standards," *Proceedings of the Institution of Mechanical Engineers, Part B: Journal of Engineering Manufacture*, vol. 227, no. 5, pp. 662-671, 2013.
- [81] P. Yang, S.-B. Xue, L. Song, and X.-w. Zhu, "Numerical simulation of geomembrane wrinkle formation," *Geotextiles and Geomembranes*, vol. 45, no. 6, pp. 697-701, 2017.
- [82] A. Fabijańska, "Subpixel edge detection in blurry and noisy images," *International Journal of Computer Science and Applications*, vol. 12, no. 2, pp. 1-19, 2015.
- [83] R. L. B. Breder, V. V. Estrela, and J. T. de Assis, "Sub-pixel accuracy edge fitting by means of B-spline," in *2009 IEEE international workshop on multimedia signal processing*, 2009: IEEE, pp. 1-5.
- [84] <https://www.datacolor.com/spyder/products/spyder-lenscal/> (accessed).
- [85] R. Schmitt, G. Mallmann, and P. Peterka, "Development of a FD-OCT for the inline process metrology in laser structuring systems," in *Optical Measurement Systems for Industrial Inspection VII*, 2011, vol. 8082: SPIE, pp. 688-696.
- [86] M. Stüber and T. Reemtsma, "Evaluation of three calibration methods to compensate matrix effects in environmental analysis with LC-ESI-MS," *Analytical and Bioanalytical Chemistry*, vol. 378, pp. 910-916, 2004.
- [87] B. Jähne, *Digital image processing*. Springer Science & Business Media, 2005.
- [88] Y. Zhou, Y. Wu, and C. Luo, "A fast dimensional measurement method for large hot forgings based on line reconstruction," *The International Journal of Advanced Manufacturing Technology*, vol. 99, pp. 1713-1724, 2018.
- [89] J. Wang, Z. Qiu, and J. Li, "Experimental research on dimensional measurement of hot parts based on CCD," in *Advanced Materials and Devices for Sensing and Imaging III*, 2008, vol. 6829: SPIE, pp. 224-229.
- [90] S.-M. Nie, J.-L. Tang, B.-F. Guo, Q. Li, S.-F. Wu, and S.-D. Song, "Research on the heavy forgings dimensional metrology based on CCD," *Suxing Gongcheng Xuebao(Journal of Plasticity Engineering)*, vol. 12, pp. 85-88, 2005.
- [91] T. B. Moeslund and T. B. Moeslund, "BLOB analysis," *Introduction to Video and Image Processing: Building Real Systems and Applications*, pp. 103-115, 2012.
- [92] W. Liu, X. Jia, Z. Jia, S. Liu, B. Wang, and J. Du, "Fast dimensional measurement method and experiment of the forgings under high temperature," *Journal of Materials Processing Technology*, vol. 211, no. 2, pp. 237-244, 2011.
- [93] L. Wu, J. Zhu, and H. Xie, "Single-lens 3D digital image correlation system based on a bilateral telecentric lens and a bi-prism: validation and application," *Applied optics*, vol. 54, no. 26, pp. 7842-7850, 2015.
- [94] B. Pan, L. Yu, and D. Wu, "High-accuracy 2D digital image correlation measurements with bilateral telecentric lenses: error analysis and experimental verification," *Experimental Mechanics*, vol. 53, pp. 1719-1733, 2013.
- [95] J. de Vries, "Barrel and pincushion lens distortion correction," *MATLAB Central File Exchange*, 2012.
- [96] Y. I. Abdel-Aziz, "Direct linear transformation from comparator coordinates into object space coordinates in close range photogrammetry," *Proc. Amer. Soc. Photogrammetry*, 1971, pp. 1-19, 1971.
- [97] A. Zatočilová, D. Paloušek, and J. Brandejs, "Image-based measurement of the dimensions and of the axis straightness of hot forgings," *Measurement*, vol. 94, pp. 254-264, 2016.

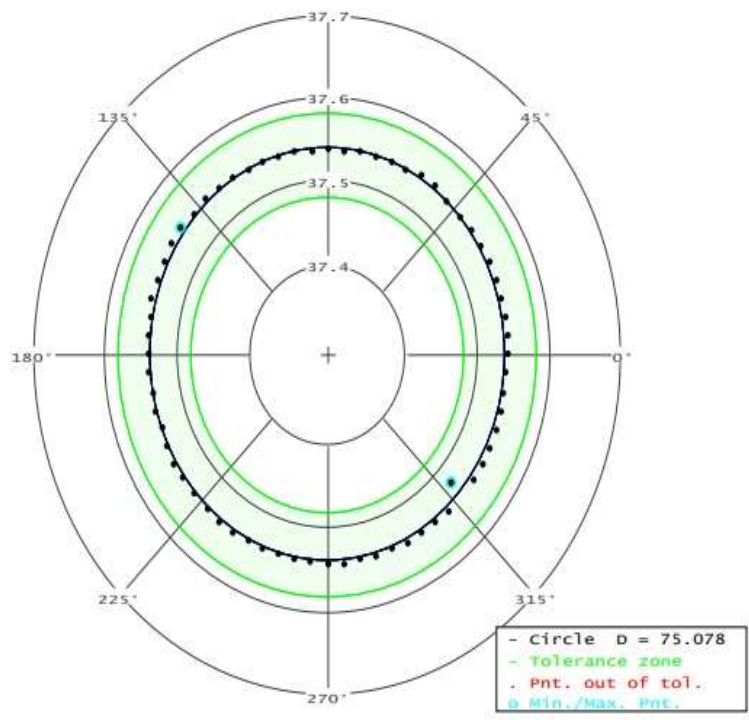
- [98] I. T. Young, J. J. Gerbrands, and L. J. Van Vliet, *Fundamentals of image processing*. Delft University of Technology Delft, 1998.
- [99] T. Koszmider and K. Strzecha, "New segmentation algorithms of metal's drop images from thermo-wet system," in *2008 International Conference on Perspective Technologies and Methods in MEMS Design*, 2008: IEEE, pp. 81-83.
- [100] R. C. Gonzalez, *Digital image processing*. Pearson education india, 2009.
- [101] S. Kumar, R. Gupta, N. Khanna, S. Chaudhury, and S. D. Joshi, "Text extraction and document image segmentation using matched wavelets and MRF model," *IEEE Transactions on Image Processing*, vol. 16, no. 8, pp. 2117-2128, 2007.
- [102] S. Zhu, X. Xia, Q. Zhang, and K. Belloulata, "An image segmentation algorithm in image processing based on threshold segmentation," in *2007 third international IEEE conference on signal-image technologies and internet-based system*, 2007: IEEE, pp. 673-678.
- [103] E. Olmedo, J. De La Calleja, A. Benitez, and M. A. Medina, "Point to point processing of digital images using parallel computing," *International Journal of Computer Science Issues (IJCSI)*, vol. 9, no. 3, p. 1, 2012.
- [104] E. Vermes, H. Childs, I. Carbone, P. Barckow, and M. G. Friedrich, "Auto-threshold quantification of late gadolinium enhancement in patients with acute heart disease," *Journal of Magnetic Resonance Imaging*, vol. 37, no. 2, pp. 382-390, 2013.
- [105] Y. Chethan, H. Ravindra, and S. B. Kumar, "Machine vision for tool status monitoring in turning Inconel 718 using blob analysis," *Materials Today: Proceedings*, vol. 2, no. 4-5, pp. 1841-1848, 2015.
- [106] A. Fabijańska, "A survey of subpixel edge detection methods for images of heat-emitting metal specimens," *International Journal of Applied Mathematics and Computer Science*, vol. 22, no. 3, pp. 695-710, 2012.
- [107] G.-S. Xu, "Sub-pixel edge detection based on curve fitting," in *2009 Second international conference on information and computing science*, 2009, vol. 2: IEEE, pp. 373-375.
- [108] M. Mizotin, "Subpixel edge detection in the problem of determining the surface tension from an axisymmetric drop profile," *Computational Mathematics and Modeling*, vol. 25, pp. 365-380, 2014.
- [109] M. Kisworo, S. Venkatesh, and G. West, "2-D edge feature extraction to subpixel accuracy using the generalized energy approach," 1991.
- [110] R. Machuca and A. L. Gilbert, "Finding edges in noisy scenes," *IEEE Transactions on Pattern Analysis and Machine Intelligence*, no. 1, pp. 103-111, 1981.
- [111] E. P. Lyvers, O. R. Mitchell, M. L. Akey, and A. P. Reeves, "Subpixel measurements using a moment-based edge operator," *IEEE Transactions on pattern analysis and machine intelligence*, vol. 11, no. 12, pp. 1293-1309, 1989.
- [112] P. I. Rockett, "The Accuracy of Sub-Pixel Localisation in the Canny Edge Detector," in *BMVC*, 1999: Citeseer, pp. 1-10.
- [113] A. Fabijańska and D. Sankowski, "Edge detection with sub-pixel accuracy in images of molten metals," in *2010 IEEE International Conference on Imaging Systems and Techniques*, 2010: IEEE, pp. 186-191.

Appendices

Appendix 1

CMM Results for diameter measurement of metal workpieces





Appendix 2

Repeated measurement results of one sample (unforged sample at room temperature)

Repeated measurement results of one sample (unforged sample at room temperature)			
Sr.no	CMM Measurement	GOM atos Measurement	Proposed System Measurement
Repeat 1	75.08	75.08	75.05
Repeat 2	75.08	75.08	75.06
Repeat 3	75.08	75.09	75.05
Repeat 4	75.08	75.09	75.05
Repeat 5	75.08	75.09	75.06
Repeat 6	75.08	75.09	75.05
Repeat 7	75.08	75.08	75.05
Repeat 8	75.08	75.08	74.09
Repeat 9	75.08	75.08	75.01
Repeat 10	75.08	75.09	75.05

Appendix 3

Proposed algorithm (code) for dimensional measurement of mild steel samples used in current research experiments

```
p=imread('DSC_0134.JPG');
out=(p(:,:,2)>=210);
figure,imshow(out)

stats = regionprops(out,'Centroid');
center=stats.Centroid;
centroids = cat(1, stats.Centroid);
imshow(out)
hold on
plot(centroids(:,1), centroids(:,2), 'b*')
hold off
stats = regionprops(out,'Centroid');

number = ceil(center);
[row,y]=size(out);

%%%%%%%%%%%%%%%%%%%%%%%%%%%%%%%%%%%%%%%%%%%%%%%%%%%%%%%%%%%%%%%%%%%%%%%%%%%%%%
number = ceil(center);
count1 =0;
col_mid = number(1);
[row,y]=size(out);
j = col_mid:y;
i=1;

for h=j(i):j(end)
    if out(number(2),h)==1
        B=[number(2),h];
        C=fliplr(B);
        count1=count1+1;
    end
end

count4 =0;
height_up = number(2);
[total_row,col_total]=size(out);

for t2=1:height_up-1
    if out(t2,number(1))==1
        k=[number(2),t2];
        l=fliplr(k);
        count4=count4+1;
    end
```

```

end

x=[number(1) C(1)];
y=[l(1) number(2)];
line(x,y,'Color','green','LineStyle','--')

%//////////code for plotting line from center towards left

    count2 =0;
width_left = number(1);
[total_row,total_col]=size(out);
for t1=1:width_left-1
if out(number(2),t1)==1
    b=[number(2),t1];
    C=fliplr(b);
break;
end
end
for t1=1:width_left-1
if out(number(2),t1)==1
count2=count2+1;
end
end

count4 =0;
height_up = number(2);
[total_row,col_total]=size(out);

for t2=1:height_up-1
if out(t2,number(1))==1
    k=[number(2),t2];
    l=fliplr(k);
count4=count4+1;
end
end
x=[C(1) number(1)];
y=[l(1) number(2)];
line(x,y,'Color','red','LineStyle','--')

%//////////code for plotting line from center to down
count3 =0;
height_down = number(2);
[total_row,total_col]=size(out);
j = height_down:total_row;
i=1;

for h2=j(i):j(end)

```

```

if out(h2,number(1))==1
    B=[h2,number(1)];
    C=fliplr(B);
    count3=count3+1;
end
end
count4 =0;
height_up = number(2);
[total_row,col_total]=size(out);

for t2=1:height_up-1
if out(t2,number(1))==1
    k=[t2,number(1)];
    l=fliplr(k);
count4=count4+1;
end
end
x=[C(1) C(1)];
y=[number(2) C(2)];
line(x,y,'Color','blue','LineStyle','--')

% ////////////////code for plotting line from center to up
count4 =0;
height_up = number(2);
[total_row,col_total]=size(out);

for t2=1:height_up-1
if out(t2,number(1))==1
    b=[t2,number(1)];
    C=fliplr(b);
    break;
end
end
for t2=1:height_up-1
if out(t2,number(1))==1
count4=count4+1;
end
end

x=[C(1) C(1)];
y=[C(2) number(2)];
line(x,y,'Color','yellow','LineStyle','--')
count5_calibrated_object=count1+count2;
count6_Calibrated_object=count3+count4;
%%%%%%%%%%%%%END
%//// from center to right till boundary of the object

number = ceil(center);
[row,y]=size(out);
number = ceil(center);

```

```

col_mid = number(1);
j = col_mid:y;
z1=1;
t11=[];
i=1;

for d1=0:1:row
    c1=(number(2)+d1);
    if out(c1,number(1))==1
        count1=0;
        for hx=j(i):j(end)
            if out(c1,hx)==1
                count1=count1+1;
            end
        end
        t11(z1)=count1-1;
        z1=z1+1;
    else break;
end

end
%////from center to left till boundary of the object

width_left = number(1);
k=width_left-1;
z2=1;
t12=[];

for d2=0:1:row
    c2=(number(2)+d2);
    if out(c2,number(1))==1
        count2=0;

for t0=k:-1:1
    if out(c2,t0)==1
        count2=count2+1;
    end
end
t12(z2)=count2-1;
    z2=z2+1;
else break;
end

end
%//// from center to up-right till boundary of the object

col_mid = number(1);
j = col_mid:y;
z3=1;
t13=[];
i=1;

```

```

for d3= number(2):-1:0
    if out(d3,number(1))==1
count3=0;
    for hx=j(i):j(end)
        if out(d3,hx)==1
            count3=count3+1;
        end
    end
    t13(z3)=count3-1;
    z3=z3+1;
else break;
end
end

%//// from center to up-left till boundary of the object

col_mid = number(1);
j = col_mid:y;
z4=1;
t14=[];
i=1;

for d4= number(2):-1:0
    if out(d4,number(1))==1
count4=0;
    for t110=k:-1:1
        if out(d4,t110)==1
            count4=count4+1;
        end
    end
    t14(z4)=count4-1;
    z4=z4+1;
else break;
end
end

Total_no_of_pixels_center_to_down =t11+t12;
Total_no_of_pixels_center_to_up =t13+t14;

%////////////////////////////////////

height_down = number(2);
[total_row,total_col]=size(out);
j = height_down:total_row;
z1a=1;
t1a=[];
i=1;

for d1a=0:1:total_col
    c1a=(number(1)+d1a);

```

```

if out(number(2),c1a)==1
count5=0;
  for h2=j(i):j(end)
    if out(h2,c1a)==1
      count5=count5+1;
    end
  end
end
t1a(z1a)=count5-1;
z1a=z1a+1;
else break;
end

end

height_up = number(2);
k1=height_up-1;

z2a=1;
t2a=[];

for d2a=0:1:total_col
  c2a=(number(1)+d2a);
  if out(number(2),c2a)==1
    count6=0;

    for tt=k1:-1:1
      if out(tt,c2a)==1
        count6=count6+1;
      end
    end
    t2a(z2a)=count6-1;
    z2a=z2a+1;
  else break;
  end

end

%////////////////////////////////////
height_down = number(2);
j = height_down:total_row;
z3a=1;
t3a=[];
i=1;
for d3a=number(1):-1:0
  if out(number(2),d3a)==1
    count7=0;
    for h2=j(i):j(end)
      if out(h2,d3a)==1
        count7=count7+1;
      end
    end
  end
end

```

```

end
    t3a(z3a)=count7-1;
    z3a=z3a+1;
else break;
end

end

height_up = number(2);
k1=height_up-1;
z4a=1;
t4a=[];
i=1;
for d4a=number(1):-1:0
    if out(number(2),d4a)==1
        count8=0;
        for ttt=k1:-1:1
            if out(ttt,d4a)==1
                count8=count8+1;
            end
        end
        t4a(z4a)=count8-1;
        z4a=z4a+1;
    else break;
end

end
Total_Height1=t1a+t2a;
Total_Height2=t3a+t4a;

%////////////////////////////////////

Original_Diameter=25;
Original_Height=60;
Pixel_value1=Original_Diameter/count5_calibrated_object
Pixel_value2=Original_Height/count6_Calibrated_object

Diameter=cat(2,Total_no_of_pixels_center_to_up,Total_no_of_pixels_center_to_down);
Height=cat(2,Total_Height1,Total_Height2);
Diameter22=Diameter*Pixel_value1;
Height22=Height*Pixel_value2;

Error_diameter= abs(Diameter22-Original_Diameter);
Error_Height=abs(Height22-Original_Height);

```